iScience

CellPress
OPEN ACCESS

Article

A Structurally Simple Vaccine Candidate Reduces Progression and Dissemination of Triple-Negative Breast Cancer

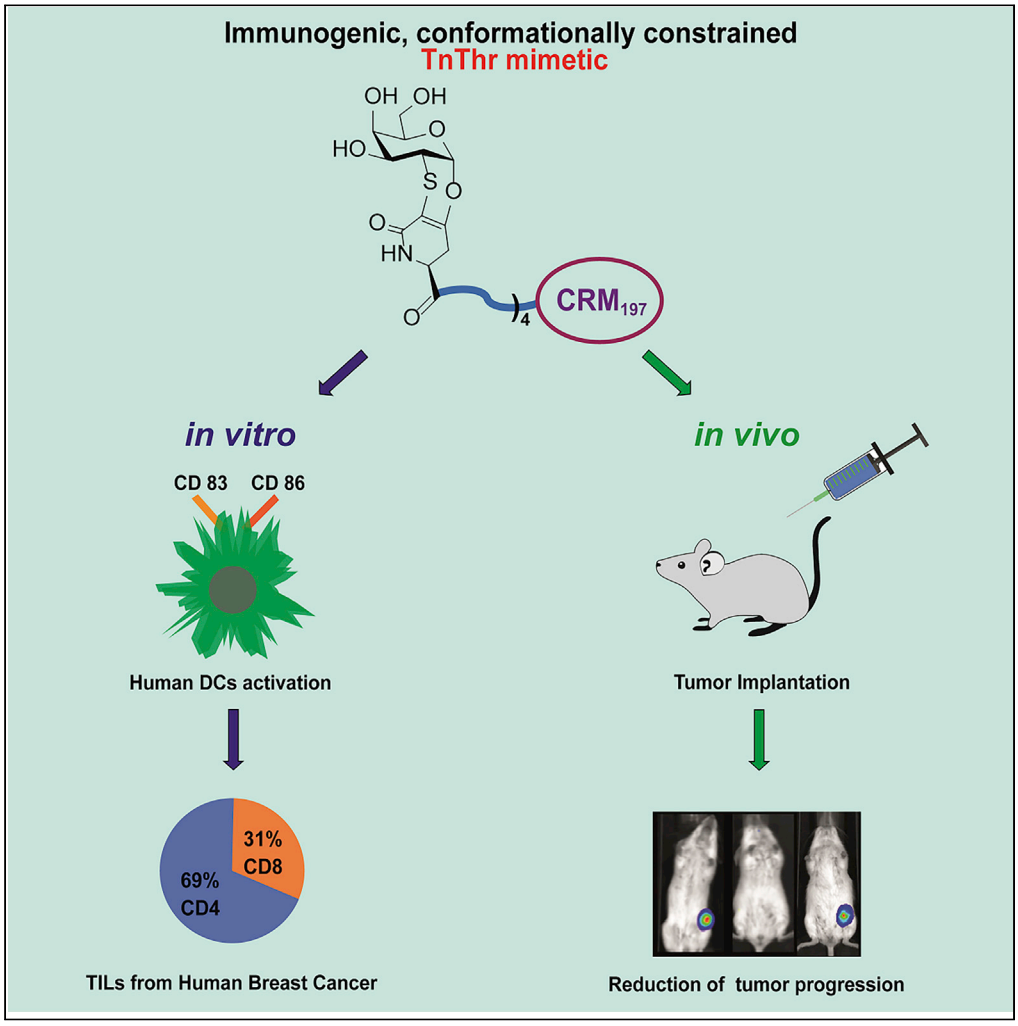

Amedeo Amedei, Fatemeh Asadzadeh, Francesco Papi, ..., Massimo Zollo, Renata Grifantini, Cristina Nativi

massimo.zollo@unina.it (M.Z.)
grifantini@ingm.org (R.G.)
cristina.nativi@unifi.it (C.N.)

HIGHLIGHTS

Structurally simple vaccine candidate reduces BC tumor size and delays lung metastasis

TnThr mimetic, fused to CRM197 adjuvant, is able to elicit T and B immune responses

TnThr mimetic-based vaccine candidate able to activate human DCs

The vaccine candidate recruits T helper CD4+ in the tumor microenvironment

Amedei et al., iScience 23, 101250
June 26, 2020
https://doi.org/10.1016/j.isci.2020.101250

iScience

CellPress
OPEN ACCESS

Article

A Structurally Simple Vaccine Candidate Reduces Progression and Dissemination of Triple-Negative Breast Cancer

Amedeo Amedei,[1] Fatemeh Asadzadeh,[2,3] Francesco Papi,[4] Maria Giuliana Vannucchi,[1] Veronica Ferrucci,[2,3] Iris A. Bermejo,[5] Marco Fragai,[4,6] Carolina Vieira De Almeida,[1] Linda Cerofolini,[6,7] Stefano Giuntini,[4,5] Mauro Bombaci,[8] Elisa Pesce,[8] Elena Niccolai,[1] Francesca Natali,[9] Eleonora Guarini,[10] Frank Gabel,[11] Chiara Traini,[1] Stefano Catarinicchia,[1] Federica Ricci,[1] Lorenzo Orzalesi,[1] Francesco Berti,[12] Francisco Corzana,[6] Massimo Zollo,[2,3,*] Renata Grifantini,[8,*] and Cristina Nativi[4,13,*]

SUMMARY

The Tn antigen is a well-known tumor-associated carbohydrate determinant, often incorporated in glycopeptides to develop cancer vaccines. Herein, four copies of a conformationally constrained mimetic of the antigen TnThr (GalNAc-Thr) were conjugated to the adjuvant CRM197, a protein licensed for human use. The resulting vaccine candidate, mime[4]CRM elicited a robust immune response in a triple-negative breast cancer mouse model, correlated with high frequency of CD4+ T cells and low frequency of M2-type macrophages, which reduces tumor progression and lung metastasis growth. Mime[4]CRM-mediated activation of human dendritic cells is reported, and the proliferation of mime[4]CRM-specific T cells, in cancer tissue and peripheral blood of patients with breast cancer, is demonstrated. The locked conformation of the TnThr mimetic and a proper presentation on the surface of CRM197 may explain the binding of the conjugate to the anti-Tn antibody Tn218 and its efficacy to fight cancer cells in mice.

INTRODUCTION

Cancer immunotherapy is nowadays a consolidated strategy, and therapeutic cancer vaccines are a matter of vast research (Bray and Soerjomataram, 2015). The use of cancer vaccines is an active, specific immunotherapy strategy to present non-self-antigens to the immune system, eliciting an antitumor immune response and leading to tumor cells' killing (Floudas et al., 2019). Cell surface-exposed carbohydrates deserve special attention, because several cancer cells can be differentiated from normal cells by the presentation on their surface of non-common glycosylation motifs (tumor-associated carbohydrate antigens [TACAs]) (Wei et al., 2018). In fact, although poorly immunogenic and usually T cell independent, carbohydrate antigens, if properly presented to the immune system, can be recognized as non-self and induce an effective immune response (Buskas et al., 2004; Danishefsky et al., 2015; Gilewski et al., 2001; Helling et al., 1995). Indeed, it has been reported about some patients with cancer able to induce natural auto-antibodies directed against native TACAs and with an improved survival rate (Livingston et al., 1994; Osinaga et al., 1996).

In the last two decades great attention has been caught by the MUC1 antigen, α-Tn (or Tn, Figure 1). The Tn is a cryptic antigen masked in normal human cells but exposed in more than 90% primary adenocarcinomas, due to the incomplete synthesis of the oligosaccharide portions, which are physiologically O-glycosylated to the MUC1 backbone. Tn antigen has been detected at early tumor stage, and its expression is associated with tumor invasiveness and metastasis (Itzkowitz et al., 1992). In breast cancer (BC) a correlation among the high level of Tn antigen expression in the primary tumor, tumor size, and a poor prognosis is known, since 20 years (Springer, 1997; Tsuchiya et al., 1999). Worldwide, BC is the most common cancer in women (20% of all cases). Among the different BC kinds, the triple-negative BC (TNBC) is the most difficult to treat for it is very aggressive, prone to metastasize, and resistant to the current anti-BC therapies (Koboldt et al., 2012).

[1]Department of Experimental and Clinical Medicine, University of Florence, Largo Brambilla 03, 50134 Firenze, Italy

[2]Department of Molecular Medicine and Medical Biotechnologies, University of Napoli "Federico II", via Pansini, 5, 80131 Napoli, Italy

[3]CEINGE Biotecnologie Avanzata, Via Gaetano Salvatore 486, 80145 Napoli, Italy

[4]Department of Chemistry, University of Florence, via della Lastruccia, 3-13, 50019 Sesto Fiorentino (FI), Italy

[5]Department of Chemistry, University of La Rioja, Madre de Dios, 53, 26006 Logroño, Spain

[6]CERM, University of Florence, via L. Sacconi, 6, 50019 Sesto Fiorentino (FI), Italy

[7]Consorzio Interuniversitario Risonanze Magnetiche di Metalloproteine (CIRMMP), via L. Sacconi, 6, 50019 Sesto Fiorentino (FI), Italy

[8]Istituto Nazionale Genetica Molecolare, Padiglione Romeo ed Enrica Invernizzi, IRCCS Ospedale Maggiore Policlinico, Milan, Italy

[9]CNR-IOM, c/o Institut Laue-Langevin, 71 avenue des Martyrs, 38000 Grenoble, France

[10]Department of Physics and Astronomy, via Sansone, 1, 50019 Sesto Fiorentino (FI), Italy

[11]Université Grenobles Alpes, CEA, CNRS, IBS, 38000 Grenoble, France

[12]GSK, Thechnical R&D, 53100 Siena, Italy

Continued

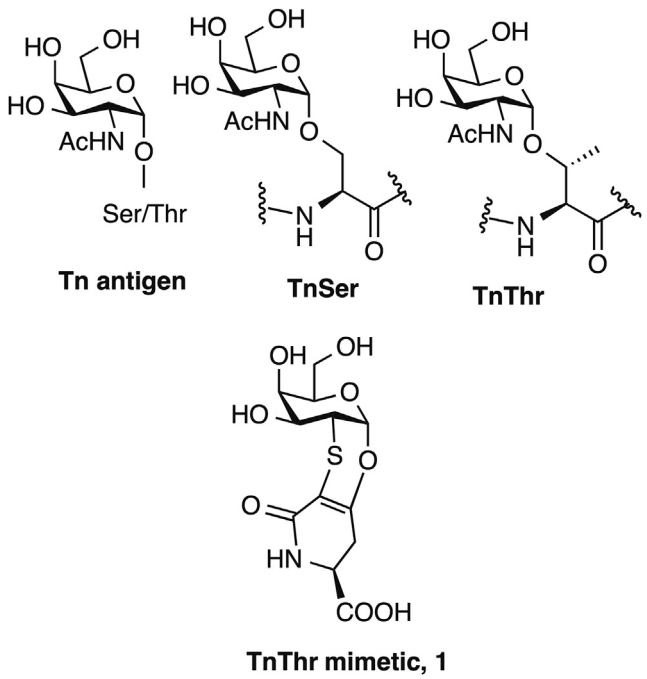

Figure 1. Structure of Tn Antigen, TnSer, TnThr, and TnThr Mimetic, 1

Structurally simple, the Tn determinant (α-O-GalNAc, linked to the MUC-1 peptide through a residue of Ser or Thr) has been the TACA selected for the development of fully or semi-synthetic cancer vaccines (Cai et al., 2012; Lakshminarayanan et al., 2012; Renaudet et al., 2008; Yin et al., 2017). Recently, relevant insights have been reported on the non-equivalence of Ser versus Thr MUC1 O-glycosylation residue (TnSer versus TnThr, Figure 1) (Grinstead et al., 2002). Noteworthy, TnThr is rather rigid in solution when compared with the more flexible TnSer; consequently in TnThr the sugar portion assumes a different spatial arrangement compared with TnSer (Mazal et al., 2013; Brister et al., 2014; Martínez-Sáez et al., 2015, 2017). This difference is mirrored in their bond state with a lower binding affinity of TnSer with respect to TnThr for anti-MUC1 SM3 antibody. Taking advantage from these findings, non-natural determinants have been proposed to obtain more antigenic structures (Compañón et al., 2019; Fernández et al., 2016; Somovilla et al., 2017). About that, few years ago we proposed a "locked" mimetic of the TnThr antigen, namely, **1** (Figure 1), which is stable and able to elicit a specific immune response *in vivo* (Richichi et al., 2014). In this study, we report on the synthesis, characterization, and immunological evaluation of CRM197 (Cross Reactive Material 197) glycoconjugates presenting residues of mimetic **1**, as candidate vaccine to treat non-responsive TNBC.

CRM197 decorated with only four residues of **1**, named **mime[4]CRM,** is able to properly activate human dendritic cells (DCs) and, of note, the administration of **mime[4]CRM** to a TNBC animal model not only produced tumor size reduction but also interfered in the lung metastasis' development. To the best of our knowledge, although specific antibodies or immune checkpoint inhibitors (passive immunotherapy) against TNBC have been approved or are in clinical trial (Force et al., 2019), no example of cancer vaccine for the active immunotherapy of TNBC is currently approved or under advanced clinical development (Vikas et al., 2018; Zeichner, 2012). In this panorama, the results herein reported represent a novelty in the non-native TACA-based vaccines research.

RESULTS AND DISCUSSION

Synthesis and Characterization of Compounds 2, 3, and Mime[4]CRM

In the design of glycoconjugate vaccines, important issues shall be taken into account, in particular (1) due to the typical weak binding interactions between lectins (i.e., macrophage galactose lectins [MGLs], Dectin-1, or DC-SIGN on DCs) and single glycans, a multivalent presentation of individual carbohydrate antigens linked to carriers (generally immunogenic proteins, peptides or synthetic scaffolds) is assembled to

[13]Lead Contact

*Correspondence:
massimo.zollo@unina.it
(M.Z.),
grifantini@ingm.org (R.G.),
cristina.nativi@unifi.it (C.N.)

https://doi.org/10.1016/j.isci.2020.101250

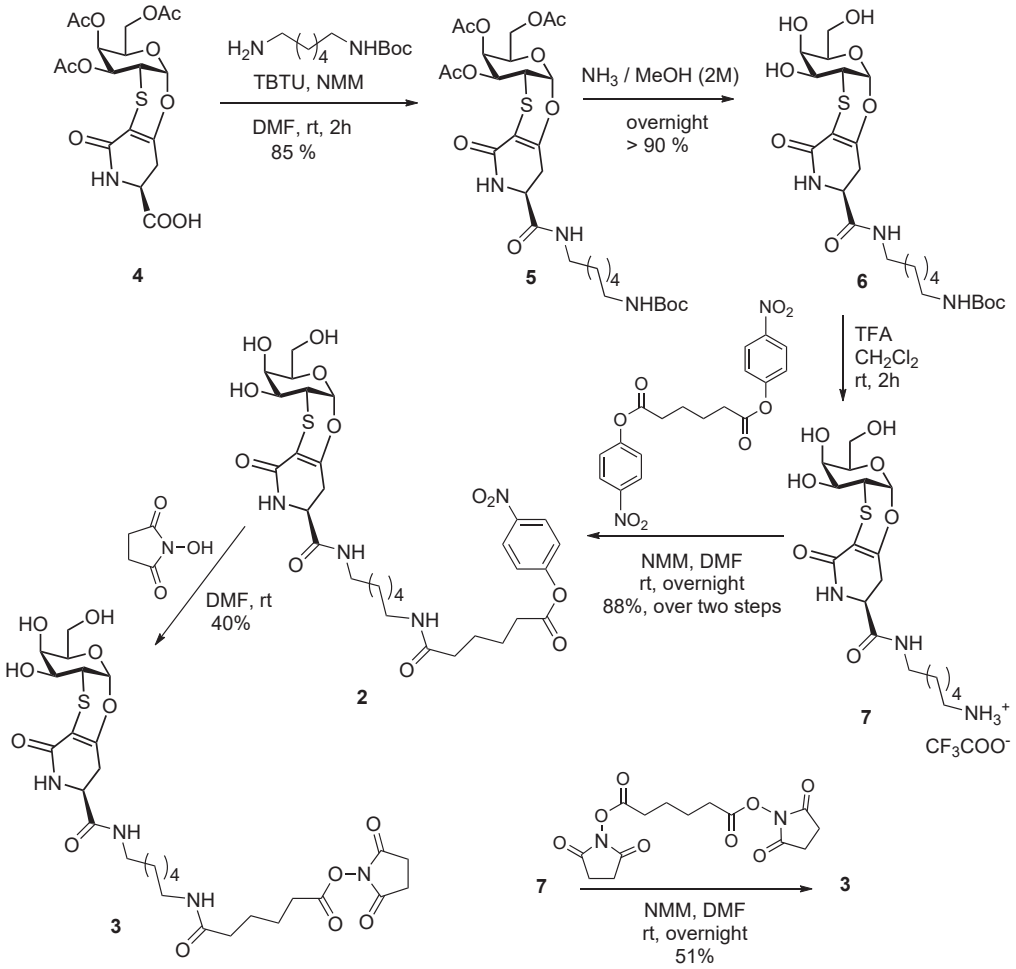

Scheme 1. Synthesis of Activated Derivatives 2 and 3

augment the binding interaction and trigger a robust recognition event and (2) to elicit TACA-specific IgG antibodies, vaccine constructs also include Toll-like ligands (Toll-like receptor) (Li and Guo, 2018; Toyokuni et al., 1994; van Duin et al., 2006) or a T helper peptide, as internal adjuvant (Renaudet et al., 2008). The outcome is the assembly of demanding constructs presenting immunodominant protein carriers, which often fail in inducing TACA-specific antibodies, eliciting undesired auto-immunity. In keeping these issues and capitalizing on the encouraging results obtained with TnThr mimetic **1** (Fallarini et al., 2017; Gracia et al., 2018; Manuelli et al., 2014; Richichi et al., 2014), we synthesized the differently activated derivatives **2** and **3**, from **4** as starting material (Scheme 1), to decorate the clinically validated carrier-adjuvant protein CRM197 under mild conditions. The acetyl derivative **4**, obtained as reported (Ardá et al., 2015), was reacted with the mono Boc-protected 1,6-diaminohexane, in the presence of 2-(1H-benzotriazole-1-yl)-1,1,3,3-tetramethylaminium tetrafluoroborate and N-methylmorpholine (NMM), in dimethylformamide (DMF), to afford derivative **5** (85%). The acetyl protecting groups were removed by treating **5** with a solution of ammonia in methanol (**6**, >90%), whereas the Boc protecting group was cleaved with trifluoroacetic acid. The trifluoroacetic salt **7** was then reacted with *para*-nitrophenyl adipates and NMM in DMF to afford compound **2** (88%, over two steps) (Scheme 1). The reaction of the activated *para*-nitrophenyl derivative **2** with N-hydroxysuccinimide produced, under mild conditions, the corresponding derivative **3** (40%) (Scheme 1). More efficiently, compound **3** was also prepared by reacting **7** at room temperature with adipic acid activated as bis-succinimide and NMM, in DMF (51%, over two steps).

CRM197 is a genetically detoxified mutant of diphtheria toxin, obtained by a single amino acid substitution (G52E) (Malito et al., 2012) and characterized by a lower immunogenicity and immunostimulatory effect

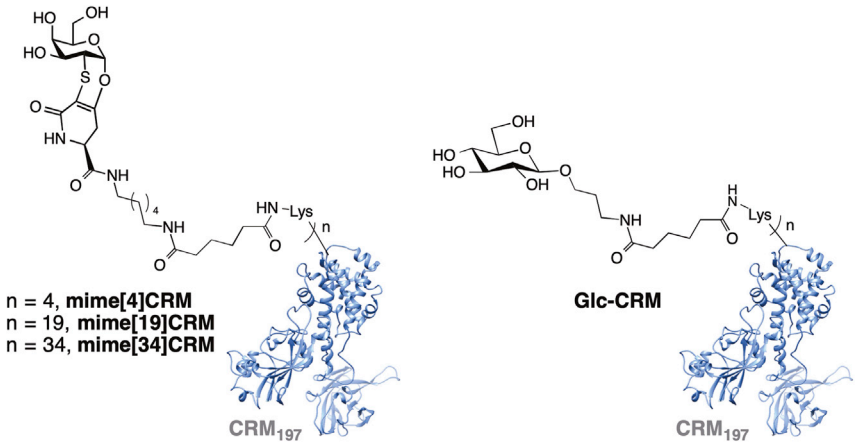

Figure 2. CRM197 Decorated with 4, 19 and 34 Residues of Mimetic 1 or with Residues of Glucose

CRM197 decorated with 4 residues (**mime[4]CRM**), 19 residues (**mime[19]CRM**), or 34 residues (**mime[34]CRM**) of TnThr mimetic **1**, and CRM197 decorated with glucose residues (**Glc-CRM**, used as control, see Supplemental Information, Data S12).

compared with diphtheria toxin (Bröker et al., 2011). Currently, CRM197 is one of the most effective carrier proteins, largely found in human conjugate vaccines, licensed to treat bacterial infections (Pecetta et al., 2016; Shinefield, 2010). This non-toxic protein is a poor B cell-mediated immunogen, also enhancing a carbohydrate-specific plasma response (Pecetta et al., 2016). In this study, the mimetic **1** was first reacted with a non-immunogenic aliphatic chain (Danishefsky et al., 2015), presenting amidic linkages and ending with a carboxylic residue activated as *para*-nitrophenyl adipate (compound **2** Scheme 1), or succinimidyl adipate (compound **3**, Scheme 1), for the subsequent conjugation to the carrier protein. According to published conditions (Tontini et al., 2013), CRM197 was treated with **2** or **3**, and, as expected, a different loading of the protein was yielded. Upon conjugation with **2**, up to four synthetic antigens were coupled to CRM197 (**mime[4]CRM**), whereas conjugation with **3** allowed to vary the loading of the protein and up to 19 or 34 synthetic glycans were grafted to CRM197 (**mime[19]CRM**, **mime[34]CRM**) (Figure 2 and Supplemental Information, Data S8–S11).

1D ^{1}H-nuclear magnetic resonance (NMR) spectra were recorded on non-functionalized CRM197 (Figure S1A), on its glycoconjugates **mime[4]CRM** (Figure S1B) and **mime[19]CRM** (Figure S1C). Significantly, although CRM197 decorated with four residues preserves its original folded structure, the protein conjugated with 19 synthetic glycans is largely unfolded. The dispersion of the NMR signals in the regions of the amide protons and methyl protons provided the main indicators for the folding state of proteins. In the spectrum of **mime[4]CRM**, these resonances are well separated, with some signals in the region between 0.5 and −1 ppm, whereas in **mime[19]CRM** the signals have narrow chemical shift dispersion without resonance lines of the protein below 0.5 ppm. On the other hand, small-angle X-ray scattering spectra recorded on **mime[19]CRM** sample confirmed that this glycoconjugate is aggregated in solution (see Figure S2).

Molecular Dynamics Simulation on Mime[4]CRM

We then performed molecular dynamics (MD) simulations on mimetic **1**. These calculations showed clear evidence of the conformational restriction imposed by the additional rings to the mimetic (root-mean-square deviation [heavy atoms] = 0.84 Å, Figure 3A) and highlighted the orientation of the amino acid with respect to the sugar moiety relative to natural TnThr. Being aware that a protruding of the TnThr mimetic residues linked to the protein is required for any immune recognition, as an example, we performed also 0.5-μs MD simulations on **mime[4]CRM** in explicit water (Figure 3B). The four unnatural counterparts were conjugated to the most exposed lysine residues displayed on the surface of the protein. According to these simulations, the tertiary structure of CRM197 is not significantly altered upon the chemical modifications and all TnThr mimetic residues are exposed to the solvent (Figure 3), which is considered essential for the efficacy of the vaccine.

Binding of Mime[4]CRM to anti-Tn Antibody Tn218

The affinity shown by the conjugate **mime[4]CRM** to the anti-Tn monoclonal antibody Tn218 (Gibadullin et al., 2017; Wua et al., 2005) was determined by SPR (Surface Plasmon Resonance) assays (Figure 4 and

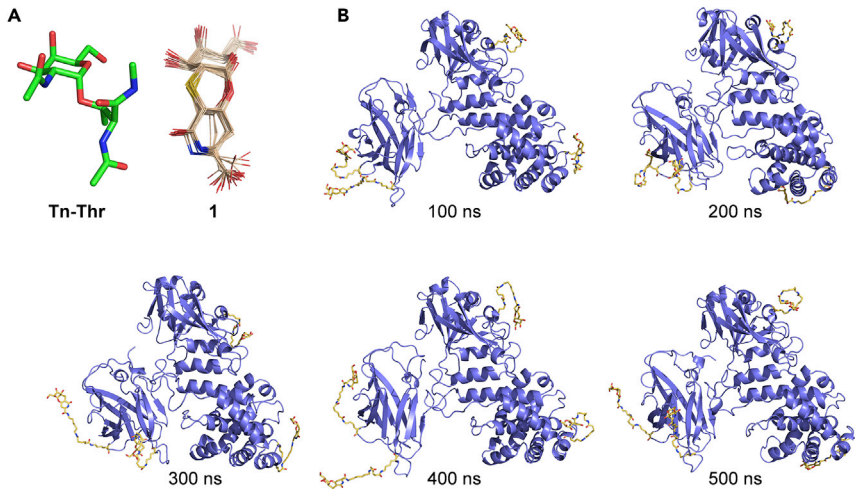

Figure 3. Molecular Dinamic Simulation on Mimetic 1and mime[4]CRM

(A) Representative conformer of **TnThr** (as a diamide derivative) in water solution, together with the structural ensemble derived from 0.5-μs MD simulation of mimetic **1**.

(B) Representative snapshot derived from 0.5-μs MD simulations of CRM197 (PDB CRM197: 4AE0) upon chemical modification with 4 molecules of mimetic **1**. A root-mean-square deviation value of 4.7 ± 1.1 Å (protein backbone), relative to the starting structure, was derived from the MD simulations. CRM197 is shown as ribbons, and the unnatural residues are represented as sticks.

Supplemental Information). The isolated mimetic **1** exhibited an affinity comparable to that of the natural Tn (Figure S3), with a K_D = 0.0160 M and 0.0125 M respectively, whereas the multipresentation of the TnThr mimetic **1** on the surface of CRM197 yielded a $K_D = 1.15 \times 10^{-5}$ M. This result attested the accessibility of **1** to the antibody and showed a binding improvement by presenting multiple copies of the TnThr mimetic on the surface of the protein (Figure 4).

Mime[4]CRM-Induced Activation of Human Dendritic Cells

DCs are central regulators of the adaptive immune response and important actors in elicitation of anti-tumoral responses. MGLs are C-type lectins exclusively expressed by human DCs and activated macrophages. A structural preference of MGLs for terminal GalNAc, including Tn antigen, has been reported (Zizzari et al., 2015; Diniz et al., 2019). We thus investigated the potential role of **mime[4]CRM** in DCs' activation and/or maturation, aiming to check the possible immunogenicity of this new vaccine candidate in humans. For that, DCs were differentiated from peripheral blood adherent mononuclear cells (PBMCs) of healthy donors, and the expression of markers CD83 and CD86 after stimulation for 48 h with **mime[4]CRM** or controls was checked (Figure 5). Flow cytometry analysis showed that **mime[4]CRM** induced activation and maturation of DCs as demonstrated by the increased expression of CD83 and CD86 markers. In contrast, **Glc-CRM** (Figure 2) and native TnThr peptide, used as controls, did not (see Supplemental Information for details). Although in-depth studies are necessary to confirm a binding interaction of MGLs with TnThr mimetic residues on CRM, these results clearly demonstrated the ability of candidate vaccine to properly activate DCs.

Therapeutic Effect of Mime[4]CRM *In Vivo* by Using Triple-Negative Breast Cancer Transplanted Model

The unique structural features and interesting *in vitro* properties of **mime[4]CRM** tethered us to assess its potential anti-tumorigenic action against the challenging TNBCs. Compared with other BC subtypes, TNBCs are more aggressive and prone to generate "*neo*" antigens (including Tn antigen) (Bianchini et al., 2016). We first verified the overall lack of toxicity of **mime[4]CRM** both on the 4T1-Luc cell line, as a cellular model of highly metastatic TNBC (Tao et al., 2008), and in human PBMC exposed to **mime[4]CRM** (from 2.3 to 57.5 μg/mL). The glucose conjugate **Glc-CRM** (see Figure 2) (Richichi et al., 2016) or CRM197 alone was also screened as control molecule. **Mime[4]CRM** did not show any influence on viability and growth rate on the two cell populations over the observation period (Figure S5 and Supplemental Information). Similar data have been obtained using the human TNBC cell line MDA-MB231 (Figure S5).

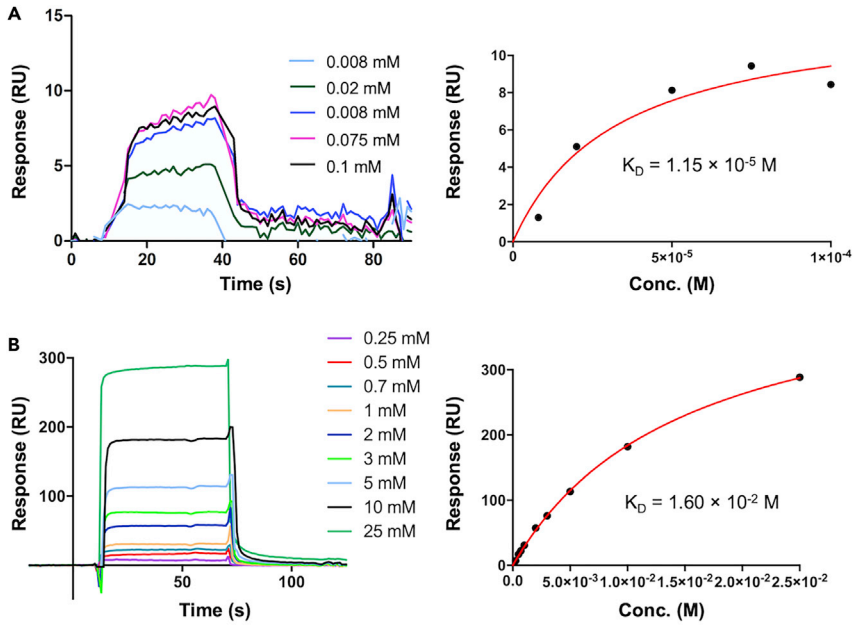

Figure 4. Affinity of Glycoconjugate mime[4]CRM to the Monoclonal anti-Tn Antibody Tn218

(A and B) SPR curves and fit obtained for **mime[4]CRM** (A) and isolated mimetic **1** (B) toward monoclonal antibody Tn218 (related to Figure S3).

The potential anti-tumorigenic action of **mime[4]CRM**, together with the activation of immune cells within the tumor microenvironment, was then evaluated *in vivo* by performing a preclinical study. For this purpose, Tn expressing (Solatycka et al., 2012) murine 4T1-luc cells (stably expressing Firefly Luciferase gene, see Supplemental Information) were implanted into the mammary fat pad gland of immunocompetent syngeneic mouse model (BALB/c mice). Of note, the use of immunocompetent mice properly allows to test the efficacy of immunomodulating compounds. Moreover, recent data showed that wild-type and huMUC1 transgenic mice produced equivalent antitumoral response against a native Tn-containing candidate vaccine (Stergiou et al., 2017).

After the tumors were established, mice were imaged (Bioluminescence Imaging, BLI, see Supplemental Information) at the time of implantation (day 0, T0) and then subcutaneously administered **mime[4]CRM** (n = 9) or CRM197 as vehicle for control group (n = 10) every week for 6 weeks (Figure 6A). As known, high-sensitivity BLI technique adequately allows the study of cell proliferation and migration *in vivo* in specific anatomical sites (Asadzadeh et al., 2017).

Mice were imaged every 7 days to monitor tumor growth *in vivo* (Figure 6B and Supplemental Information for dissection of the tumor growth from T0 to T42). Mice were then sacrificed at T28, T42, and T54. The obtained results clearly showed that the trend of total flux was significantly reduced after a week ($p < 0.01$) and also after 3 weeks ($p < 0.05$) of treatment (T14 and T28 post-implantation, respectively) in the group of mice that received **mime[4]CRM** compared with the vehicle group (Figure 6C), thus demonstrating an antitumorigenic action *in vivo* of **mime[4]CRM**. Remarkably, the reduction in the primary tumor growth between the two groups of mice was still visible after 4 weeks of treatment (i.e., after T28), even though it did not reach statistical significance (data not shown). This was likely due to an untimely interruption of the immunization schedule, along with a substantial tumor burden activation typical of highly aggressive 4T1 cells.

The absence of body and organs' weight loss (Figures 6D and S6) in treated mice confirmed that there was no significant acute toxicity induced by **mime[4]CRM**, in line with our *in vitro* data.

The immune cells (both lymphoid and myeloid cell populations) infiltrating 4T1 mammary tumor sections from mice (two mice, #9 and #19) treated for 3 weeks (T28 post-implantation, Figure 6A) with CRM197 and

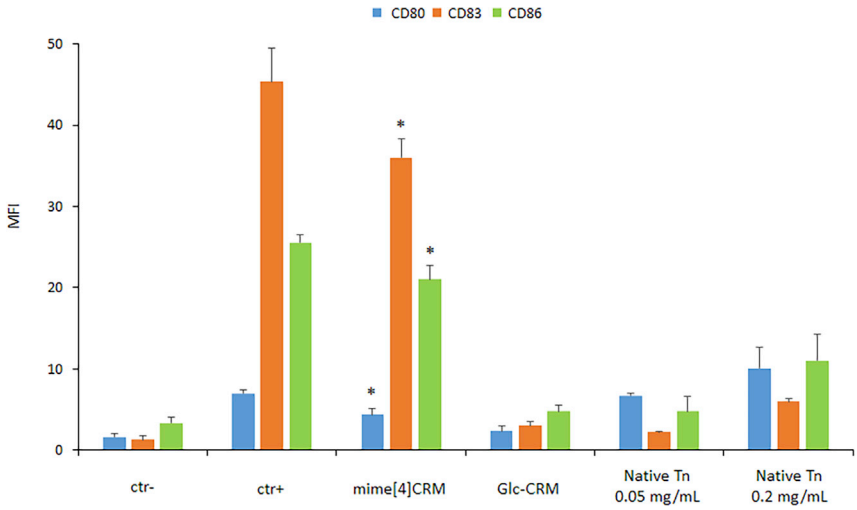

Figure 5. Evaluation of Human DCs' Activation

DCs isolated from three healthy donors have been stimulated with **mime[4]CRM**, **Glc-CRM,** or native Tn. Glc-CRM and native Tn showed some effect in DCs activation, whereas **mime[4]CRM** increased the expression of CD83 and CD86 markers. The data (median ±SD) of CD80, CD83, and CD86 expression on negative control (ctr−), positive control (ctr+, lipopolysaccharide), added with 0.2 mg/mL **mime[4]CRM**, with 0.2 mg/mL **Glc-CRM,** or with native Tn (0.05 or 0.2 mg/mL). The difference between **mime[4]CRM** treatment and the ctr− was assessed using paired t test; *$p < 0.05$ (see Supplemental Information for detail).

mime[4]CRM, respectively, were investigated by immunofluorescence analyses, by using antibodies directed against CD4 (T lymphocytes), TCR (T lymphocytes), CD11c (DCs), PD1 (immunosuppressive marker mostly expressed on T cells surface), FOXP3 (T regulatory cells [Tregs]), CD68 (granulocytes), F4/80 (macrophages), and CD163 (pro-tumorigenic M2 macrophages) (Figure 7). These markers allowed to investigate the role of **mime[4]CRM** in triggering *in vivo* immune cells exerting inhibitory effects or, conversely, promote tumor spread (i.e., CD4+FOXP3+PD1+, immunosuppressive regulatory T lymphocytes; CD68+ F4/80+ CD163+ M2-type macrophages) (Aras and Zaidi, 2017).

The data obtained showed increased levels of both T cells (CD4+TCR+) and peripheral DCs expressing CD4+ (CD4+CD11c+) in mice treated with **mime[4]CRM** (Figures 7A and 7B). This suggests that the candidate vaccine is able to modulate the recruitment of both antigen-presenting cells (APCs, i.e., DCs) and T helper CD4+ in the tumor microenvironment of the treated mice. Furthermore, the tumor sections from the same treated mouse also showed a significant reduction of CD4+ T cells expressing the immunosuppressive marker PD1 (PD1+CD4+, Figure 7C) and the transcriptional factor FOXP3 (Figure 7D), thus indicating a reduction in the quote of immunosuppressive Tregs in the TNBC microenvironment.

Of interest, in the **mime[4]CRM**-treated mouse's sections, data also showed a significant reduction in the pro-tumorigenic M2-polarized tumor-associated macrophages (TAMs; i.e., CD68+ CD163+; F4/80+ CD163+; Figures 7E and 7F). Moreover, the reduction of immunosuppressive T lymphocytes (i.e., PD1+ CD4+) was also shown in the tumor tissues from mice after 42 days from tumor cell implantation (T42), thus suggesting a long-lasting effect of **mime[4]CRM** in inhibiting immunosuppressive markers (e.g., PD1) in the tumor microenvironment of TNBC (data not shown). In contrast, the decrease of Tregs (FOXP3+ CD4+) in the same **mime[4]CRM**-treated mice was not substantially observed, thus inferring a loss of regulation of conventional T lymphocytes at T42 (results did not reach a statistical significance; data not shown).

Altogether, immunofluorescence staining indicates that **mime[4]CRM** vaccine has a clear potential role in modulating the recruitment and phenotype of CD4+ T cells and, as a consequence, on the polarization status of TAMs in the TNBC tumor microenvironment.

As 4T1 cells, used in this study as a cellular model of TNBC, are highly metastatic, the presence of lung metastases was evaluated by performing *in vivo* analyses 42 days after 4T1 TNBC cells were

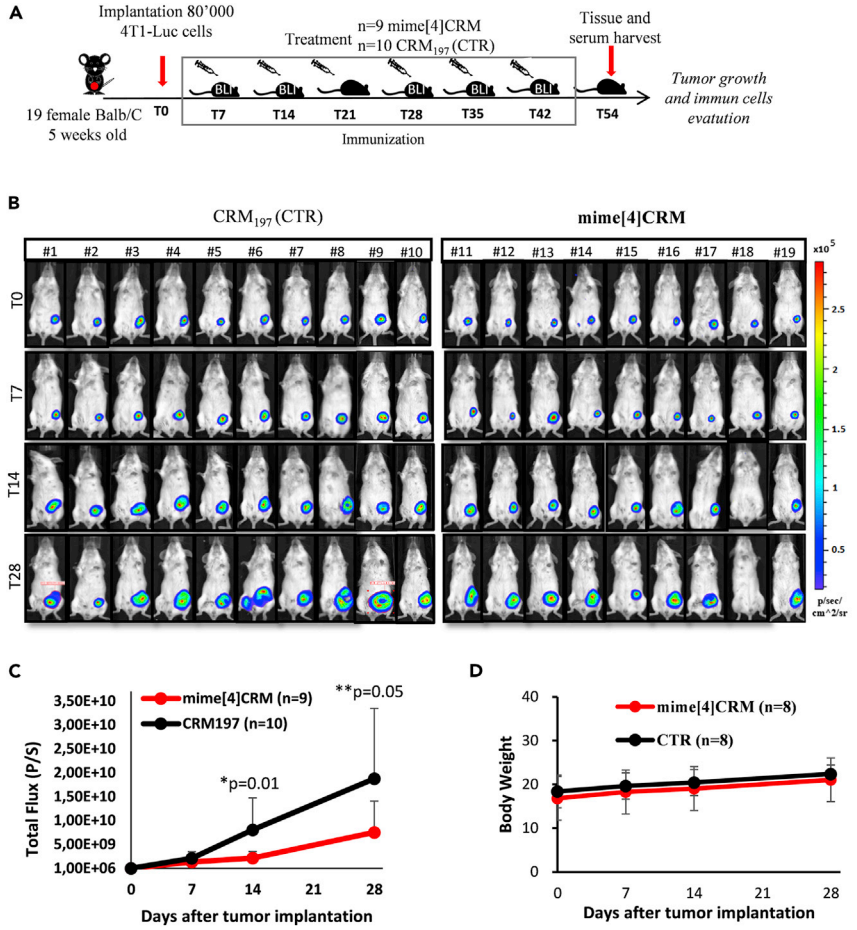

Figure 6. Description of the Vaccine Therapy Using Mime[4]CRM in Transplanted Mammary BC Cells and Their Rate of Proliferation *In Vivo*

(A) Representative scheme for the *in vivo* preclinical trial showing 4T1-Luc cells' injection into the mammary fat pad of n = 19 syngeneic BALB/c mice (at T0), and the weekly subcutaneous administration of **mime[4]CRM** (17 mg/kg/weekly) started after 7 days from the time of cell implantation. CRM197 was administered to the control group.

(B) Representative BLI images of mice orthotopically transplanted using 4T1-Luc cells implanted (n = 10 control mice, n = 9 treated mice). Mice were imaged every 7 days via *in vivo* BLI to monitor tumor growth from time of implantation (T0) to 28 days after tumor implantation.

(C) Quantification of photon emission (p/s) from the region of interest (ROI) in mice treated with **mime[4]CRM** or with CRM197 as vehicle. The differences in total flux (photons/seconds, P/S) between the two groups of mice indicated a statistically significant reduction of tumor growth (14 days of treatment: 3.7-fold reduction; 28 days of treatment: 2-fold reduction) as measured by luminescence signal emission from tumorigenic 4T1-LUC cells after 1 week and 3 weeks from tumor injection (*$p < 0.01$, **$p < 0.05$, see Supplemental Information for detail). The values are expressed as mean ± SD.

(D) Evaluation of drug toxicity using mice body weight in **mime[4]CRM**-treated and control mice. The values are expressed as mean ± SD. No significant differences were observed between the two groups (related to Figure S5).

implanted. At T42, our *in vivo* BLI analyses indicated the presence of lung metastases in seven of nine controls and four of eight **mime[4]CRM**-treated mice (Figures 8A and 8B). In contrast, as determined through *ex vivo* BLI imaging, the presence of metastatic foci was detected in eight of nine control mice (seven mice at T42 and one mouse at T54, Figure 8B), and in four of eight **mime[4]CRM**-treated mice (one mouse at T42 and three mice at T54, Figure 8A). Therefore, although we cannot exclude the presence of lung micro-metastases at T42 in the **mime[4]CRM**-treated group of mice because they might not be detectable with the *in vivo* BLI technology, data showed a clear effect of our candidate vaccine in modulating lung metastasis development.

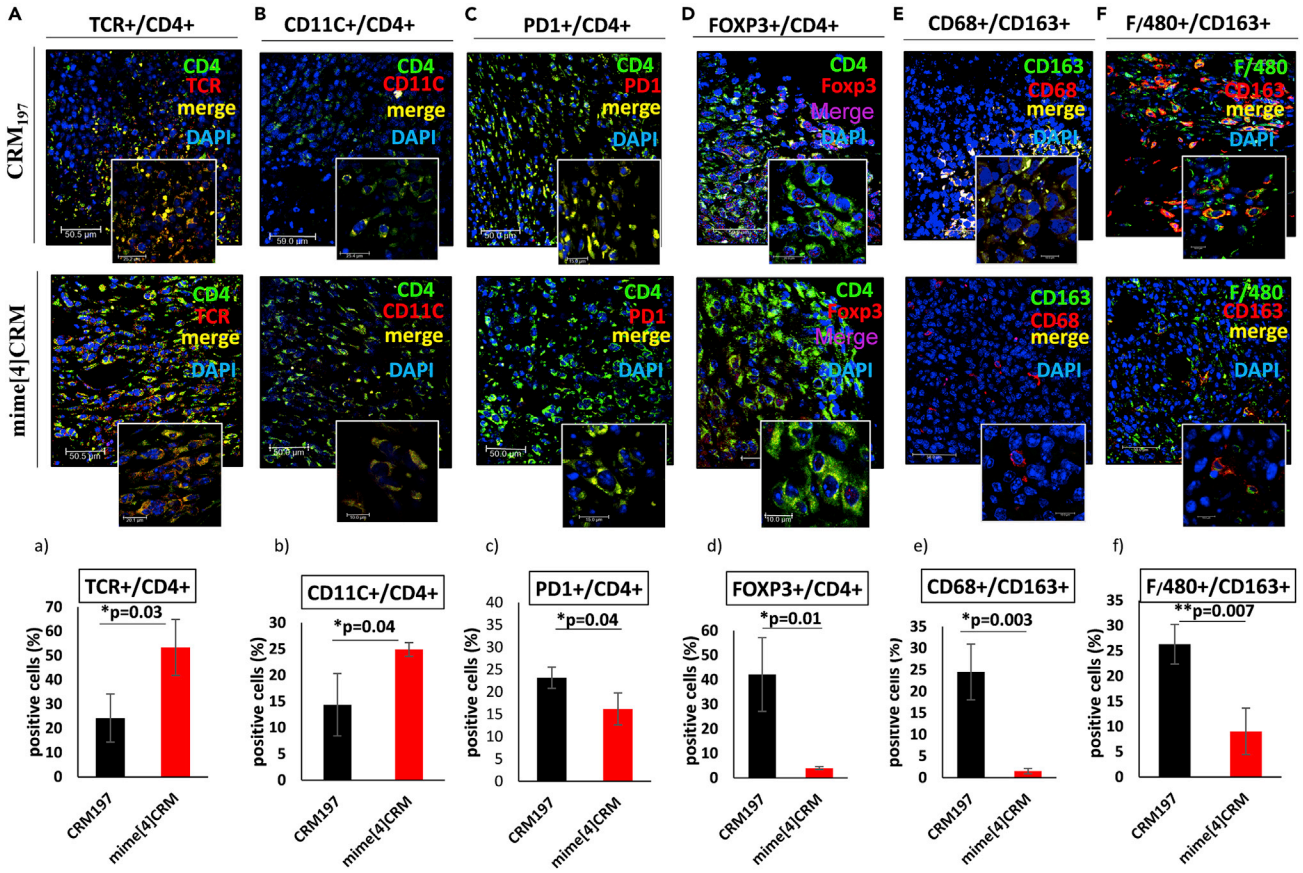

Figure 7. Representative Immunofluorescence (IF) Staining of Primary Mammary Tumor Sections from Transplanted Mice Treated with Mime[4] CRM or with CRM197 as a Vehicle

(A–F) IF double staining with (A) T cell receptor (TCR, marker of T cells, red) and CD4 (expressed by both T helper and dendritic cells, green), (B) CD11c (marker of DCs, red) and CD4 (green), (C) programmed cell death protein 1 (PD1, marker of immunosuppressive immune cells, red) and CD4 (green), (D) FOXP3 (marker of regulatory T cells, Tregs, red) and CD4 (green), (E) CD163 (specific marker of M2-polarized macrophages, red) and CD68 (marker of macrophages, green), and (F) CD163 (red) and F4/80 (marker of macrophages, green). DAPI was used to stain the nuclei (blue) in yellow or in pink, the overlays indicating (A) CD4+TCR+ (T lymphocytes), (B) CD4+ CD11c+ (DCs), (C) CD4+ PD1+ (immunosuppressive lymphocytes), (D) CD4+ FOXP3+ (T regulatory cells), and (E and F) CD68+ CD163+ and F4/80+ CD163+ cells (M2 macrophages). Magnification 63×. (a–f) Graphs showing the percentage of positive cells counted in fluorescence staining by using ImageJ software (n = 3 different sections for each tumor were screened within the tumor mass and images and cell positivity were counted). Mice treated with **mime[4]CRM**, instead of CRM197, showed a statistically significant increase of T helper lymphocytes (CD4+ TCR+, $*p < 0.03$; a) and DCs (CD4+ CD11c+, $*p < 0.04$, b) and a reduction of immunosuppressive lymphocytes (CD4+ PD1+, $*p < 0.04$, c), T regulatory cells (CD4+FOXP3+, $*p < 0.01$, d), and M2 tumor-associated macrophages (TAMs; i.e., CD68+ CD163+, $*p < 0.003$ and F4/80+ CD163+ cells $**p < 0.007$, e and f). The values are expressed as mean ± SD. $*p < 0.05$; $**p < 0.007$. See Supplemental Information for detail.

To investigate the immunoediting of mice treated with **mime[4]CRM** compared with control mice, the composition of immune cell infiltrate was also analyzed at T54 (i.e., 2 weeks after the last treatment) in the lung (Figure S6) and in BC (Figure S7) tissue, by H&E staining and by immunohistochemistry (two mice and two sections/mouse) using antibodies against CD4, CD8, and FOXP3 markers. In BC, the results showed a statistically significant increase of CD4-positive cells in **mime[4]CRM**-treated compared with CRM197-treated mice, whereas no significant differences were seen for CD8 and FOXP3 markers between the two groups (see Supplemental Information and Figure S7).

Of note, H&E staining showed a cell infiltrate in the lung of the groups of treated mice (Figures S6B, S6F, and S6G) compared with untreated mice (Figure S6A). However, it is important to note that in CRM197-treated mice the organ presented numerous metastatic cell masses (Figure S6B), whereas **mime[4]CRM**-treated mice showed just a single metastatic cell mass (Figure S6G). The composition of the immune cell infiltrate in CRM197-treated mice consisted of several CD4-positive cells diffused in the entire organ,

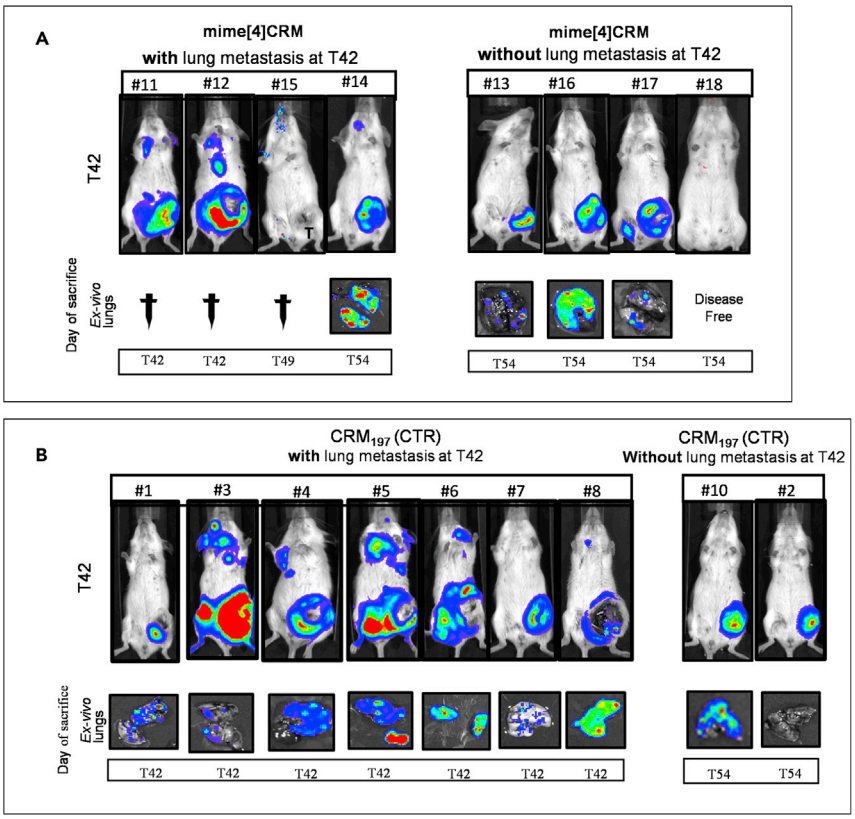

Figure 8. *In Vivo* and *Ex Vivo* Analyses to Evaluate the Presence of Lung Metastases

(A and B) *In vivo* BLI analyses showed only 50% of the **mime[4]CRM**-treated mice (four of eight animals) developed lung metastases (A), whereas the presence of metastatic foci was found in seven of nine control mice (i.e.,78%) at T42 (B). *Ex vivo* BLI analyses proved the presence of metastatic foci in eight of nine control mice (seven mice at T42 and one mouse at T54, B lower panel) and in four of eight **mime[4]CRM**-treated mice (one mouse at T42 and three mice at T54, A lower panel).

although more numerous in the metastatic masses (Figure S6C), whereas the FOXP3- and CD8-positive cells were confined to the metastatic mass (Figures S6D and S6E). Conversely, in **mime[4]CRM**-treated mouse carrying the metastatic mass, there were numerous and dispersed CD4-positive cells (Figure S6H), but very few FOXP3-positive cells limited to the metastatic mass (Figure S6J).

Furthermore, we investigated the potential ability of **mime[4]CRM** to decrease Prune-1 protein levels in the treated mice. This protein had previously been reported to be overexpressed in 4T1 cells (Virgilio et al., 2012) and positively correlated to advanced stage in metastatic BC (D'Angelo et al., 2004; Zollo et al., 2005). However, immunofluorescence analyses performed on primary tumor sections derived from **mime[4]CRM**-treated and vehicle mice did not show differences in Prune-1 levels (data not shown), thus suggesting that the ability of the vaccine **mime[4]CRM** to reduce tumor outgrowth does not involve the down-regulation of Prune-1 levels *in vivo*, confirming its action on the modulation of immune infiltrating cells by activating the lymphocytes component.

Cumulative survival analyses between the two groups of mice revealed that seven of nine (77.7%) controls and two of eight treated (25%) mice died at T42, thus indicating a clear trend of therapeutic benefit in **mime[4]CRM**-treated versus control mice in the observed period (long rank test $p < 0.083$, data not shown).

Anti-TnThr Mimetic 1-Specific Antibody Response Elicited by mime[4]CRM Immunization

Results so far described show that mice engrafted with 4T1 cancer cells and immunized with **mime[4]CRM** in a therapeutic experimental setting have a reduced tumor burden and, remarkably, impaired distal

dissemination. The antibody response introduced by the vaccine was analyzed by measuring the IgG serum titers elicited upon immunization against the glycan portion of **mime[4]CRM**. To detect mimetic **1**-specific antibodies, mice sera collected during immunization (T28 and T42) were tested by ELISA on plates coated with the hexapeptide Ala-Pro-Asp-H_2NSer-Arg-Pro **8** (as negative control, see Supplemental Information) or with the glycosylated Ala-Pro-Asp-HNSer(mimetic **1**)-Arg-Pro hexapeptide (**9**, see Supplemental Information). Immunization with **mime[4]CRM** induced predominantly IgG (almost exclusively IgG1, whereas IgG2a was barely detectable), and to a lower lever IgM (mean titer 1:1,350 and 1:600 respectively), compared with control mice (mean titer 1:600 and 1:100, respectively) (see Figure S8). Sera were then tested for binding on the surface of 4T1 cancer cells by flow cytometry. Notably, mice immunized with **mime[4]CRM** elicited antibodies that can better recognize native Tn antigen expressed by BC cells than control mice (approximately 3-fold increase in mean fluorescence intensity, see Figure S9).

A preliminary analysis of serum cytokines revealed a higher level of anti-tumor Th17 cytokines after immunization with **mime[4]CRM** (Figure S10). This result was not unexpected, because the ability of Tn glycosylation in inducing interleukin (IL)-17 responses was recently described (Freire et al., 2011). Th17 cells producing IL-17 have been detected in patients with ovarian cancer (Kryczek et al., 2009) and in mouse tumor models (Kryczek et al., 2007). Although relevance of IL17+ T lymphocytes in anti-cancer immunity is still controversial, it may contribute to protective tumor immunity by recruiting effector cells to the tumor microenvironment (Amedei et al., 2013; Kryczek et al., 2009; Martin-Orozco et al., 2009). In our study, the presence of IL-17 in serum of immunized mice is an additional evidence of **mime[4]CRM** immunomodulatory activity on T cells.

Isolation of Mime[4]CRM-Specific T Cells

Capitalizing on these notable results, 12 patients with BC were enrolled to assess the presence of **mime[4]CRM**-specific T cells, as in the peripheral blood as in the tumor tissues. In detail, the PBMCs were cultured in the presence of medium alone or with **mime[4]CRM**. The presence of **mime[4]CRM**-specific T cells was documented in 8 (67%) of the 12 patients. Thus, we isolated **mime[4]CRM**-specific T cells, by cloning the tumor-infiltrating cells of the same patients with BC. We obtained a total of 90 T cell clones and 15 (17%) that were specific for **mime[4]CRM**. Of note, evaluating the profile of cellular markers of the intra-tumoral **mime[4]CRM**-specific T cells, we found that 69% were CD4+, whereas 31% were CD8+ (see Figure S11 and Supplemental Information). This last evidence demonstrates the ability of **mime[4]CRM** to stimulate T cells in patients with BC. A compelling hypothesis is that this might be due to an activation of Tn-specific T cell response spontaneously elicited in cancer tissues.

In conclusion, the results reported in this study demonstrated a therapeutic efficacy of the glycoconjugate **mime[4]CRM** in inhibiting tumor growth in mice. The efficacy, likely correlated with a higher frequency of CD4+ T cells and a lower frequency of M2-type macrophages, was assessed in mice inoculated with 4T1-Luc cells and treated with **mime[4]CRM**. Specific IgGs were elicited in mice immunized with **mime[4]CRM**, which recognized native Tn antigen on BC cells better than sera from control mice. **Mime[4]CRM** properly activated human DCs and was able to modulate the recruitment of both APCs and T helper CD4+ in the tumor microenvironment of treated mice. In addition, the isolation from patients with BC of tumor-infiltrating lymphocytes specific for **mime[4]CRM** highlighted the intrinsic immunogenicity of the candidate vaccine and its ability to stimulate a specific immune response. These results are unprecedented for a TACA mimetic-based construct. Mice *in vivo* and human *ex vivo* immunogenicity of **mime[4]CRM**, characterized by a carbohydrate determinant quite different from that of the native TACA, could be of great interest for the design of structurally innovative cancer vaccines.

Limitations of the Study

The study provided preclinical data demonstrating the efficacy of **mime[4]CRM** as cancer vaccine for TNBC. The predictive value of the proposed TNBC mouse cancer model for **mime[4]CRM** as human vaccine deserves further investigations. In particular, efforts should be focused to assess **mime[4]CRM** efficiency in the stimulation of the Tn-specific T and B human lymphocytes naturally induced in oncologic patients affected by different Tn-positive cancers.

Resource Availability

Lead Contact

Further information and requests for resources and reagents should be directed to and will be fulfilled by the Lead Contact, Cristina Nativi (cristina.nativi@unifi.it).

Materials Availability

All unique/stable reagents generated in this study are available from the Lead Contact with a completed Materials Transfer Agreement.

METHODS

All methods can be found in the accompanying Transparent Methods supplemental file.

SUPPLEMENTAL INFORMATION

Supplemental Information can be found online at https://doi.org/10.1016/j.isci.2020.101250.

ACKNOWLEDGMENTS

Authors thank Dr. F.P. Pennino (University of Naples) for his initial contribution to the animal settings, Dr. X. Ferhati, G. Salerno, and Ms. A. Mazzara (University of Florence) for initial contribution to CRM glycosylation. We thank MIUR-Italy (Progetto Dipartimenti di Eccellenza 2018–2022 allocated to Dept. of Chemistry and Prin 2015), CISM (University of Florence) for MALDI-MS, CEINGE for supporting the use of mice facility and animal regulation study, PON 01–02388/1 2007–2013, and POR Rete delle Tecnologie in Campania Movie. I.A.B. thanks the Asociación Española Contra el Cáncer *en La Rioja* for a grant. F.C. was supported by Ministerio de Ciencia, Innovación y Universidades (project RTI2018-099592-B-C21).

AUTHOR CONTRIBUTIONS

A.A. designed and analyzed DCs tests and human *ex vivo* tests; A.A. and M.G.V. designed and analyzed the IHC tests; F.A. prepared and performed the *in vivo* tests; F.A., V.F., and M.Z. analyzed the *in vivo* data and performed quantitative immunofluorescence analysis; F.C. designed and analyzed MD and SPR assays; I.A.B. performed MD and SPR experiments, F.P. performed chemical syntheses; F.P. performed peptides' synthesis and functionalization; F.P. and S.G. performed CRM glycosylation; L.C. performed NMR studies; M.F. designed and analyzed the NMR experiments; M.B. and E.P. performed the serum *in vitro* tests; E.N. and C.V.D.A. performed DCs, E.N. and F.R. performed human *ex vivo* experiments, F.N., E.G., and F.G. designed and run SAXS experiments; C.T. and S.C. prepared and performed IHC assays; L.O. prepared human tissues samples, F.B., M.F., and C.N. designed and analyzed the CRM glycosylation experiments; M.Z. designed the *in vivo* experiments; R.G. designed and analyzed the serum *in vitro* tests; R.G. and C.N. co-wrote the paper; C.N. directed the project. A.A. and F.A. are co-first authors. All authors discussed the results and commented on the paper.

DECLARATION OF INTERESTS

F.B. is an employee of the GSK group of companies. All the other authors declare no competing financial interests.

Received: March 23, 2020
Revised: May 4, 2020
Accepted: June 2, 2020
Published: June 26, 2020

REFERENCES

Amedei, A., Niccolai, E., Benagiano, M., Della Bella, C., Cianchi, F., Bechi, P., Taddei, A., Bencini, L., Farsi, M., Cappello, P., et al. (2013). Ex vivo analysis of pancreatic cancer-infiltrating T lymphocytes reveals that ENO-specific Tregs accumulate in tumor tissue and inhibit Th1/Th17 effector cell functions. Cancer Immunol. Immunother. *62*, 1249–1260.

Aras, S., and Zaidi, M.R. (2017). TAMeless traitors: macrophages in cancer progression and metastasis. Br. J. Cancer *117*, 1583–1591.

Ardá, A., Bosco, R., Sastre, J., Cañada, F.J., André, S., Gabius, H.-J., Richichi, B., Jiménez-Barbero, J., and Nativi, C. (2015). Structural insights into the binding of sugar receptors (lectins) to a synthetic tricyclic tn mimetic and its glycopeptide version. Eur. J. Org. Chem. *2015*, 6823–6831.

Asadzadeh, M., Ahmad, S., Al-Sweih, N., and Khan, Z. (2017). Population structure and molecular genetic characterization of 5-flucytosine-susceptible and -resistant clinical

Candida dubliniensis isolates from Kuwait. PLoS One *12*, e0175269.

Bianchini, G., Balko, J.M., Mayer, I.A., Sanders, M.E., and Gianni, L. (2016). Triple-negative breast cancer: challenges and opportunities of a heterogeneous disease. Nat. Rev. Clin. Oncol. *13*, 674–690.

Bray, F., and Soerjomataram, I. (2015). The changing global burden of cancer: transitions in human development and implications for cancer prevention and control. In Cancer: Disease Control Priorities, Third Edition, *Volume 3*, H. Gelband, P. Jha, R. Sankaranarayanan, and S. Horton, eds. (The International Bank for Reconstruction and Development/The World Bank), pp. 23–44.

Brister, M.A., Pandey, A.K., Bielska, A.A., and Zondlo, N.J. (2014). OGlcNAcylation and phosphorylation have opposing structural effects in tau: phosphothreonine induces particular conformational order. J. Am. Chem. Soc. *136*, 3803–3816.

Bröker, M., Costantino, P., DeTora, L., McIntosh, E.D., and Rappuoli, R. (2011). Biochemical and biological characteristics of cross-reacting material 197 CRM197, a non-toxic mutant of diphtheria toxin: use as a conjugation protein in vaccines and other potential clinical applications. Biologicals *39*, 195–204.

Buskas, T., Li, Y., and Boons, G.-J. (2004). The immunogenicity of the tumor-associated antigen Lewisy may be suppressed by a bifunctional cross-linker required for coupling to a carrier protein. Chemistry *10*, 3517–3524.

Cai, H., Huang, Z.-H., Shi, L., Sun, Z.-Y., Zhao, Y.-F., Kunz, H., and Li, Y.-M. (2012). Variation of the glycosylation pattern in MUC1 glycopeptide BSA vaccines and its influence on the immune response. Angew. Chem. Int. Ed. *51*, 1719–1723.

Compañón, I., Guerreiro, A., Mangini, V., Castro-López, J., Escudero-Casao, M., Avenoza, A., Busto, J.H., Castillón, S., Jiménez-Barbero, J., Asensio, J.L., et al. (2019). Structure-based design of potent tumor-associated antigens: modulation of peptide presentation by single-atom O/S or O/Se substitutions at the glycosidic linkage. J. Am. Chem. Soc. *141*, 4063–4072.

Danishefsky, S.J., Shue, Y.-K., Chang, M.N., and Wong, C.-H. (2015). Development of globo-H cancer vaccine. Acc. Chem. Res. *48*, 643–652.

Diniz, A., Coelho, H., Dias, J.S., van Vliet, S.J., Jiménez-Barbero, J., Corzana, F., Cabrita, E.J., and Marcelo, F. (2019). The plasticity of the carbohydrate recognition domain dictates the exquisite mechanism of binding of human macrophage galactose-type lectin. Chemistry *25*, 13945–13955.

van Duin, D., Medzhitov, R., and Shaw, A.C. (2006). Triggering TLR signaling in vaccination. Trends Immunol. *27*, 49–55.

D'Angelo, A., Garzia, L., André, A., Carotenuto, P., Aglio, V., Guardiola, O., Arrigoni, G., Cossu, A., Palmieri, G., Aravind, L., and Zollo, M. (2004). Prune cAMP phosphodiesterase binds nm23-H1 and promotes cancer metastasis. Cancer Cell *5*, 137–149.

Fallarini, S., Brittoli, A., Fiore, M., Lombardi, G., Renaudet, O., Richichi, B., and Nativi, C. (2017). Immunological characterization of a rigid α-Tn mimetic on murine iNKT and human NK cells. Glycoconj. J. *34*, 553–562.

Fernández, E.M.S., Navo, C.D., Martínez-Sáez, N., Gonçalves-Pereira, R., Somovilla, V.J., Avenoza, A., Busto, J.H., Bernardes, G.J.L., Jiménez-Osés, G., Corzana, F., et al. (2016). Tn antigen mimics based on sp2-iminosugars with affinity for an anti-MUC1 antibody. Org. Lett. *18*, 3890–3893.

Floudas, C.S., Brar, G., and Greten, T.F. (2019). Immunotherapy: current status and future perspectives. Dig. Dis. Sci. *64*, 1030–1040.

Force, J., Leal, J.H.S., and McArthur, H.L. (2019). Checkpoint blockade strategies in the treatment of breast cancer: where we are and where we are heading. Curr. Treat. Options Oncol. *20*, 35.

Freire, T., Lo-Man, R., Bay, S., and Leclerc, C. (2011). Tn glycosylation of the MUC6 protein modulates its immunogenicity and promotes the induction of Th17-biased T cell responses. J. Biol. Chem. *286*, 7797–7811.

Gibadullin, R., Farnsworth, D.W., Barchi, J.J., and Gildersleeve, J.C. (2017). GalNAc-tyrosine is a ligand of plant lectins, antibodies, and human and murine macrophage galactose-type lectins. ACS Chem. Biol. *12*, 2172–2182.

Gilewski, T., Ragupathi, G., Bhuta, S., Williams, L.J., Musselli, C., Zhang, X.-F., Bencsath, K.P., Panageas, K.S., Chin, J., Hudis, C.A., et al. (2001). Immunization of metastatic breast cancer patients with a fully synthetic globo H conjugate: A phase I trial. Proc. Natl. Acad. Sci. U S A *98*, 3270–3275.

Gracia, R., Marradi, M., Salerno, G., Pérez-Nicado, R., Pérez-San Vicente, A., Dupin, D., Rodriguez, J., Loinaz, I., Chiodo, F., and Nativi, C. (2018). Biocompatible single-chain polymer nanoparticles loaded with an antigen mimetic as potential anticancer vaccine. ACS Macro Lett. *7*, 196–200.

Grinstead, J.S., Koganty, R.R., Krantz, M.J., Longenecker, B.M., and Campbell, A.P. (2002). Effect of glycosylation on MUC1 humoral immune recognition: NMR studies of MUC1 glycopeptide-antibody interactions. Biochemistry *41*, 9946–9961.

Helling, F., Zhang, S., Shang, A., Adluri, S., Calves, M., Koganty, R., Longenecker, B.M., Yao, T.-J., Oettgen, H.F., and Livingston, P.O. (1995). GM2-KLH conjugate vaccine: increased immunogenicity in melanoma patients after administration with immunological adjuvant QS-21. Cancer Res. *55*, 2783–2788.

Itzkowitz, S.H., Bloom, E.J., Lau, T.S., and Kim, Y.S. (1992). Mucin associated Tn and sialosyl-Tn antigen expression in colorectal polyps. Gut *33*, 518–523.

Koboldt, D.C., Fulton, R.S., McLellan, M.D., Schmidt, H., Kalicki-Veizer, J., McMichael, J.F., Fulton, L.L., Dooling, D.J., Ding, L., Mardis, E.R., et al. (2012). Comprehensive molecular portraits of human breast tumours. Nature *490*, 61–70.

Kryczek, I., Wei, S., Zou, L., Altuwaijri, S., Szeliga, W., Kolls, J., Chang, A., and Zou, W. (2007). Cutting edge: Th17 and regulatory T cell dynamics and the regulation by IL-2 in the tumor microenvironment. J. Immunol. *178*, 6730–6733.

Kryczek, I., Banerjee, M., Cheng, P., Vatan, L., Szeliga, W., Wei, S., Huang, E., Finlayson, E., Simeone, D., Welling, T.H., et al. (2009). Phenotype, distribution, generation, and functional and clinical relevance of Th17 cells in the human tumor environments. Blood *114*, 1141–1149.

Lakshminarayanan, V., Thompson, P., Wolfert, M.A., Buskas, T., Bradley, J.M., Pathangey, L.B., Madsen, C.S., Cohen, P.A., Gendler, S.J., and Boons, G.-J. (2012). Immune recognition of tumor-associated mucin MUC1 is achieved by a fully synthetic aberrantly glycosylated MUC1 tripartite vaccine. Proc. Natl. Acad. Sci. U S A *109*, 261–266.

Li, Q., and Guo, Z. (2018). Recent advances in Toll like receptor-targeting glycoconjugate vaccines. Molecules *23*, 1583.

Livingston, P.O., Wong, G.Y., Adluri, S., Tao, Y., Padavan, M., Parente, R., Hanlon, C., Calves, M.J., Helling, F., and Ritter, G. (1994). Improved survival in stage III melanoma patients with GM2 antibodies: a randomized trial of adjuvant vaccination with GM2 ganglioside. J. Clin. Oncol. *12*, 1036–1044.

Malito, E., Bursulaya, B., Chen, C., Surdo, P.L., Picchianti, M., Balducci, E., Biancucci, M., Brock, A., Berti, F., Bottomley, M.J., et al. (2012). Structural basis for lack of toxicity of the diphtheria toxin mutant CRM197. Proc. Natl. Acad. Sci. U S A *109*, 5229–5234.

Manuelli, M., Fallarini, S., Lombardi, G., Sangregorio, C., Nativi, C., and Richichi, B. (2014). Iron oxide superparamagnetic nanoparticles conjugated with a conformationally blocked α-Tn antigen mimetic for macrophage activation. Nanoscale *6*, 7643–7655.

Martin-Orozco, N., Muranski, P., Chung, Y., Yang, X.O., Yamazaki, T., Lu, S., Hwu, P., Restifo, N.P., Overwijk, W.W., and Dong, C. (2009). T helper 17 cells promote cytotoxic T cell activation in tumor immunity. Immunity *31*, 787–798.

Martínez-Sáez, N., Castro-López, J., Valero-González, J., Madariaga, D., Compañón, I., Somovilla, V.J., Salvadó, M., Asensio, J.L., Jiménez-Barbero, J., Avenoza, A., et al. (2015). Deciphering the non-equivalence of serine and threonine O-glycosylation points: implications for molecular recognition of the Tn antigen by an anti-MUC1 antibody. Angew. Chem. Int. Ed. *54*, 9830–9834.

Martínez-Sáez, N., Peregrina, J.M., and Corzana, F. (2017). Principles of mucin structure: implications for the rational design of cancer vaccines derived from MUC1-glycopeptides. Chem. Soc. Rev. *46*, 7154–7175.

Mazal, D., Lo-Man, R., Bay, S., Pritsch, O., Dériaud, E., Ganneau, C., Medeiros, A., Ubillos, L., Obal, G., Berois, N., et al. (2013). Monoclonal antibodies toward different Tn-amino acid backbones display distinct recognition patterns on human cancer cells. Implications for effective immuno-targeting of cancer. Cancer Immunol. Immunother. *62*, 1107–1122.

Osinaga, E., Babino, A., Grosclaude, J., Cairoli, E., Batthyany, C., Bianchi, S., Signorelli, S.,

Varangot, M., Muse, I., and Roseto, A. (1996). Development of an immuno-lectin-enzymatic assay for the detection of serum cancer-associated glycoproteins bearing Tn determinant. Int. J. Oncol. *8*, 401–406.

Pecetta, S., Tontini, M., Faenzi, E., Cioncada, R., Proietti, D., Seubert, A., Nuti, S., Berti, F., and Romano, M.R. (2016). Carrier priming effect of CRM197 is related to an enhanced B and T cell activation in meningococcal serogroup A conjugate vaccination. Immunological comparison between CRM197 and diphtheria toxoid. Vaccine *34*, 2334–2341.

Renaudet, O., BenMohamed, L., Dasgupta, G., Bettahi, I., and Dumy, P. (2008). Towards a self-adjuvanting multivalent B and T cell epitope containing synthetic glycolipopeptide cancer vaccine. ChemMedChem *3*, 737–741.

Richichi, B., Thomas, B., Fiore, M., Bosco, R., Qureshi, H., Nativi, C., Renaudet, O., and BenMohamed, L. (2014). A cancer therapeutic vaccine based on clustered Tn-antigen mimetics induces strong antibody-mediated protective immunity. Angew. Chem. Int. Ed. *53*, 11917–11920.

Richichi, B., Pastori, C., Gherardi, S., Venuti, A., Cerreto, A., Sanvito, F., Toma, L., Lopalco, L., and Nativi, C. (2016). GM-3 lactone mimetic interacts with CD4 and HIV-1 env proteins, hampering HIV-1 infection without inducing a histopathological alteration. ACS Infect. Dis. *2*, 564–571.

Shinefield, H.R. (2010). Overview of the development and current use of CRM197 conjugate vaccines for pediatric use. Vaccine *28*, 4335–4339.

Solatycka, A., Owczarek, T., Piller, F., Piller, V., Pula, B., Wojciech, L., Podhorska-Okolow, M., Dziegiel, P., and Ugorski, M. (2012). MUC1 in human and murine mammary carcinoma cells decreases the expression of core 2 β1,6-N-acetylglucosaminyltransferase and β-galactoside α2,3-sialyltransferase. Glycobiology *22*, 1042–1054.

Somovilla, V.J., Bermejo, I.A., Albuquerque, I.S., Martínez-Sáez, N., Castro-López, J., García-Martín, F., Compañón, I., Hinou, H., Nishimura, S.-I., Jiménez-Barbero, J., et al. (2017). The use of fluoroproline in MUC1 antigen enables efficient detection of antibodies in patients with prostate cancer. J. Am. Chem. Soc. *139*, 18255–18261.

Springer, G.F. (1997). Immunoreactive T and Tn epitopes in cancer diagnosis, prognosis, and immunotherapy. J. Mol. Med. *75*, 594–602.

Stergiou, N., Glaffig, M., Jonuleit, H., Schmitt, E., and Kunz, H. (2017). Immunization with a synthetic human MUC1 glycopeptide vaccine against tumor-associated MUC1 breaks tolerance in human MUC1 transgenic mice. ChemMedChem *12*, 1424–1428.

Tao, K., Fang, M., Alroy, J., and Sahagian, G.G. (2008). Imagable 4T1 model for the study of late stage breast cancer. BMC Cancer *8*, 228.

Tontini, M., Berti, F., Romano, M.R., Proietti, D., Zambonelli, C., Bottomley, M.J., De Gregorio, E., Del Giudice, G., Rappuoli, R., Costantino, P., et al. (2013). Comparison of CRM197, diphtheria toxoid and tetanus toxoid as protein carriers for meningococcal glycoconjugate vaccines. Vaccine *31*, 4827–4833.

Toyokuni, T., Dean, B., Cai, S., Boivin, D., Hakomori, S., and Singhal, A.K. (1994). Synthetic vaccines: synthesis of a dimeric Tn antigen-lipopeptide conjugate that elicits immune responses against Tn-expressing glycoproteins. J. Am. Chem. Soc. *116*, 395–396.

Tsuchiya, A., Kanno, M., Kawaguchi, T., Endo, Y., Zhang, G.-J., Ohtake, T., and Kimijima, I. (1999). Prognostic relevance of tn expression in Breast Cancer. Breast Cancer *6*, 175.

Vikas, P., Borcherding, N., and Zhang, W. (2018). The clinical promise of immunotherapy in triple-negative breast cancer. Cancer Manag. Res. *10*, 6823–6833.

Virgilio, A., Spano, D., Esposito, V., Di Dato, V., Citarella, G., Marino, N., Maffia, V., De Martino, D., De Antonellis, P., Galeone, A., and Zollo, M. (2012). Novel pyrimidopyrimidine derivatives for inhibition of cellular proliferation and motility induced by h-prune in breast cancer. Eur. J. Med. Chem. *57*, 41–50.

Wei, M.-M., Wang, Y.-S., and Ye, X.-S. (2018). Carbohydrate-based vaccines for oncotherapy. Med. Res. Rev. *38*, 1003–1026.

Wua, A.M., Wub, J.H., Kuoa, H.-W., and Herpa, A. (2005). Further characterization of the binding properties of two monoclonal antibodies recognizing human Tn red blood cells. J. Biomed. Sci. *12*, 153–166.

Yin, X.-G., Chen, X.-Z., Sun, W.-M., Geng, X.-S., Zhang, X.-K., Wang, J., Ji, P.-P., Zhou, Z.-Y., Baek, D.J., Yang, G.-F., et al. (2017). IgG antibody response elicited by a fully synthetic two-component carbohydrate-based cancer vaccine candidate with α-galactosylceramide as built-in adjuvant. Org. Lett. *19*, 456–459.

Zeichner, S.B. (2012). The failed theratope vaccine: 10 years later. J. Am. Osteopath. Assoc. *112*, 482–483.

Zizzari, I.G., Napoletano, C., Battisti, F., Rahimi, H., Caponnetto, S., Pierelli, L., Nuti, M., and Rughetti, A. (2015). MGL receptor and immunity: when the ligand can make the difference. J. Immunol. Res. *2015*, 450695.

Zollo, M., Andrè, A., Cossu, A., Sini, M.C., D'Angelo, A., Marino, N., Budroni, M., Tanda, F., Arrigoni, G., and Palmieri, G. (2005). Overexpression of h-prune in breast cancer is correlated with advanced disease status. Clin. Cancer Res. *11*, 199–205.

iScience, Volume *23*

Supplemental Information

A Structurally Simple Vaccine Candidate Reduces Progression and Dissemination of Triple-Negative Breast Cancer

Amedeo Amedei, Fatemeh Asadzadeh, Francesco Papi, Maria Giuliana Vannucchi, Veronica Ferrucci, Iris A. Bermejo, Marco Fragai, Carolina Vieira De Almeida, Linda Cerofolini, Stefano Giuntini, Mauro Bombaci, Elisa Pesce, Elena Niccolai, Francesca Natali, Eleonora Guarini, Frank Gabel, Chiara Traini, Stefano Catarinicchia, Federica Ricci, Lorenzo Orzalesi, Francesco Berti, Francisco Corzana, Massimo Zollo, Renata Grifantini, and Cristina Nativi

Supplemental Information

Supplemental Figures and legends

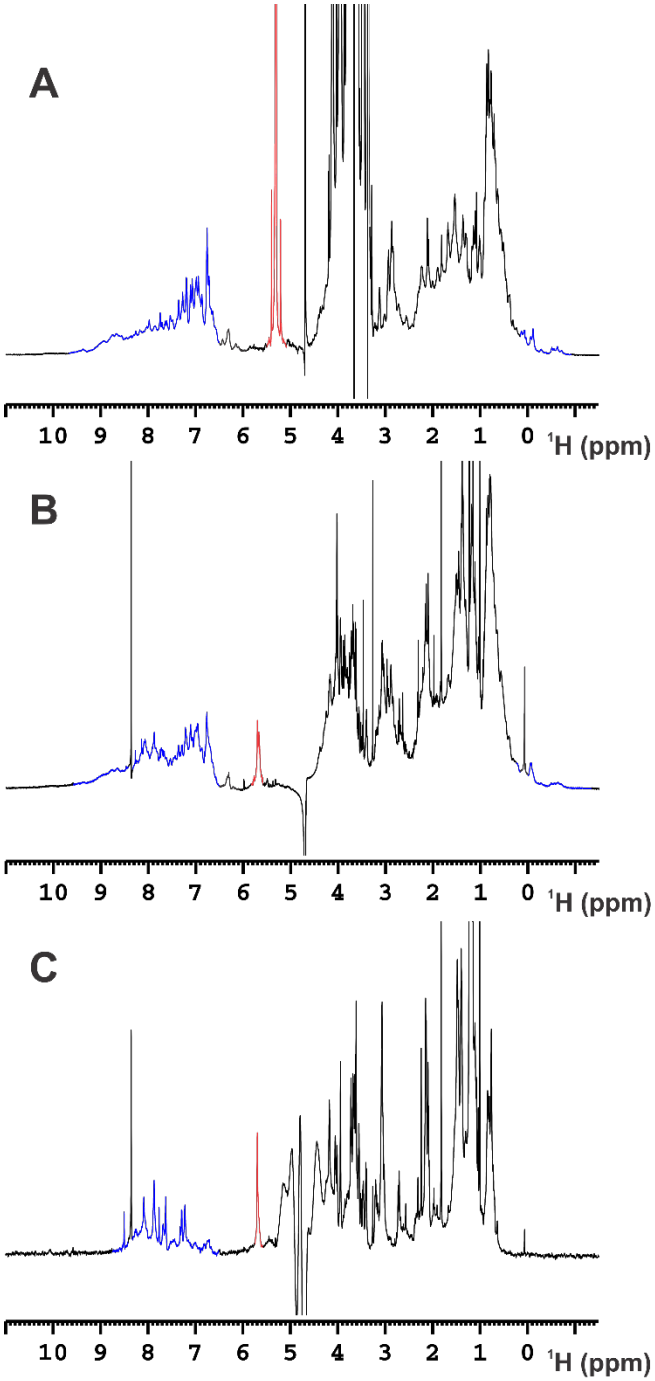

Figure S1. 1D 1H NMR spectra of free CRM197 (panel A), and of its glycoconjugates **mime[4]CRM** (panel B) and **mime[19]CRM** (panel C). The spectra were recorded at 298 K and 900 MHz. The signal of the anomeric proton of sucrose present in the formulation buffer of free CRM197 (panel A) and the anomeric protons of the synthetic glycans conjugated to the protein (in panel B and C) have been highlighted in red. The signals of the amide and methyl protons have been highlighted in blue. In the free CRM197 (panel A) and in **mime[4]CRM** (panel B) the amide signals are spread out over 3 ppm (from 9.5 to 6.5 ppm) while in **mime[19]CRM** (panel C) the spreading is sizably reduced (from 8.5-6.5 ppm). In **mime[19]CRM** the signals of methyl protons in the region from 1 to -1 ppm are completely missing. Related to Figure 2.

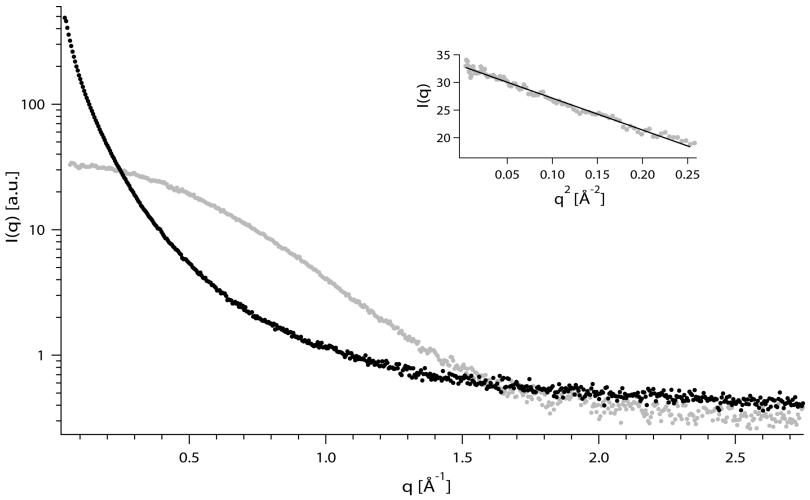

Figure S2. SAXS spectra of **mime[19]CRM** (black symbols) and CRM197 (grey symbols), recorded at the BioSAXS beamline BM29 (ESRF, Grenoble, France) at 37 °C. Inset: Guinier fit of the scattering intensity in the small angles region. Related to Figure 2.

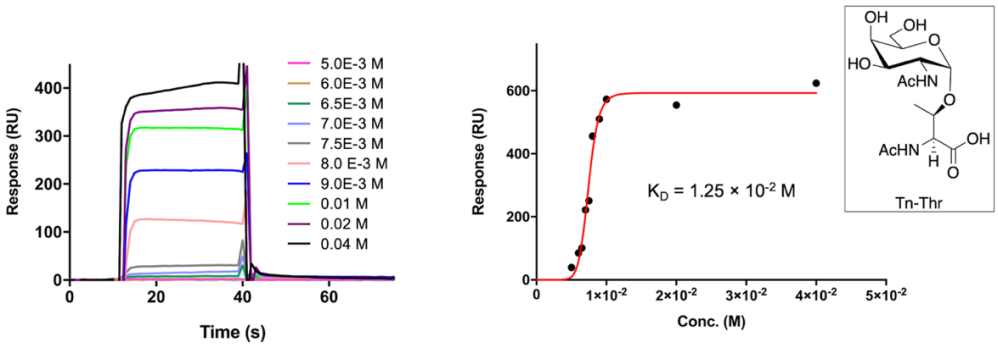

Figure S3. SPR curves obtained for native TnThr towards monoclonal antibody Tn218. Related to Figure 4.

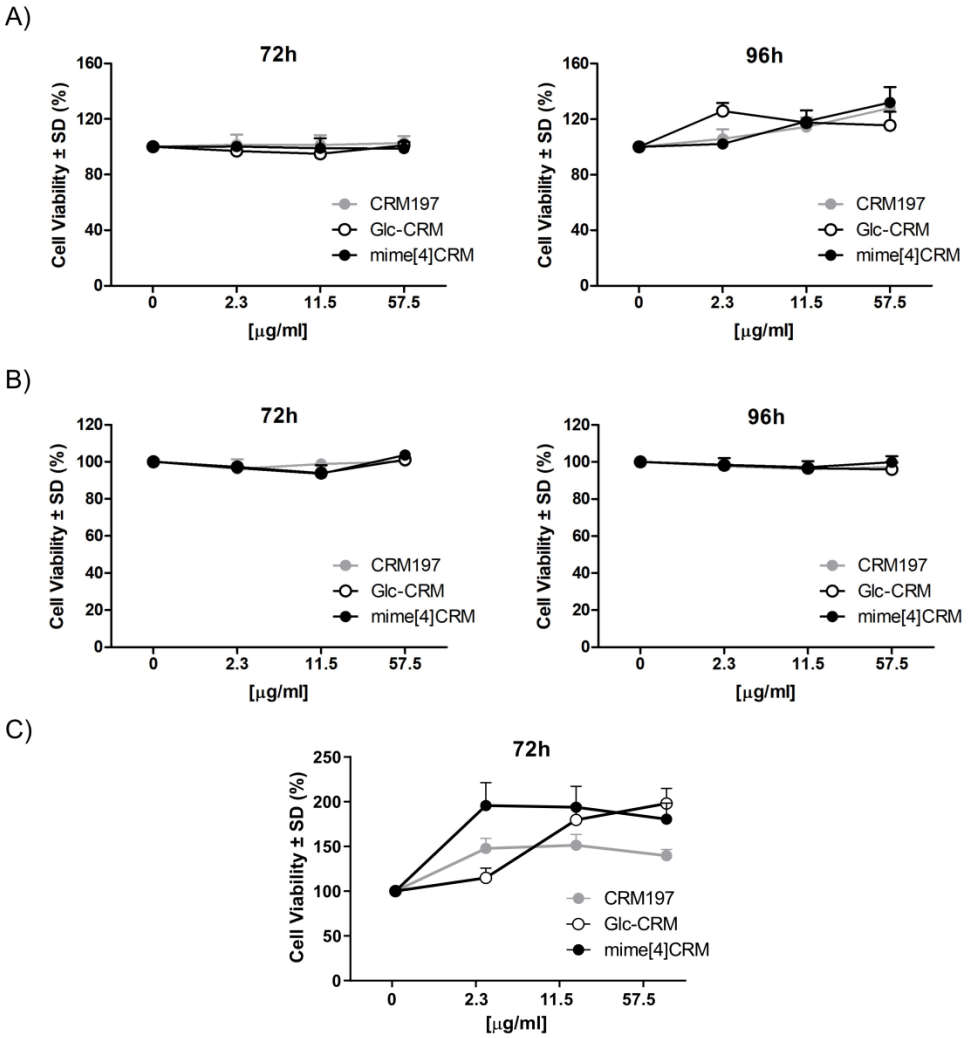

Figure S4. Cell viability upon exposure to **mime[4]CRM** 4T1 mouse breast cancer cells (upper panel, A), Human PBMC (central panel, B) and MDA-MB231 human TNBC (lower panel, C) were seeded in 96w plates (10,000 cells/w, in triplicate) and incubated for 72 or 96 h with the indicated concentrations of either **mime[4]CRM** or Glc-CRM or CRM197 alone. Cell viability was assessed Presto Blu staining compared to untreated cells run in parallel. Related to Figure 6.

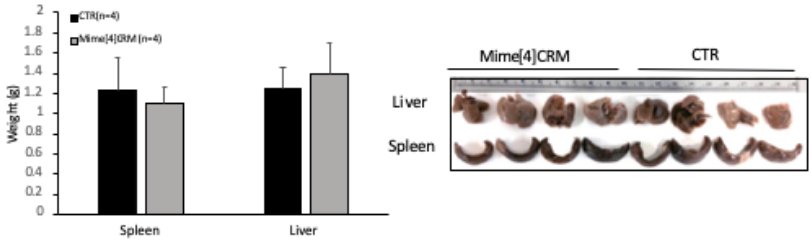

Figure S5. Control *vs*. treated mice's spleen and lung weight (n=4 mice: n=1 at T28, n=3 at T42 or T54). Related to Figure 6.

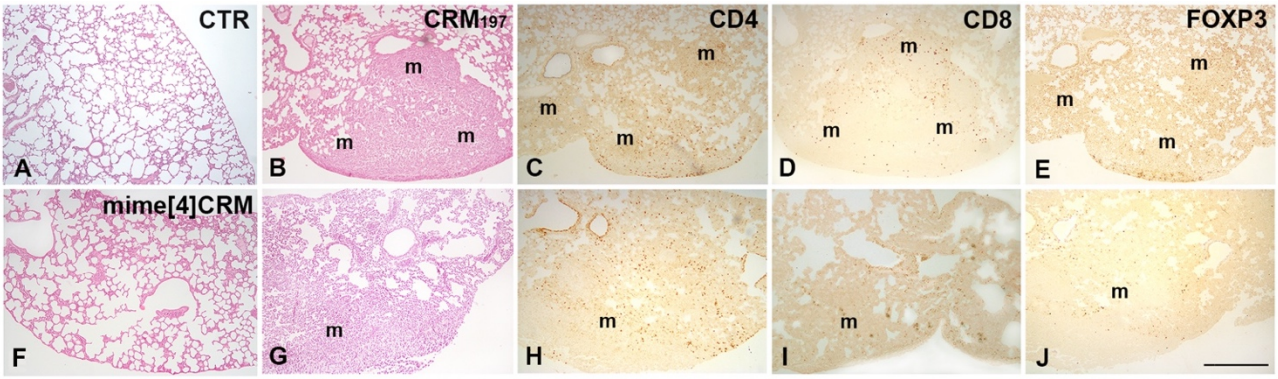

Figure S6. H&E staining in control mice (A, untreated), in CRM197 (B, control) or mime[4]CRM (F,G) treated mice at T54. CD4- CD8- FOXP3-immunolabeling in CRM197 (C-E) or **mime[4]CRM** (H-J) treated mice at T54. In mice treated with CRM197, H&E staining showed the presence of a cell infiltrate and several metastatic cell masses (m) that strongly altered the parenchyma architecture (B); the immunolabeling shows numerous CD4-, CD8- and FOXP3-positive cells (C-E). In **mime[4]CRM**-treated mice, the integrity of the parenchyma is partially conserved in mice (F) except for the section that showed metastasis (G). In this mouse there were numerous and dispersed CD4-positive cells (H) but few FOXP3-positive cells, concentrated in the metastatic mass (J). Bar=100 μm. Related to Figure 6.

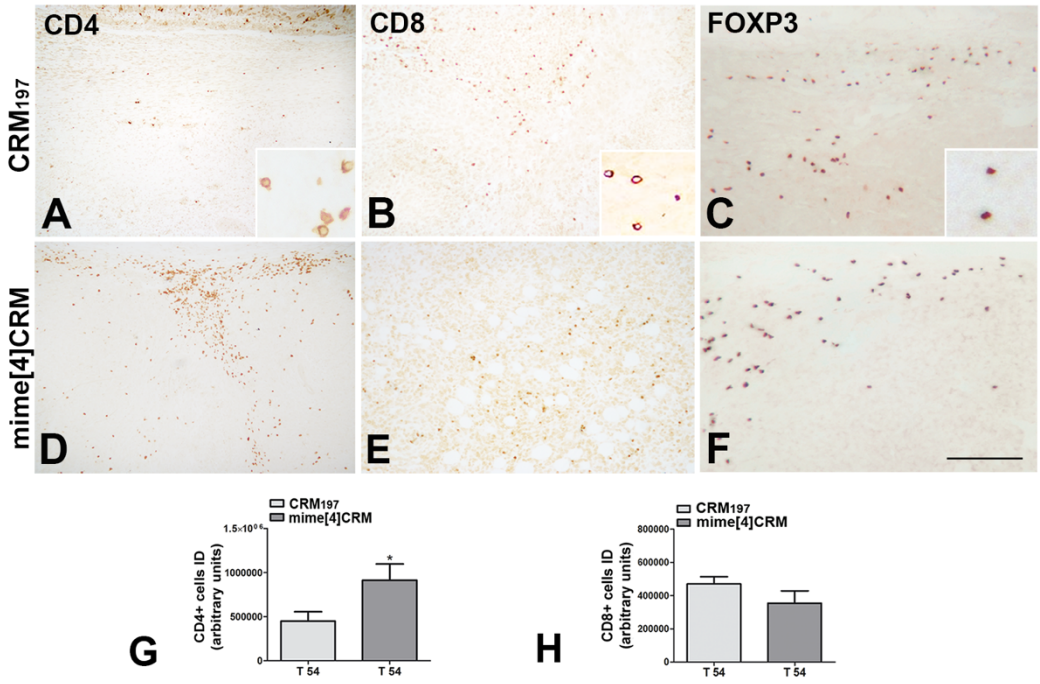

Figure S7. Representative immunofluorescence for the CD4, CD8 and FOXP3 lymphocyte markers in breast cancer sections from mice treated with CRM197 (A-C) or mime[4]CRM (C-F) at T54. The CD4 and CD8 immunolabeling is located along the cell contour (inset in A and B). The FOXP3 immunolabeling is nuclear (inset in C). Quantitation of the CD4 positive cells shows a significant increase in **mime[4]CRM**-treated mice with respect to CRM197 ones at T54 (G) (*P=0.035). No significant difference in CD8 positive cells is observed between the two groups (H). Bar A,B,D,E = 100 μm; C,F = 50 μm; insets = 25μm. Related to Figure 7.

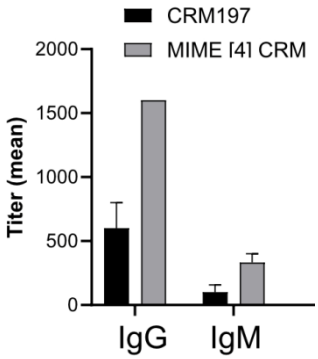

Figure S8. ELISA titers of IgM and IgG antibodies elicited against mimetic **1** by immunization with **mime[4]CRM** and control. Serial dilutions of sera from mice immunized with **mime[4]CRM** or with CRM197 (collected at day 42) were tested by ELISA on Covalink 96w plates coated either with the glycosylated hexapeptide, AlaProAsp-HNSer(mimetic **1**)ArgPro, or with AlaProAsp-H_2NSer-ArgPro (as negative control). For detection, plates were added with HRP conjugated goat anti-mouse IgM and anti-mouse IgG secondary antibodies and detection was done with TMB substrate and optical density reading at 450 nm. Related to Figure 8.

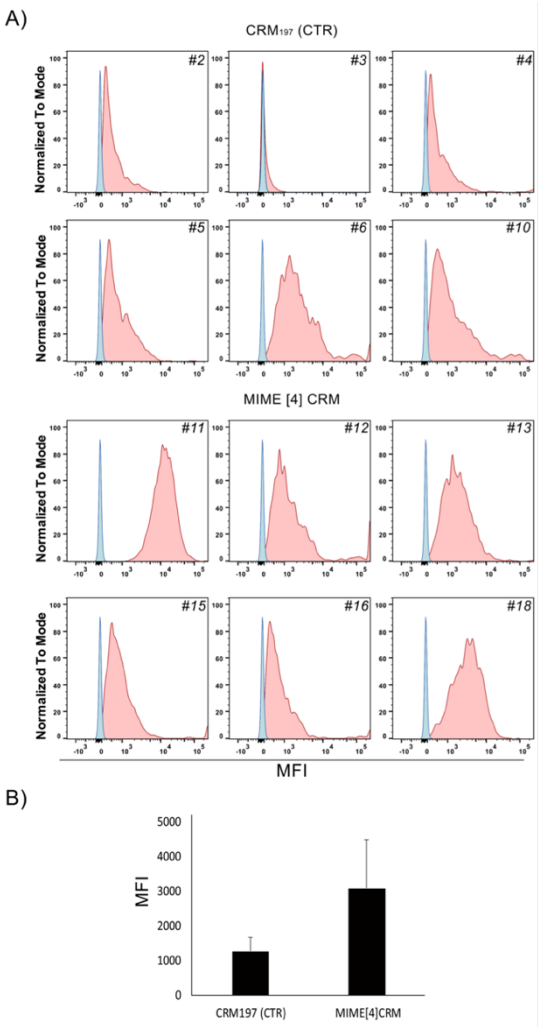

Figure S9. Binding of sera from immunized mice on the 4T1 BC cell line detected by FACS. A) FACS staining of sera from mice immunized with **mime[4]CRM** and from control mice immunized with CRM197 (red peak) compared to pre-immune sera (light blue peak) (representative data of 6 sera/group are shown in the Figure). In the X axis, binding of sera on the surface of 4T1 cells is expressed as Mean Fluorescence Unit (MFI). Mouse number is reported within each group. B) Average of MFI values of mice immunized with **mime[4]CRM** and control mice (CTR). Related to Figure 7.

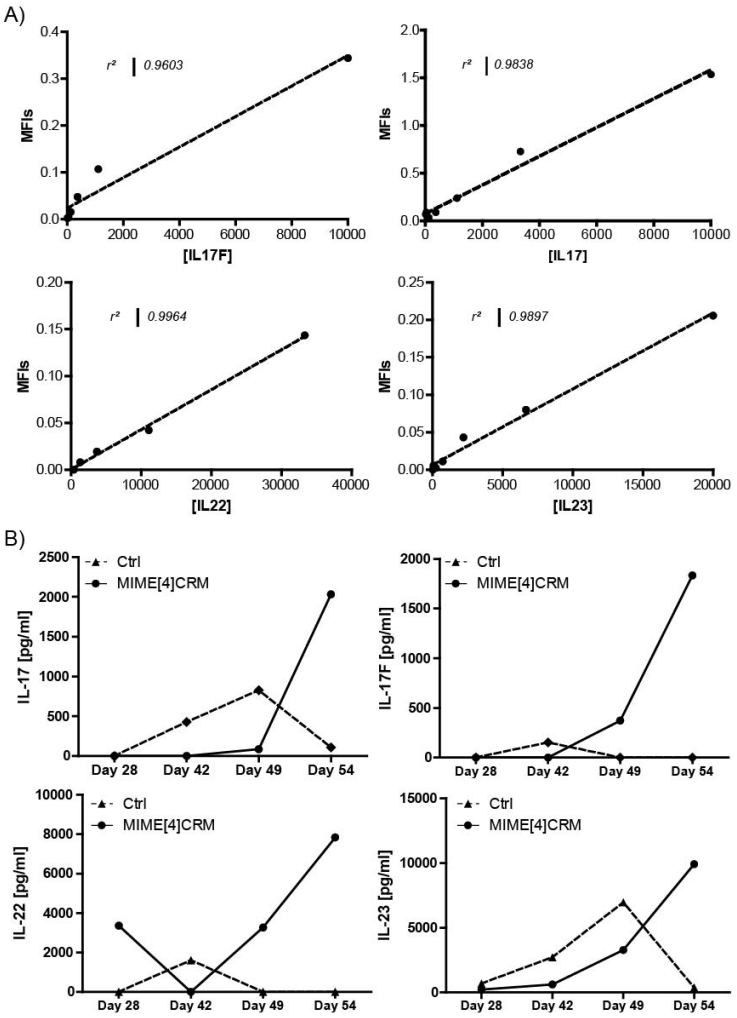

Figure S10. Quantification of serum cytokines showing a differential concentration in mice that developed or not metastasis after vaccination with **mime[4]CRM**. Th17 cytokines IL-17, IL-17F, IL-22, and IL-23, are higher in sera of **mime[4]CRM**-treated mice than in controls; serum concentrations of the other cytokines were barely detectable or were similar among the two groups. Related to Figure 8.

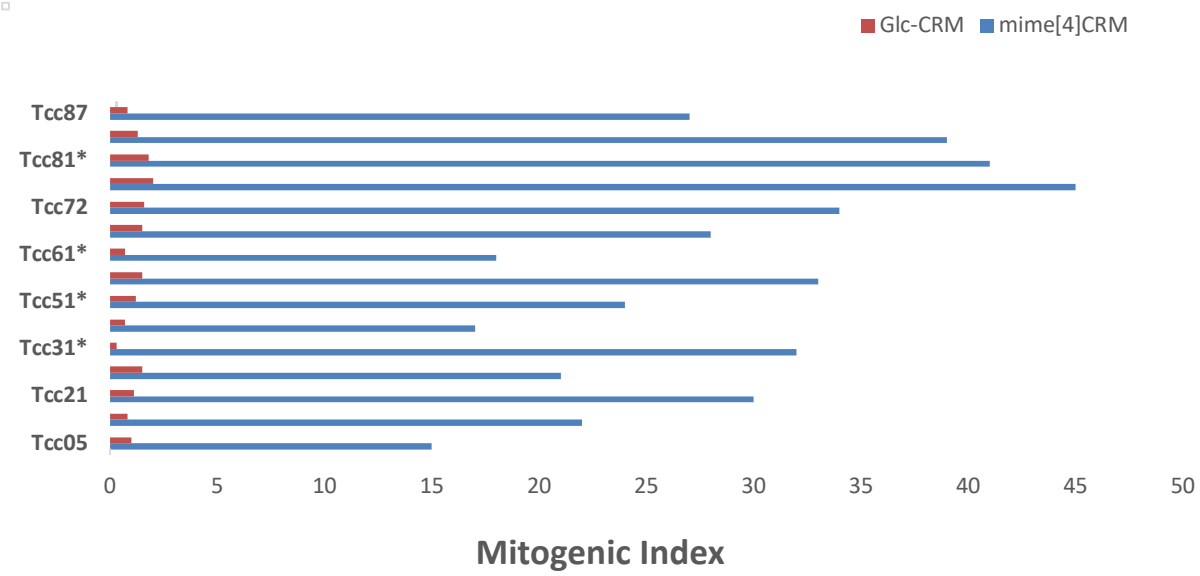

Figure S11. Correlation of mitogenic index (MI) of **mime[4]CRM**-specific T cells when stimulated with **mime[4]CRM** or **Glc-CRM**. Both $CD4^+$ and $CD8^+$ (those with asterisk) T cells clones (Tccs) showed an increased

MI when stimulated with **mime[4]CRM**, and very marginally with **Glc-CRM**, thereby displaying a specificity for the mimetic. Related to Figure 7.

Table S1. Bioluminescence analysis from *in vivo* mice trial showed in Figure 6.

Total Flux (P/S)										
	Controls (CRM)									
Mice number	**1**	**2**	**3**	**4**	**5**	**6**	**7**	**8**	**9**	**10**
T0	6,06E+05	1,91E+06	1,12E+06	4,90E+05	3,88E+06	4,86E+06	5,74E+06	3,46E+06	5,45E+06	3,03E+05
T7	9,74E+07	2,37E+09	1,02E+09	1,82E+09	7,95E+06	3,22E+09	3,23E+09	3,03E+09	3,71E+09	2,54E+09
T14	1,32E+09	4,47E+09	6,98E+09	2,46E+10	5,35E+09	7,35E+09	2,79E+09	1,07E+10	1,18E+10	5,05E+09
T28	1,64E+09	1,79E+09	1,43E+10	1,51E+10	2,37E+10	2,43E+10	1,62E+10	1,30E+10	4,41E+10	6,03E+09

Treatments (mime[4]CRM)								
11	**12**	**13**	**14**	**15**	**16**	**17**	**18**	19
9,39E+05	8,43E+04	7,67E+06	1,02E+06	2,96E+06	2,69E+06	4,05E+05	1,89E+06	1,00E+06
8,48E+07	3,47E+08	4,80E+09	2,54E+09	2,99E+09	1,69E+09	6,91E+06	6,43E+08	1,76E+09
4,17E+09	2,10E+09	2,11E+09	2,18E+09	1,01E+09	3,46E+09	8,50E+08	0,00E+00	3,34E+09
7,39E+09	4,69E+09	2,32E+09	1,51E+10	1,74E+08	6,43E+09	1,62E+10	0,00E+00	1,54E+10

Table S2. Count data of the immunofluorescence staining presented in Figure 7.

	DAPI	TCR/CD4	DAPI	CD11c/CD4	DAPI	PD1/CD4	DAPI	FOXP3/CD4	DAPI	CD163/CD68	DAPI	CD163/F480
CRM #1	280	40	152	26	200	45	174	92	255	66	214	50
CRM #2	213	52	179	33	198	42	240	60	303	53	130	40
CRM #3	170	58	172	13	120	31	165	80	202	61	230	57
Total Number	663	150	503	72	518	118	579	232	760	180	574	147
mime[4]CRM #1	220	115	126	30	160	30	290	10	352	3	209	30
mime[4]CRM #2	199	130	148	39	165	20	300	12	304	5	220	13
mime[4]CRM #3	177	75	163	40	170	30	260	12	380	8	190	13
Total Number	596	320	437	109	495	80	850	34	1036	16	619	56

Supplemental Data

Data S1. Related to Scheme 1. ^{1}H, ^{13}C, 2D NMR and ESI-MS spectra of compound **2**.

^{1}H at 500 MHz in CD_3OD - 25 deg

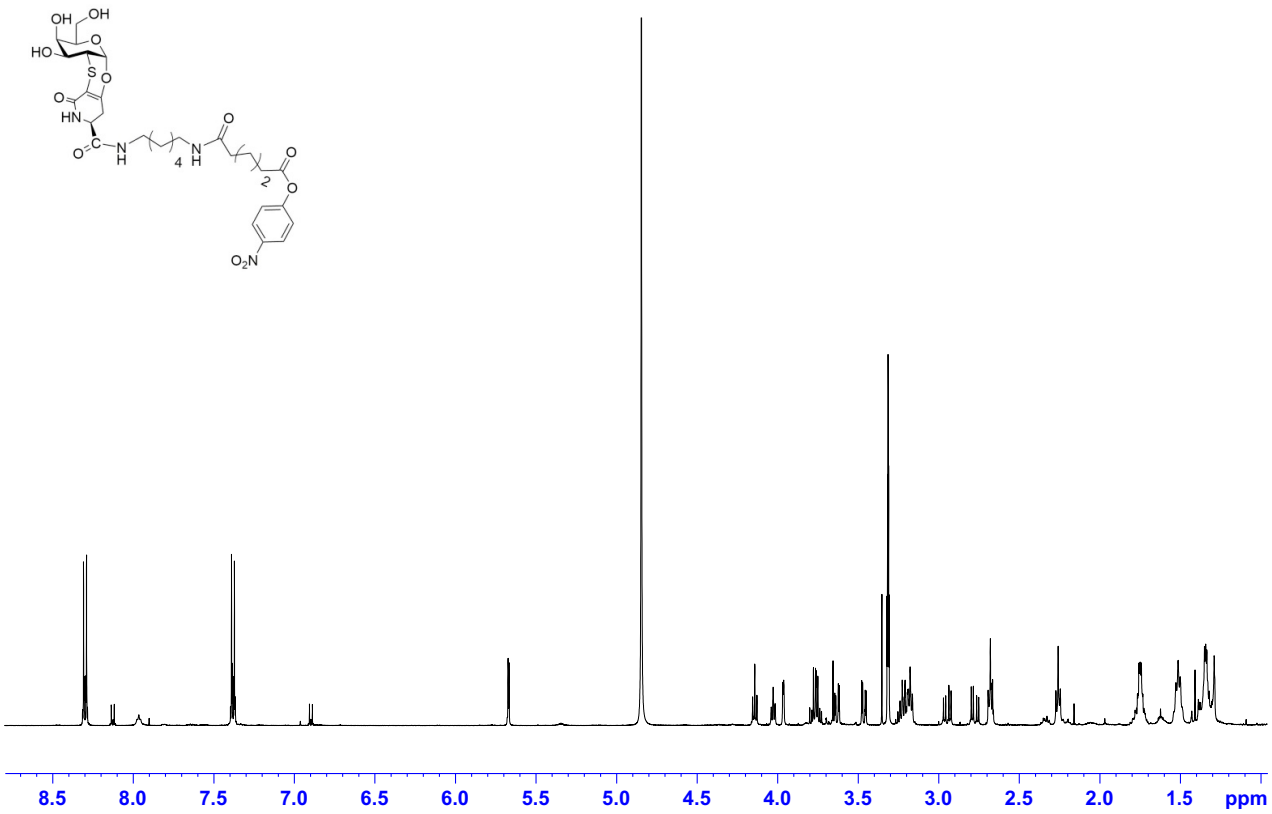

^{13}C at 125 MHz in CD_3OD - 25 deg

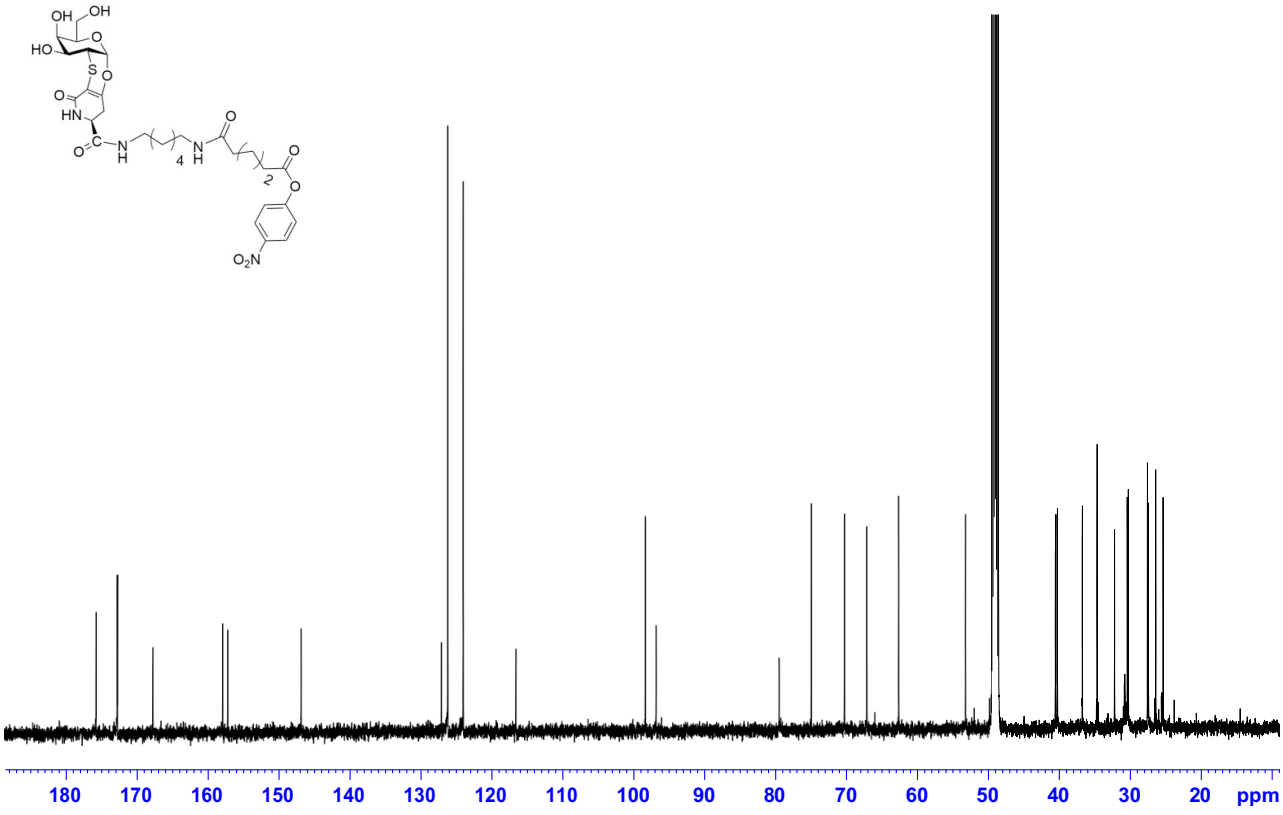

HSQC at 500 MHz in CD_3OD - 25 deg

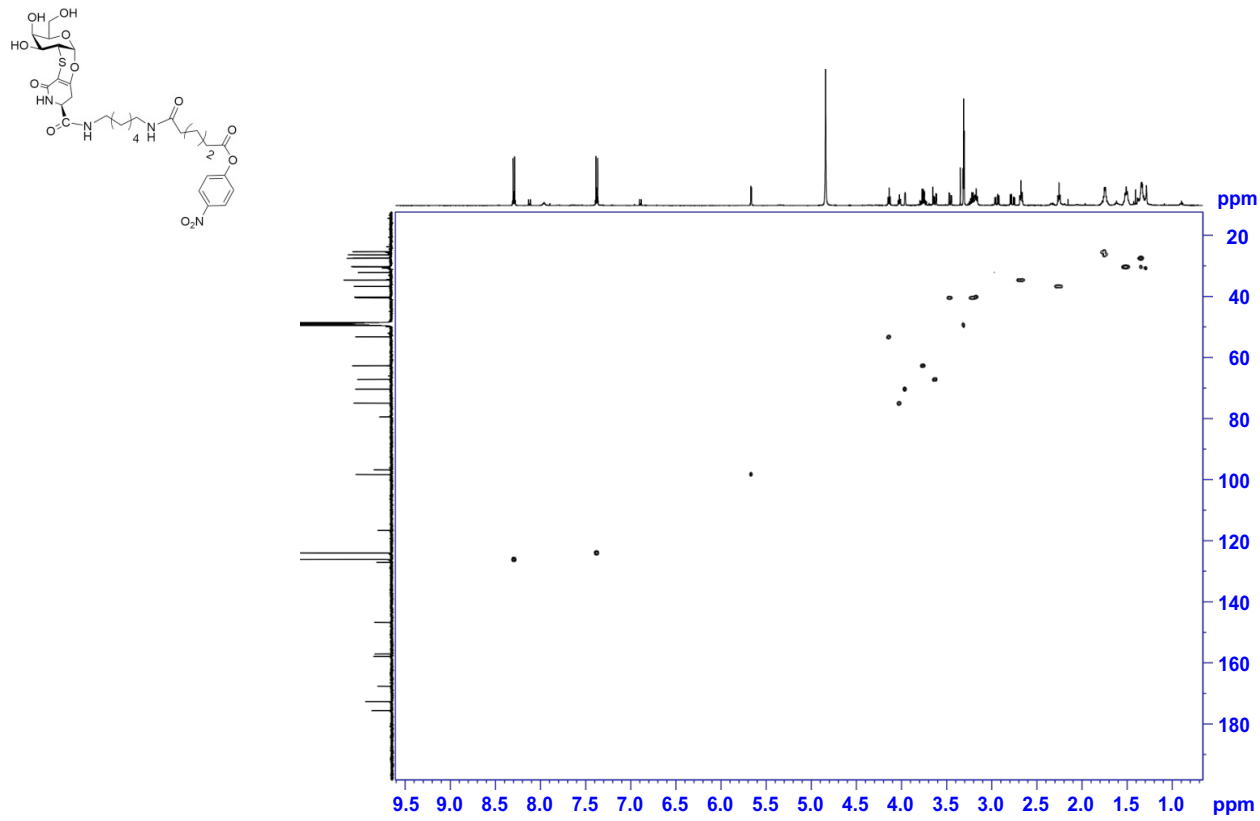

COSY at 500 MHz in CD_3OD - 25 deg

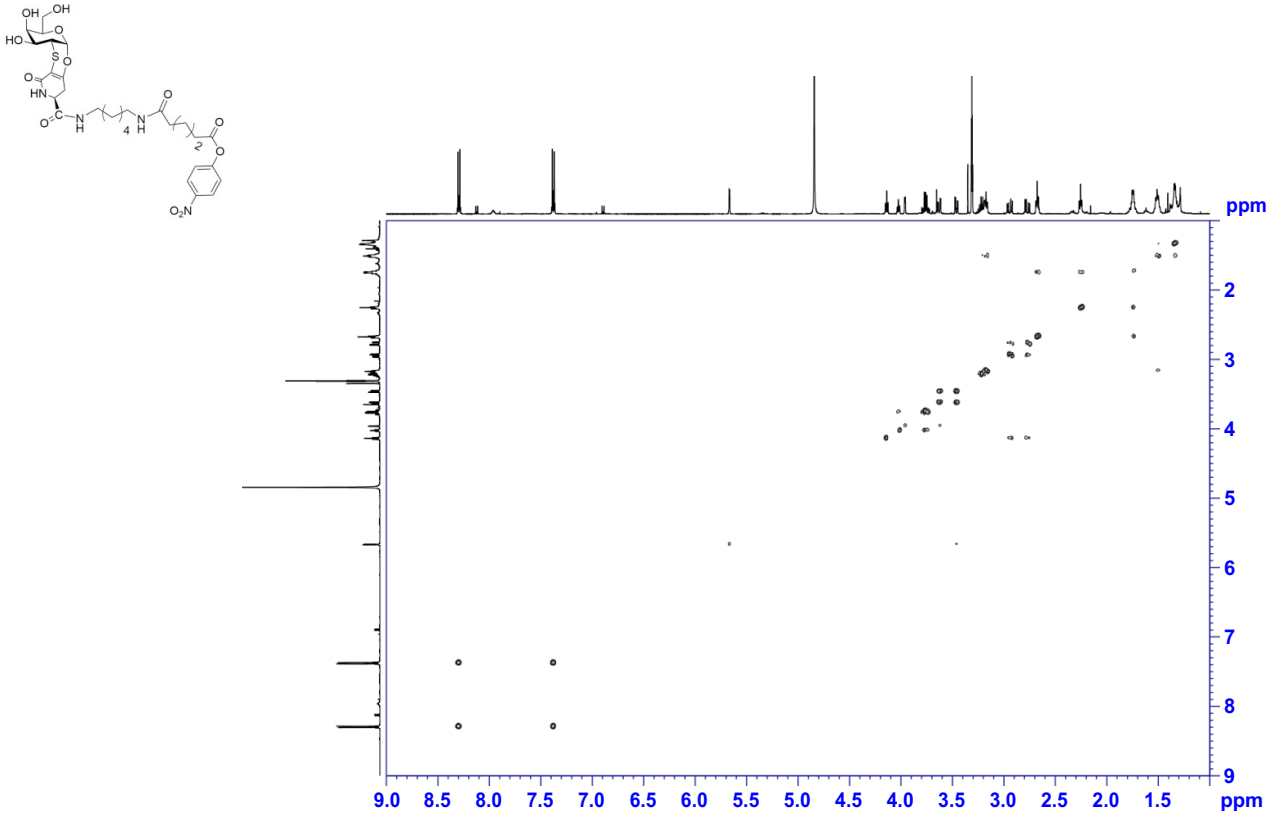

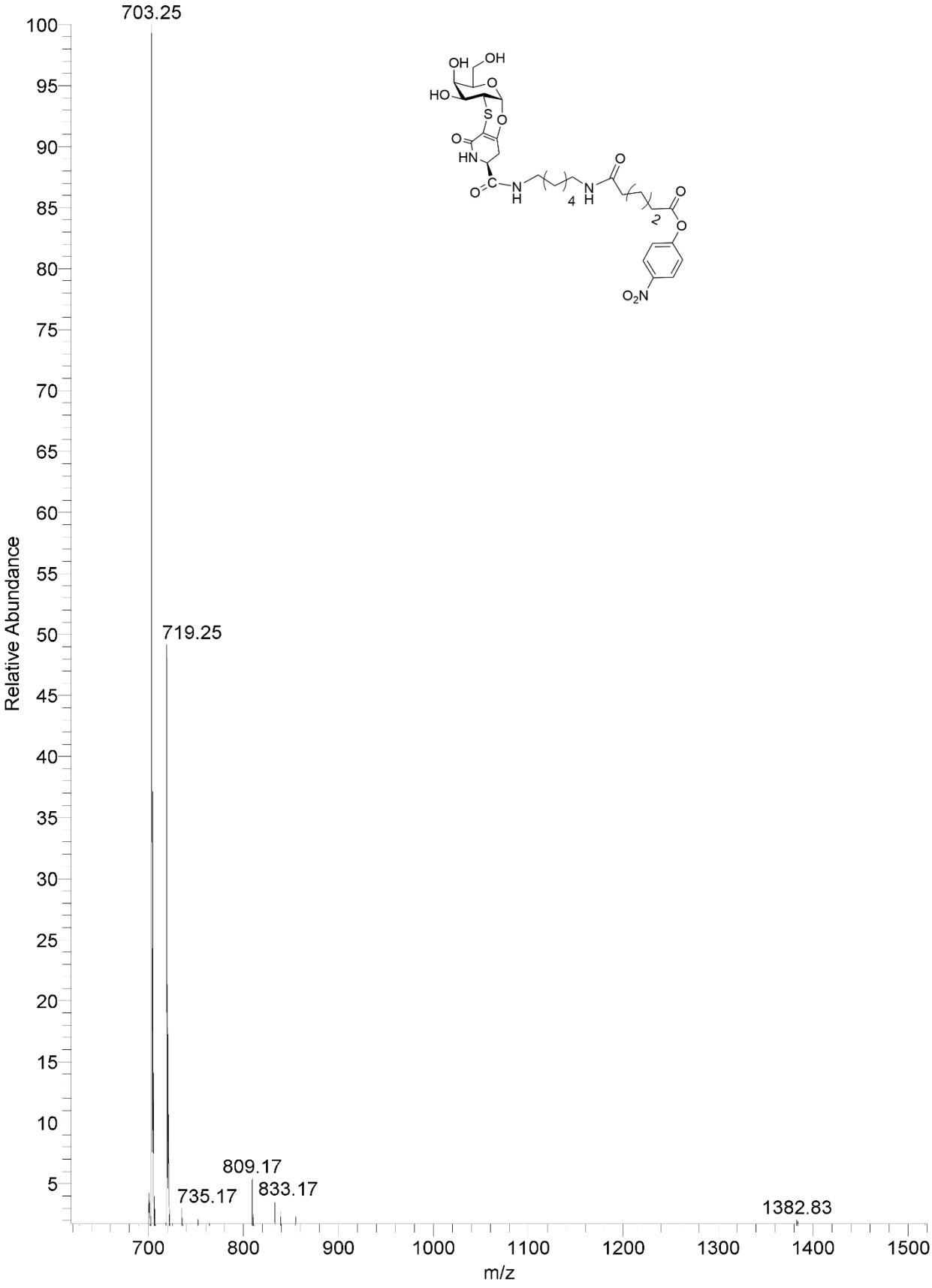
703.25
719.25
809.17
833.17
735.17
1382.83
Relative Abundance
m/z
100
95
90
85
80
75
70
65
60
55
50
45
40
35
30
25
20
15
10
5
700
800
900
1000
1100
1200
1300
1400
1500
OH
OH
HO
O
S
O
O
HN
O
C
N
H
4
N
H
O
2
O
O
O_2N

Data S2. Related to Scheme 1. ^{1}H, ^{13}C, 2D NMR and ESI-MS spectra of compound **3**.

^{1}H at 500 MHz in CD_3OD - 25 deg

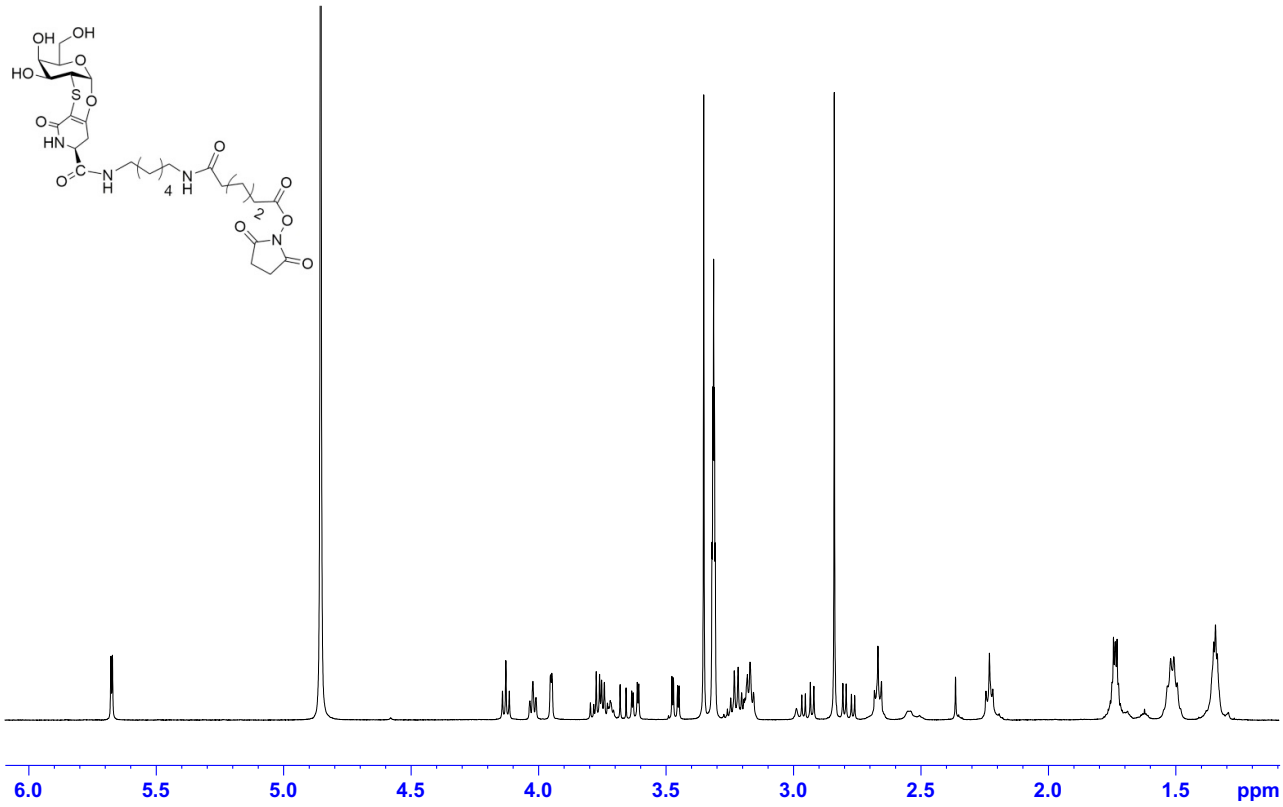

^{13}C at 125 MHz in CD_3OD - 25 deg

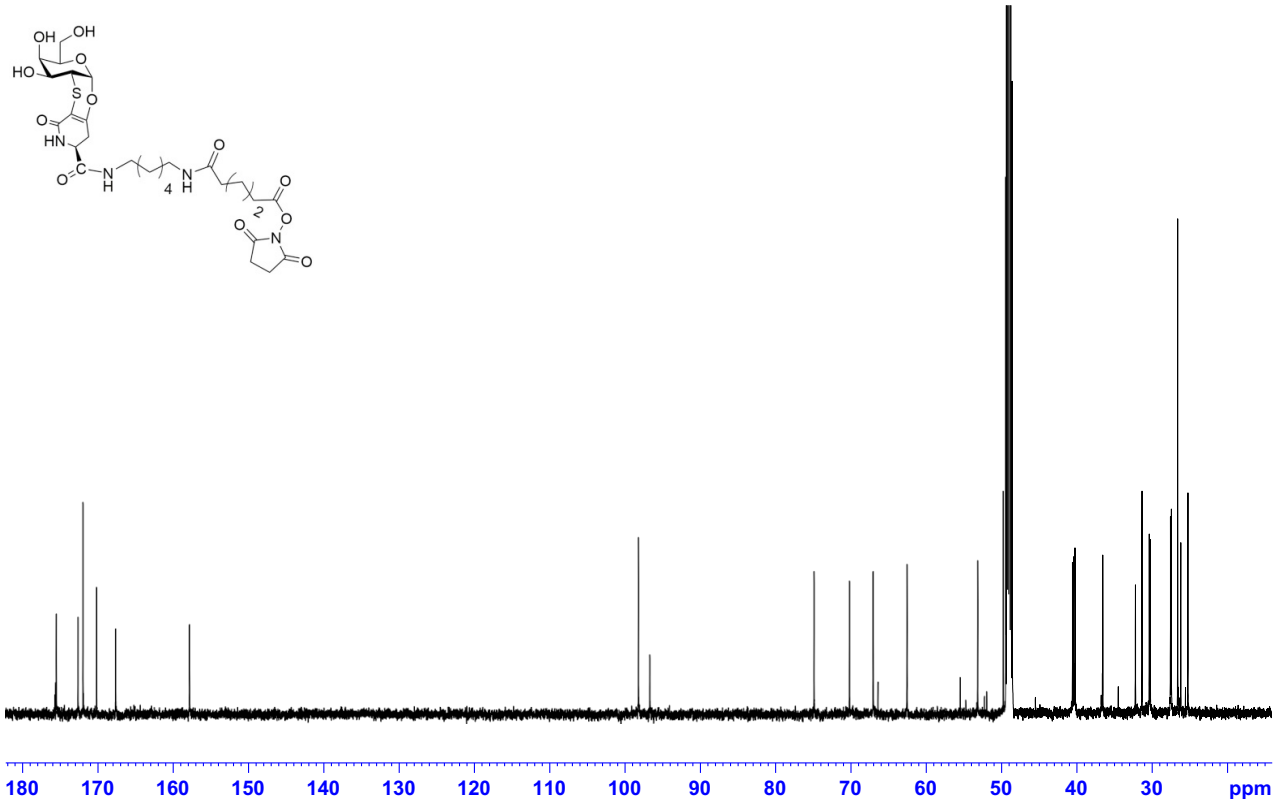

HSQC at 500 MHz in CD_3OD - 25 deg

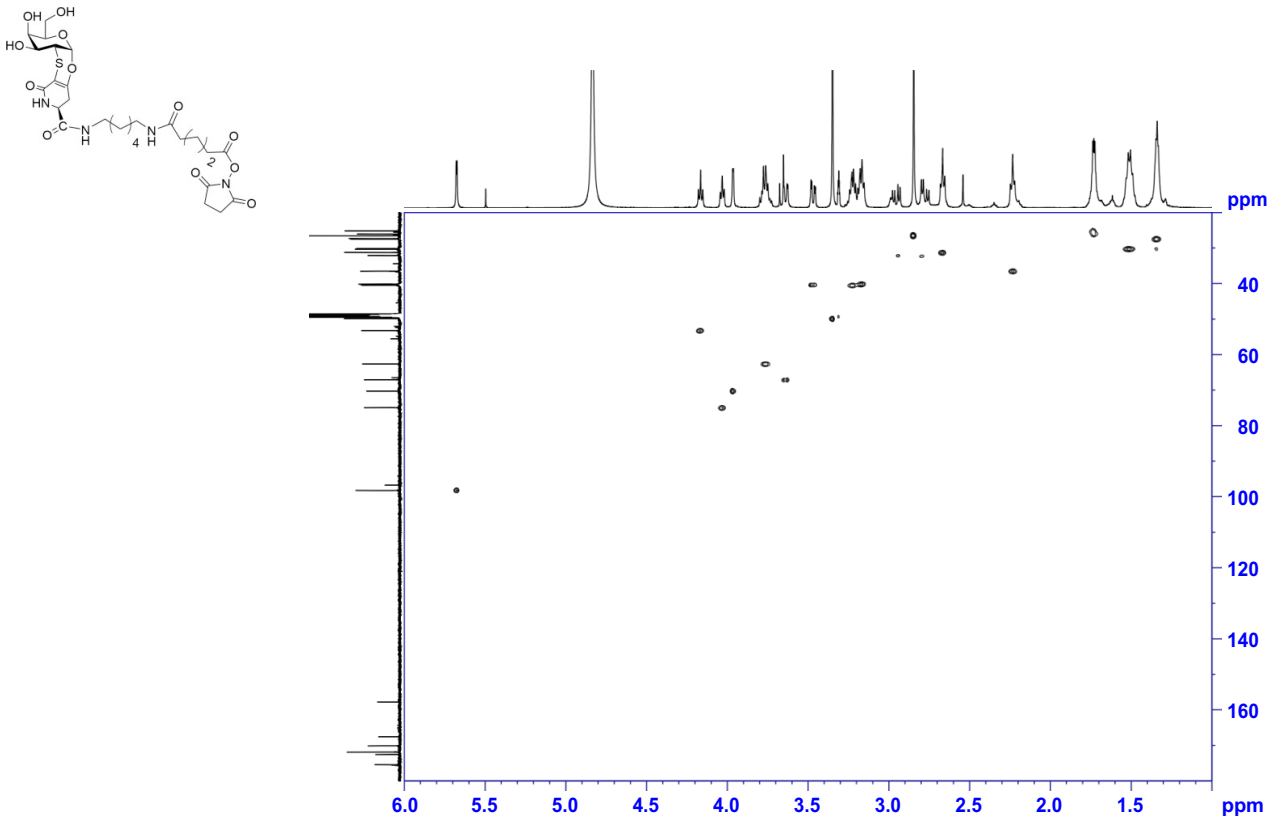

COSY at 500 MHz in CD_3OD - 25 deg

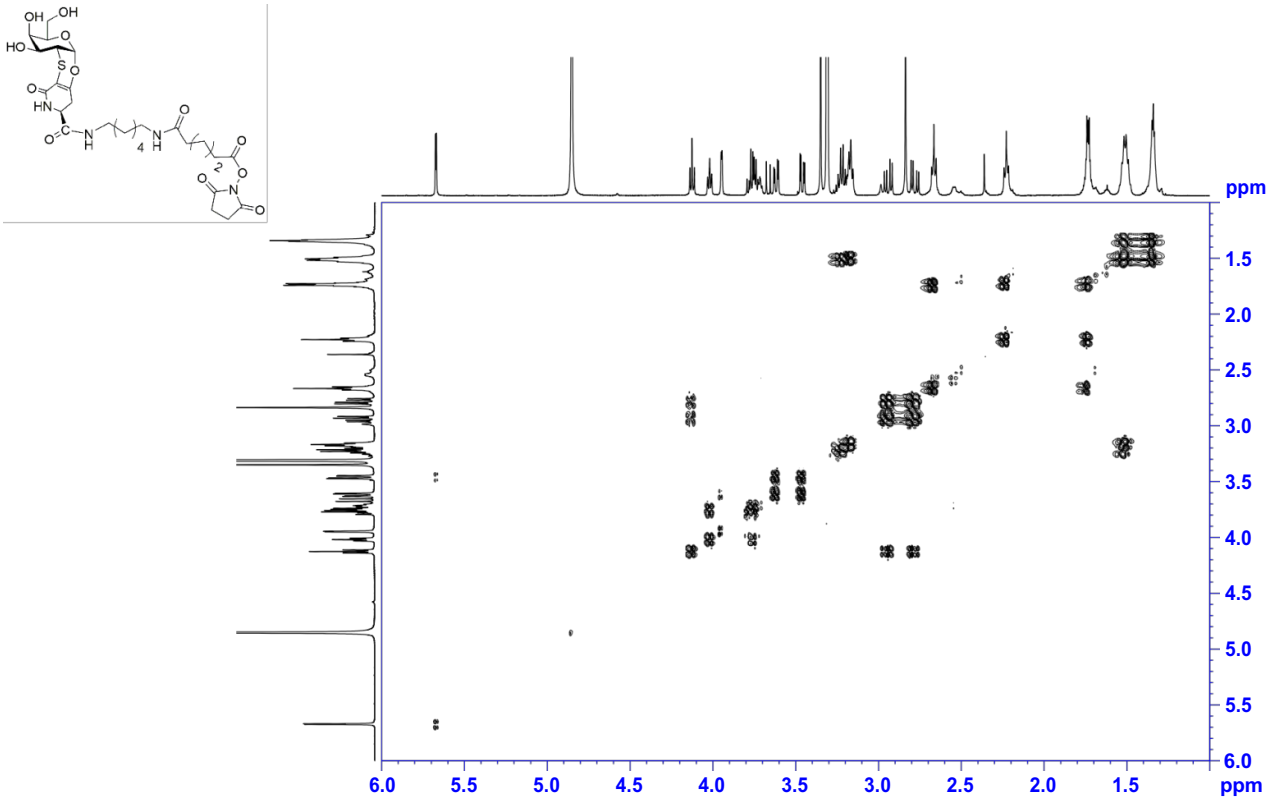

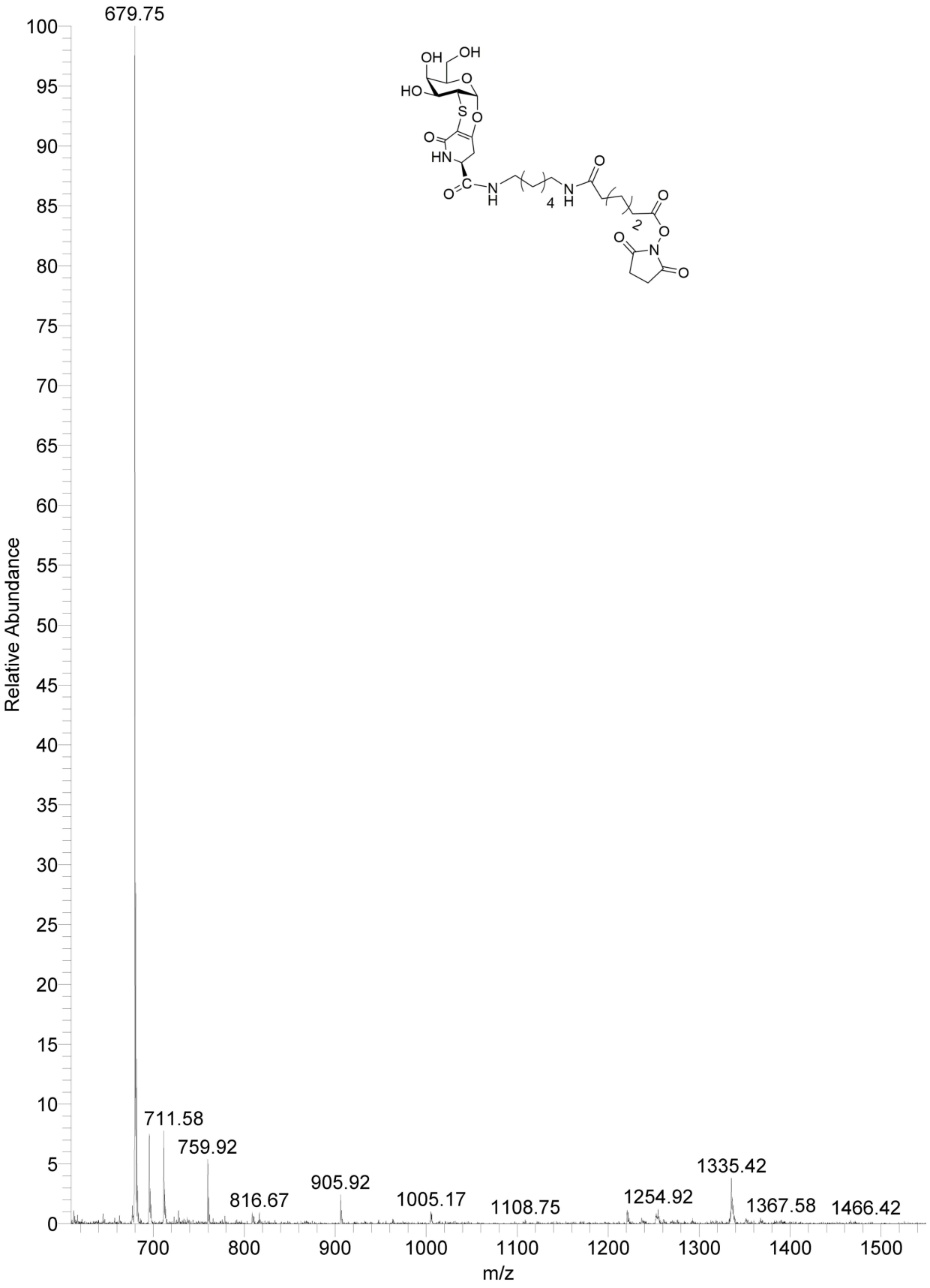
679.75
711.58
759.92
816.67
905.92
1005.17
1108.75
1254.92
1335.42
1367.58
1466.42
Relative Abundance
m/z
100
95
90
85
80
75
70
65
60
55
50
45
40
35
30
25
20
15
10
5
0
700
800
900
1000
1100
1200
1300
1400
1500
OH
OH
HO
O
S
O
O
HN
O
C
N
H
4
N
H
O
2
O
O
N
O
O

Data S3. Related to Scheme 1. ^{1}H, ^{13}C, 2D NMR and ESI-MS spectra of compound **5**.

^{1}H at 500 MHz in $CDCl_3$ - 25 deg

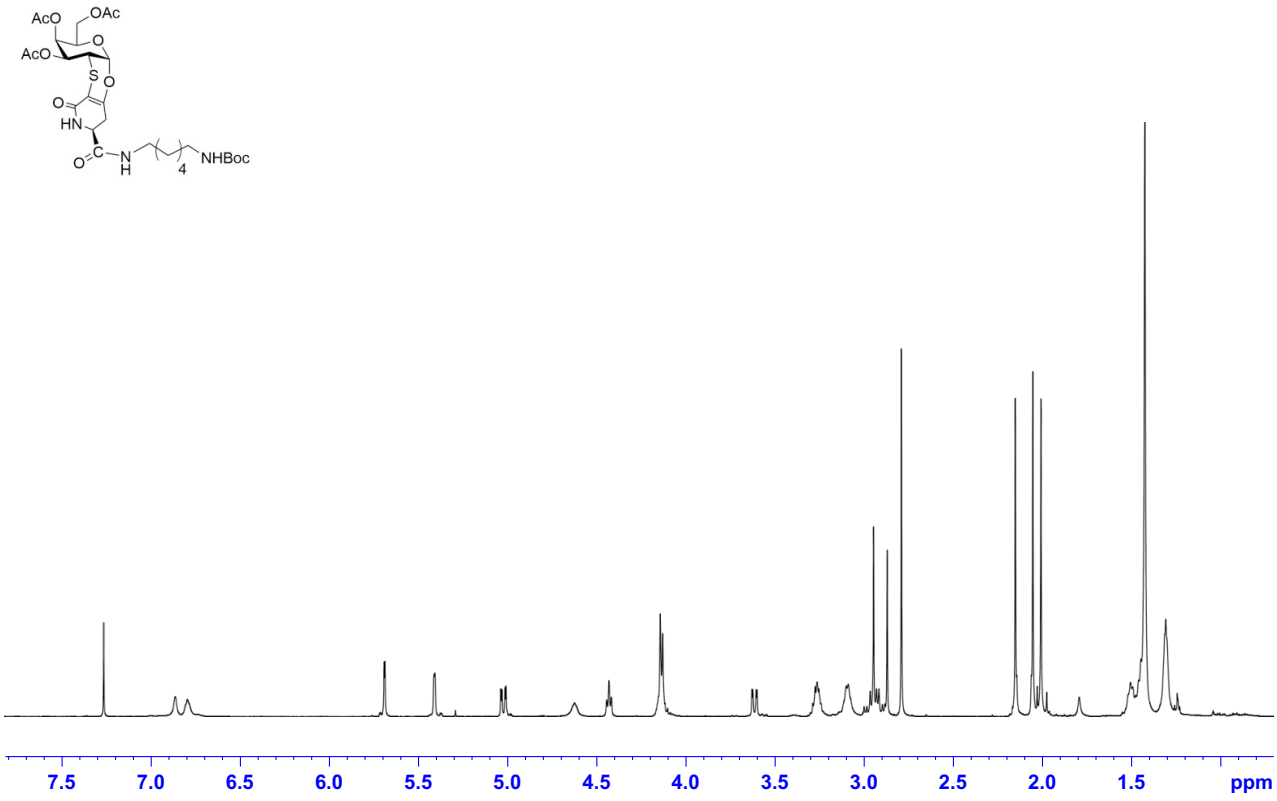

^{13}C at 125 MHz in $CDCl_3$ - 25 deg

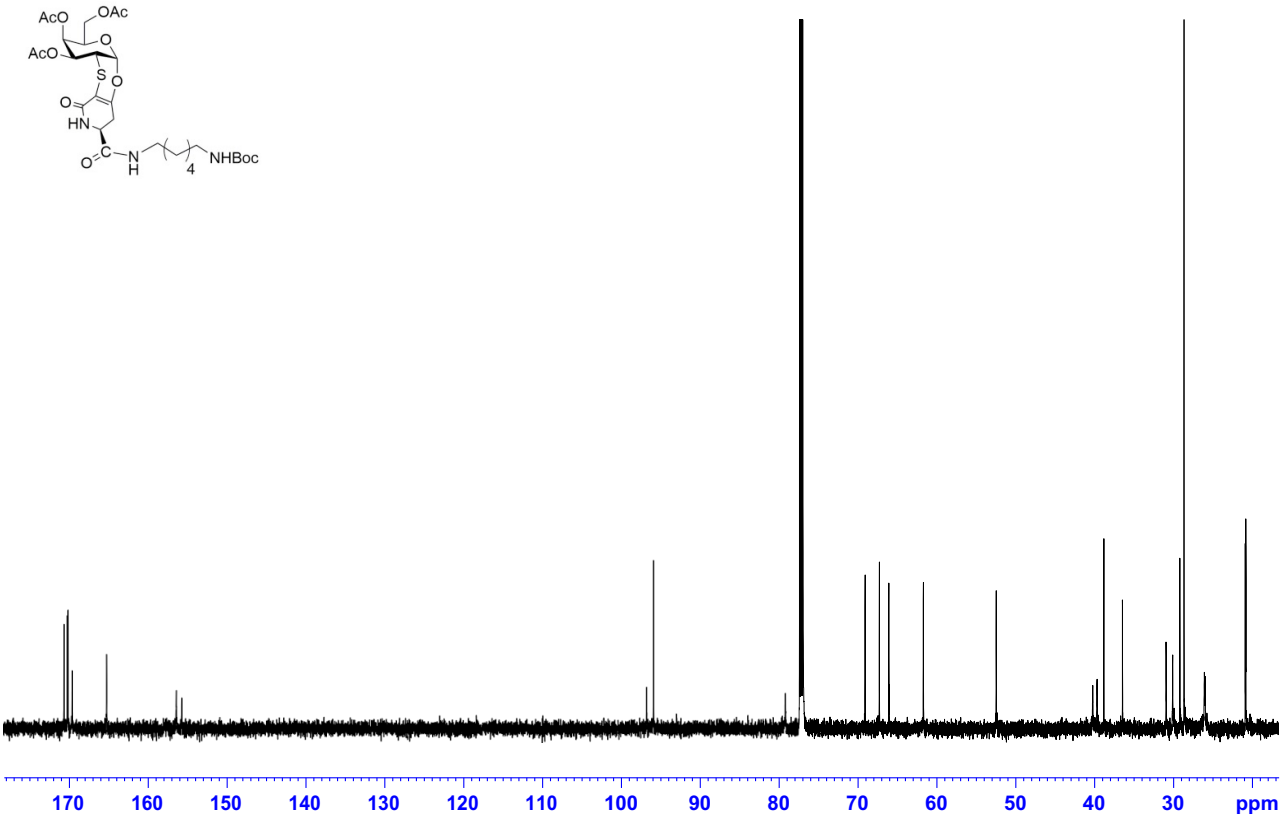

HSQC at 500 MHz in $CDCl_3$ - 25 deg

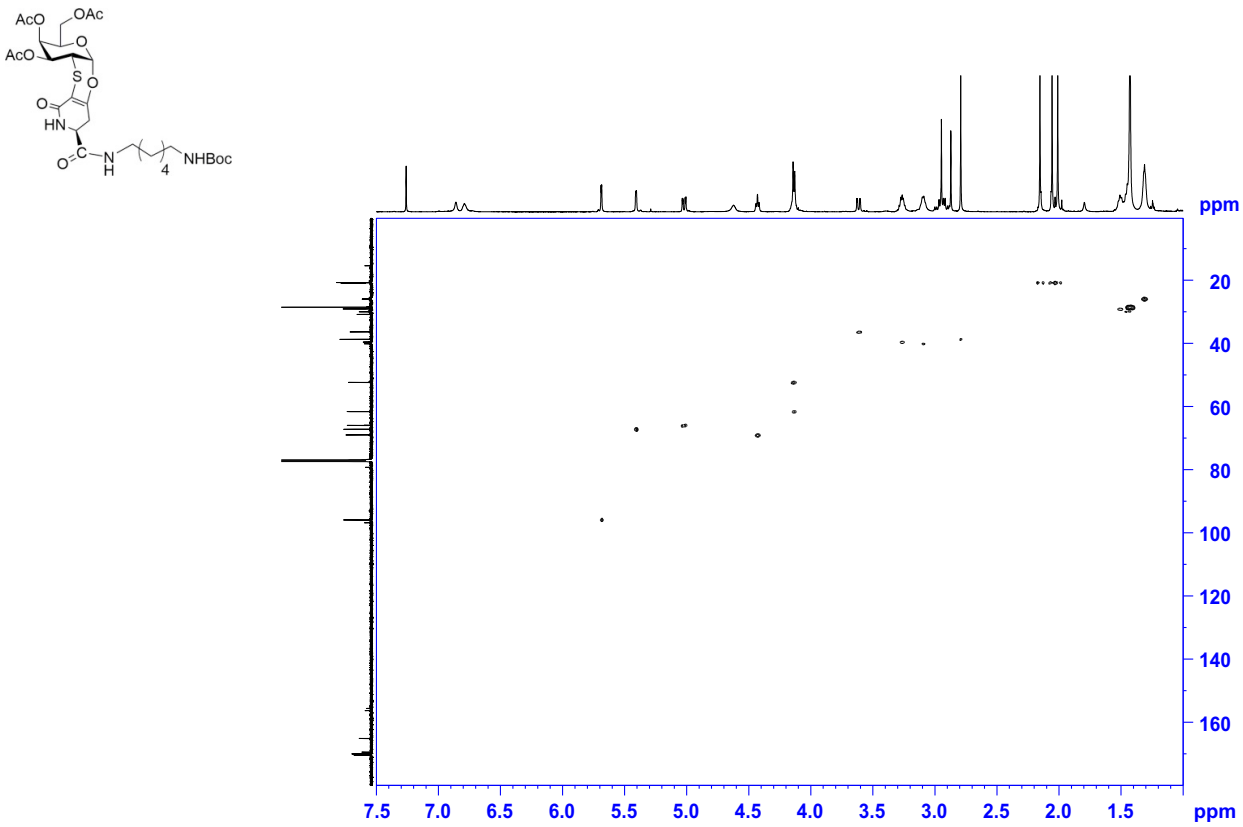

COSY at 500 MHz in $CDCl_3$ - 25 deg

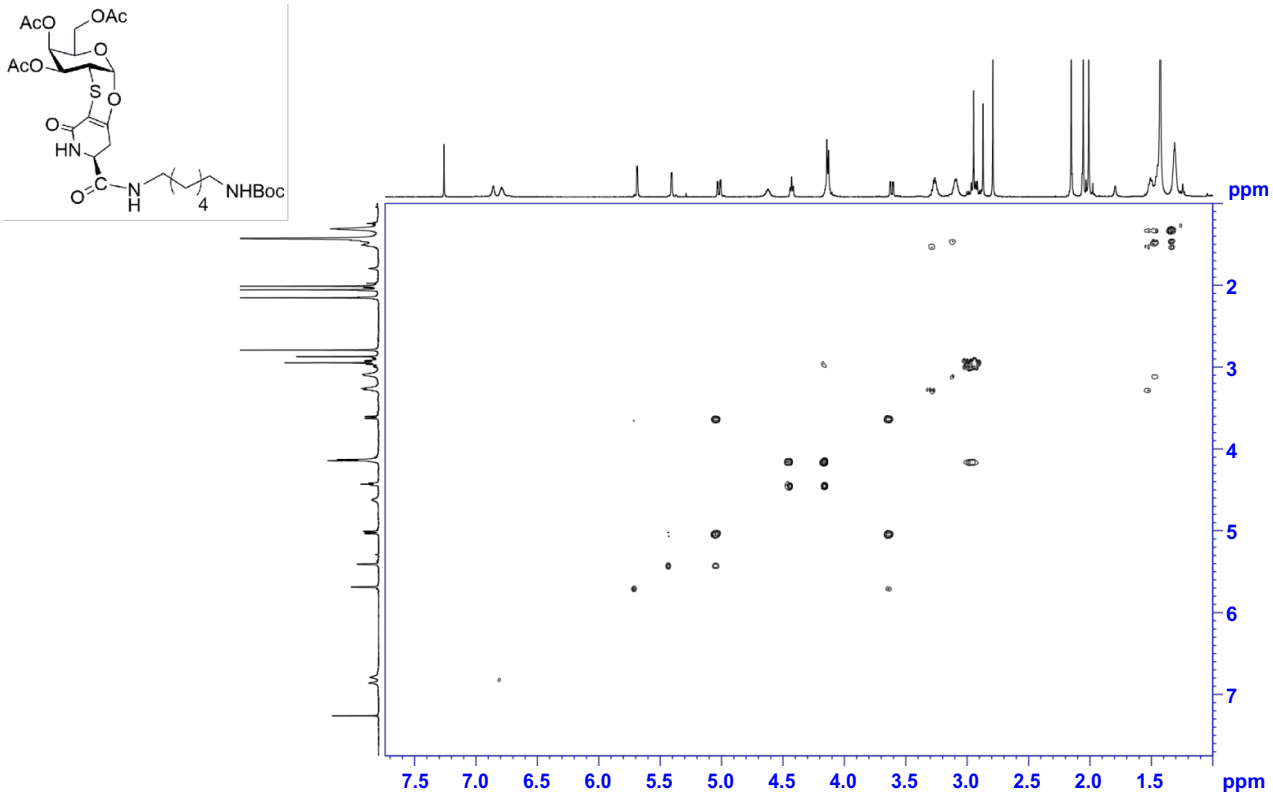

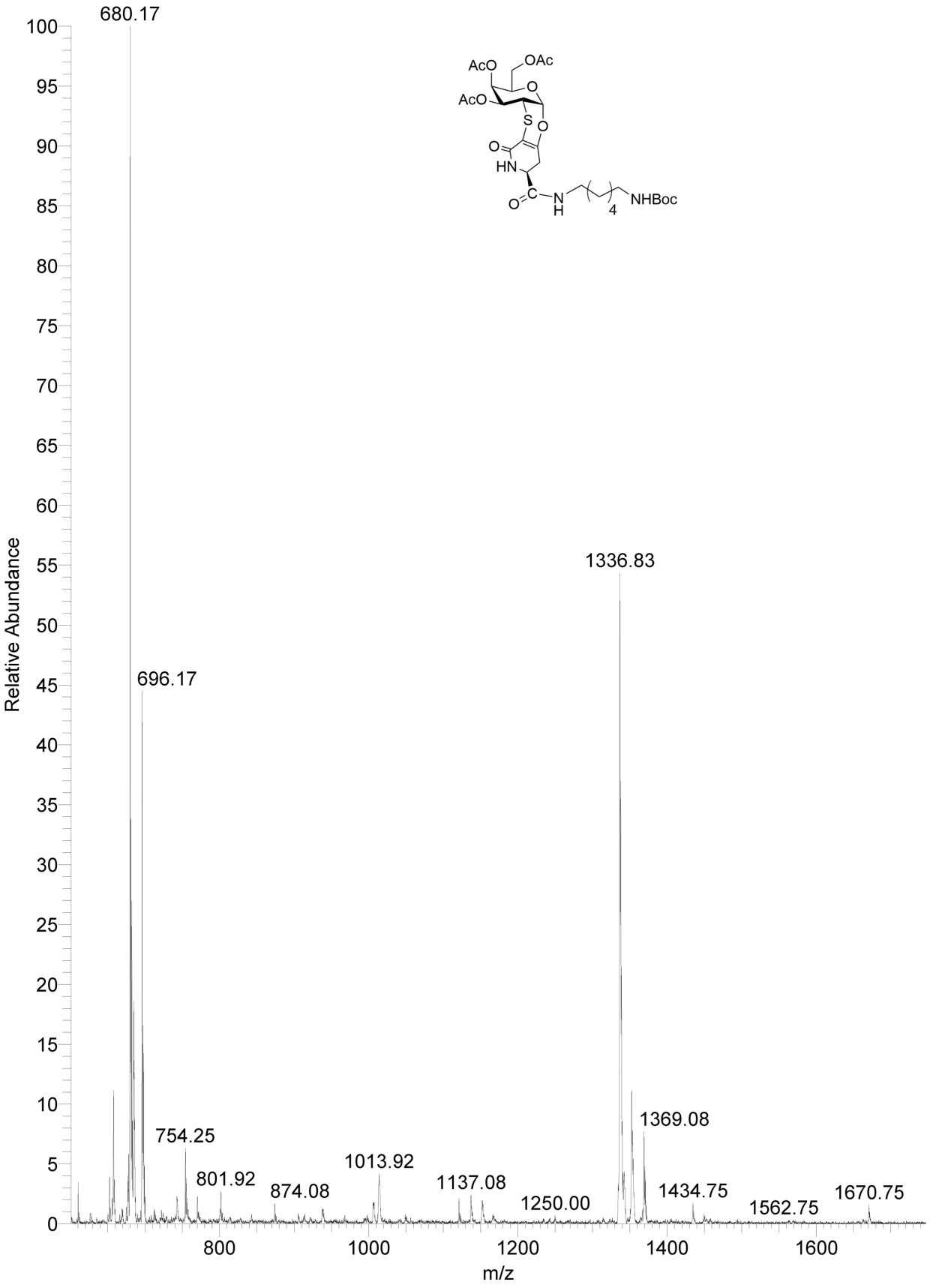
680.17
696.17
754.25
801.92
874.08
1013.92
1137.08
1250.00
1336.83
1369.08
1434.75
1562.75
1670.75
Relative Abundance
m/z
AcO
OAc
AcO
O
S
O
O
HN
O
C
N
H
4
NHBoc

Data S4. Related to Scheme 1. ^{1}H, ^{13}C, 2D NMR and ESI-MS spectra of compound **6**.

^{1}H at 500 MHz in CD_3OD - 25 deg

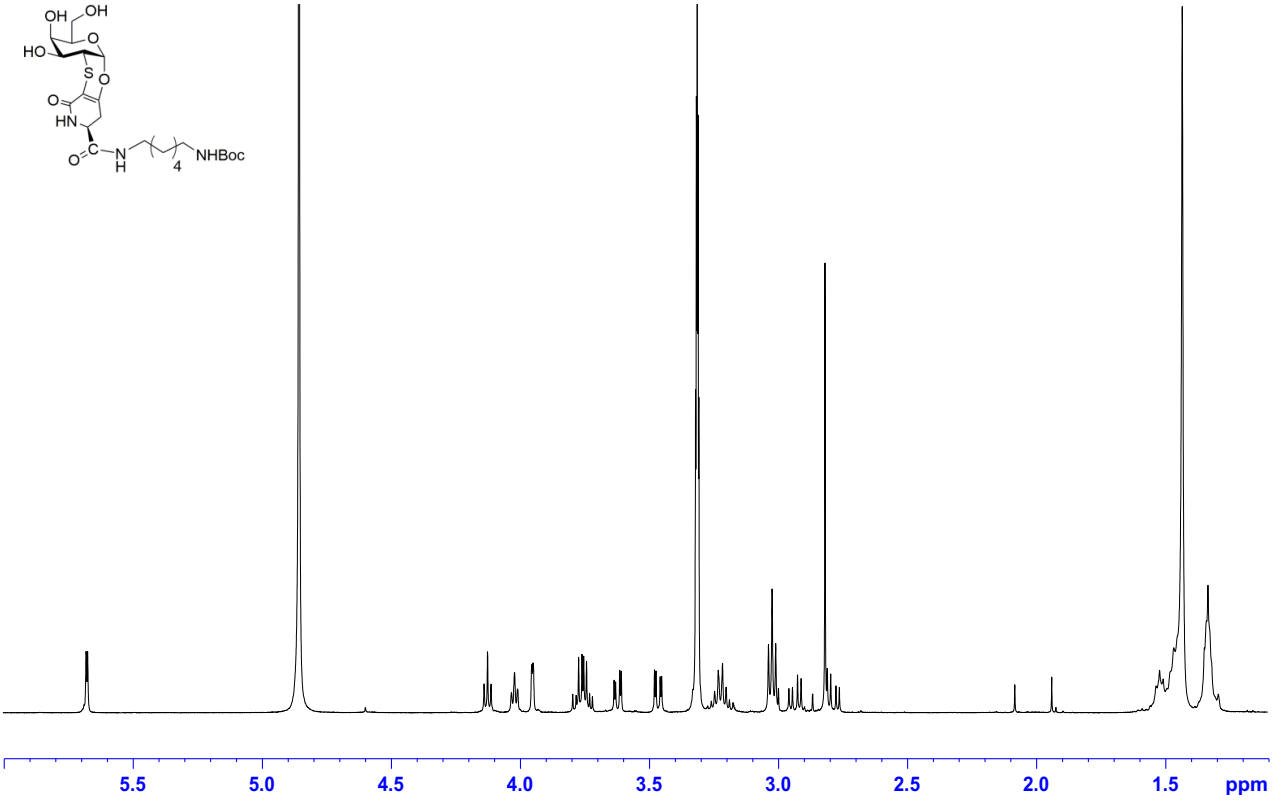

^{13}C at 125 MHz in CD_3OD - 25 deg

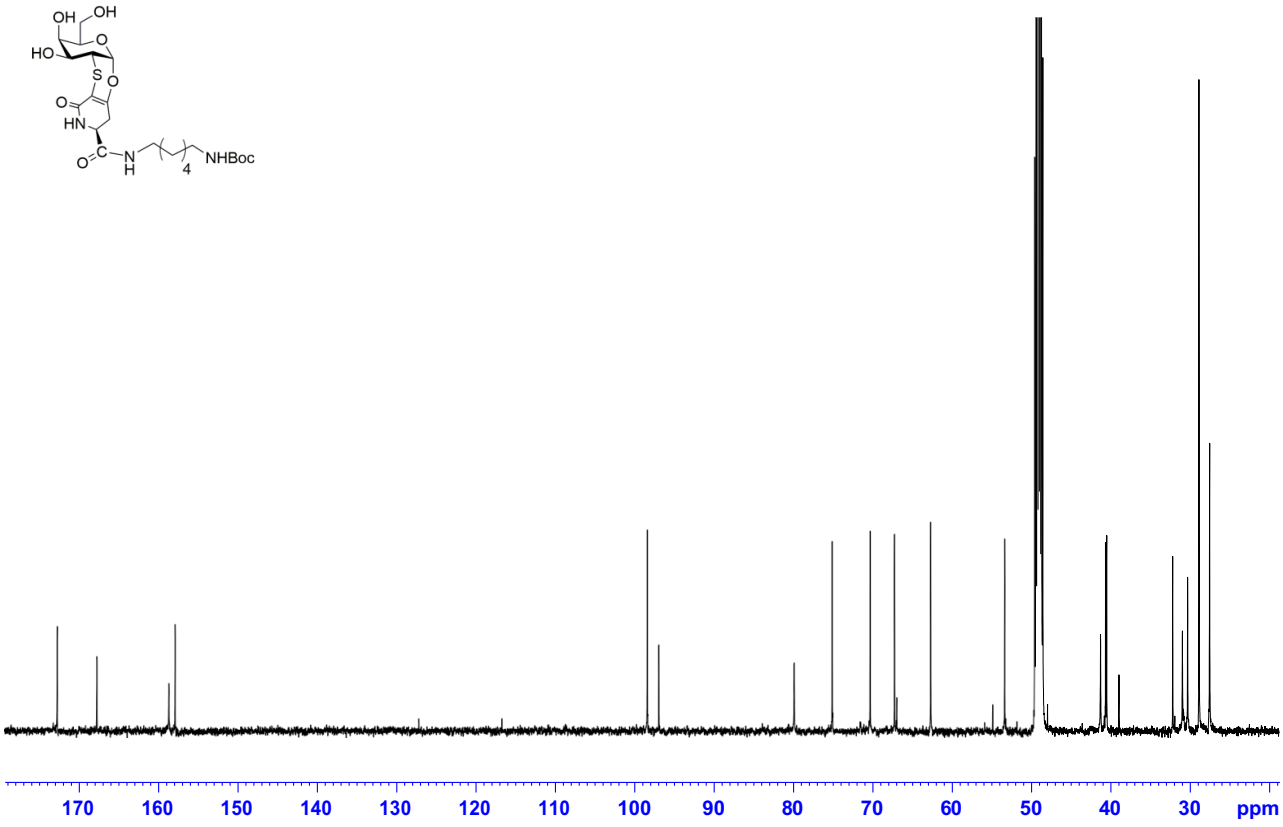

HSQC at 500 MHz in CD_3OD - 25 deg

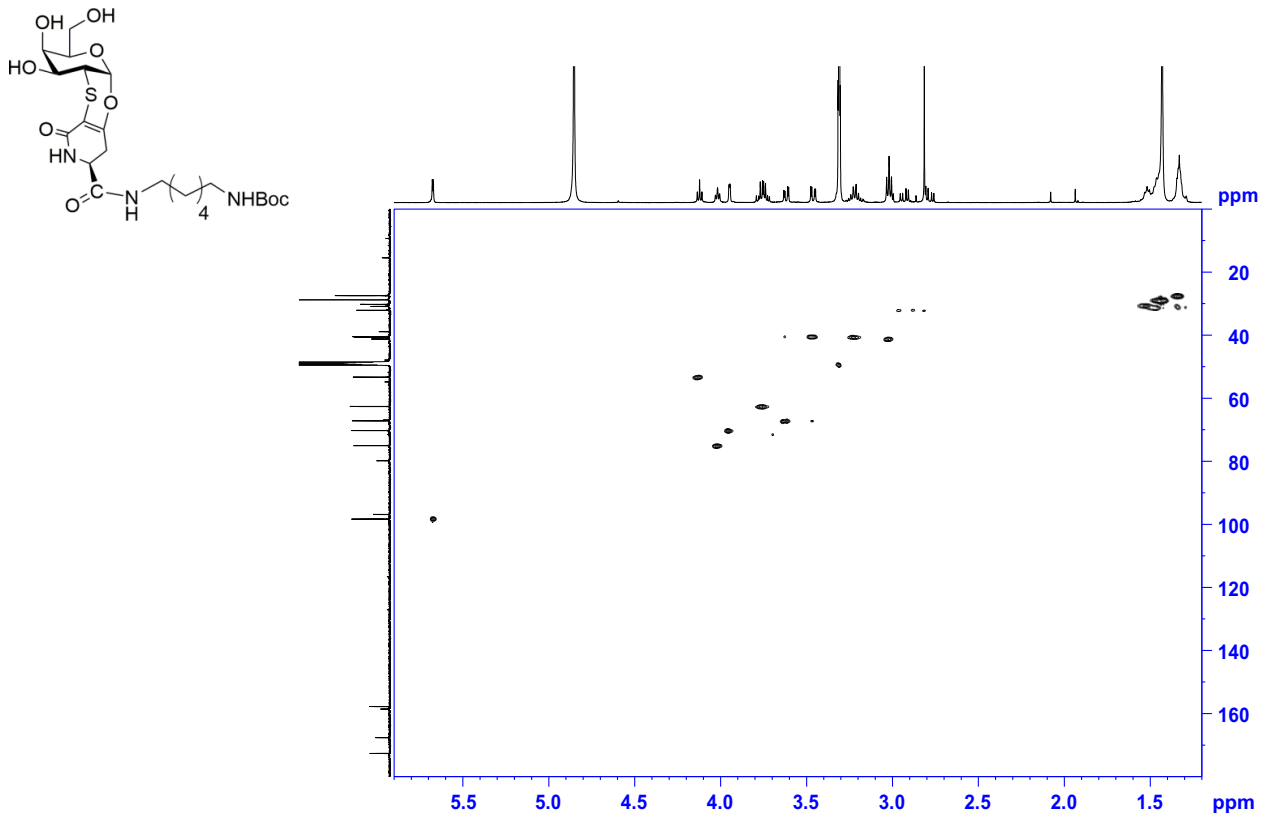

COSY at 500 MHz in CD_3OD - 25 deg

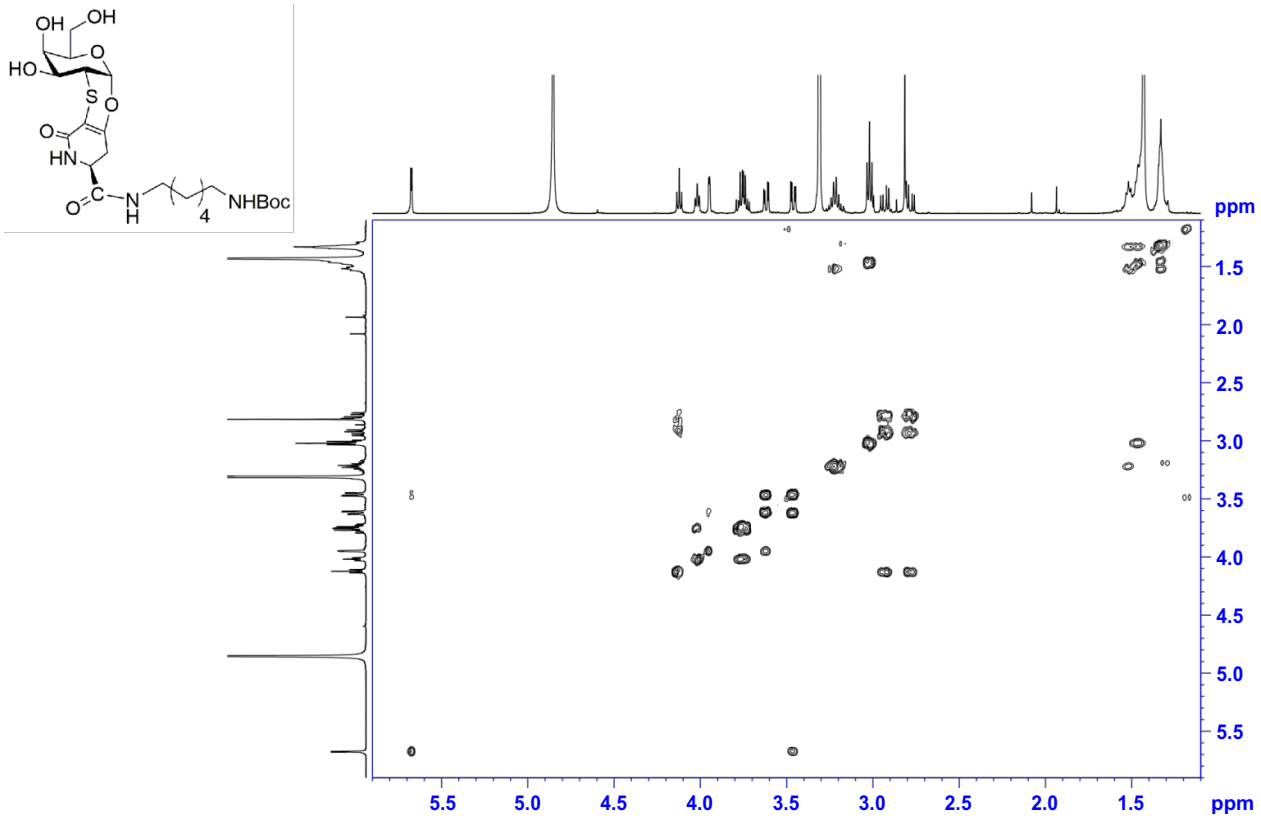

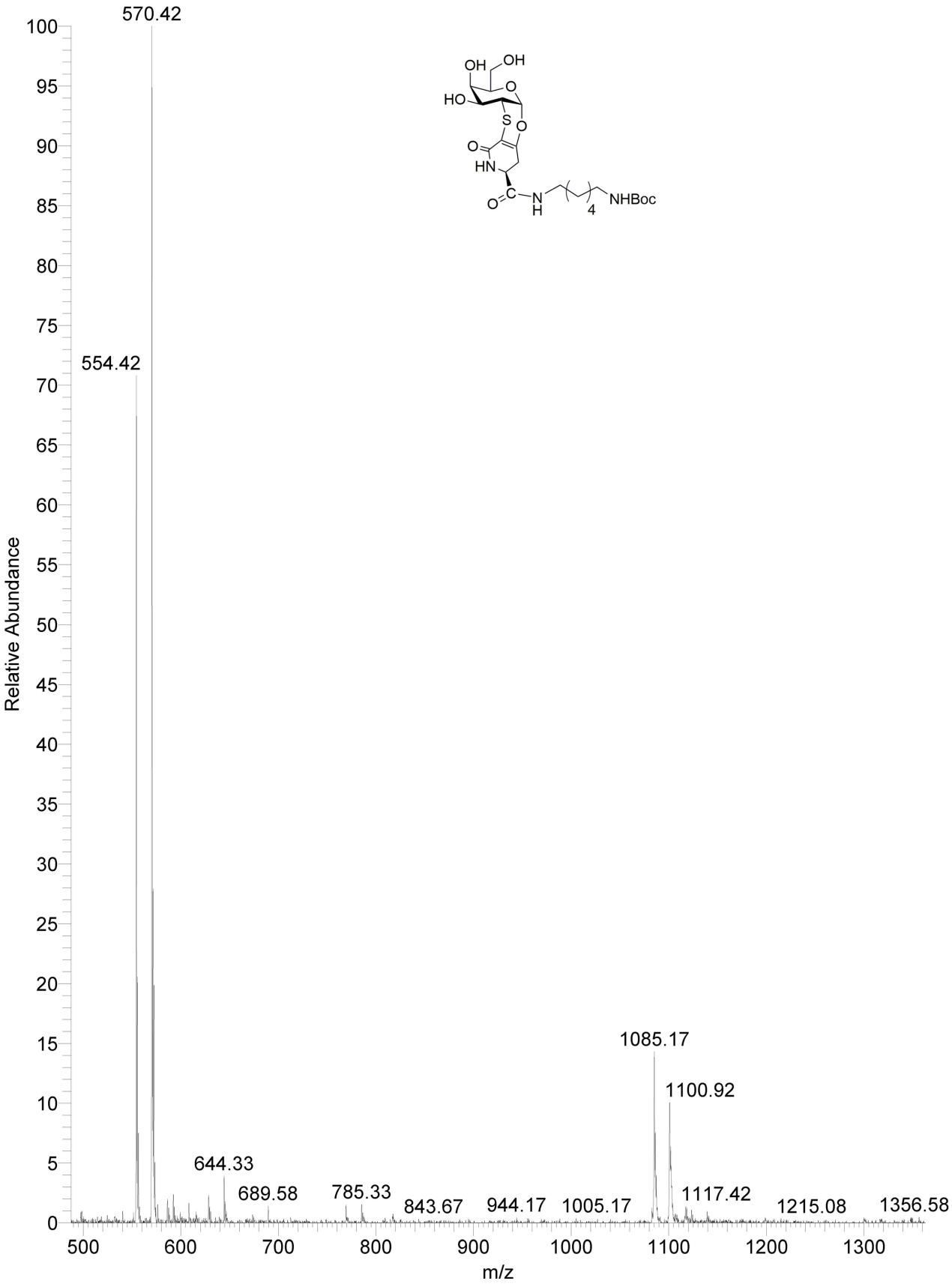
570.42
554.42
644.33
689.58
785.33
843.67
944.17
1005.17
1085.17
1100.92
1117.42
1215.08
1356.58
Relative Abundance
m/z
OH
OH
HO
O
S
O
O
HN
C
O
N
H
4
NHBoc

Data S5. Related to Scheme 1. ^{1}H NMR spectrum of compound **7**.

^{1}H at 500 MHz in CD_3OD - 25 deg

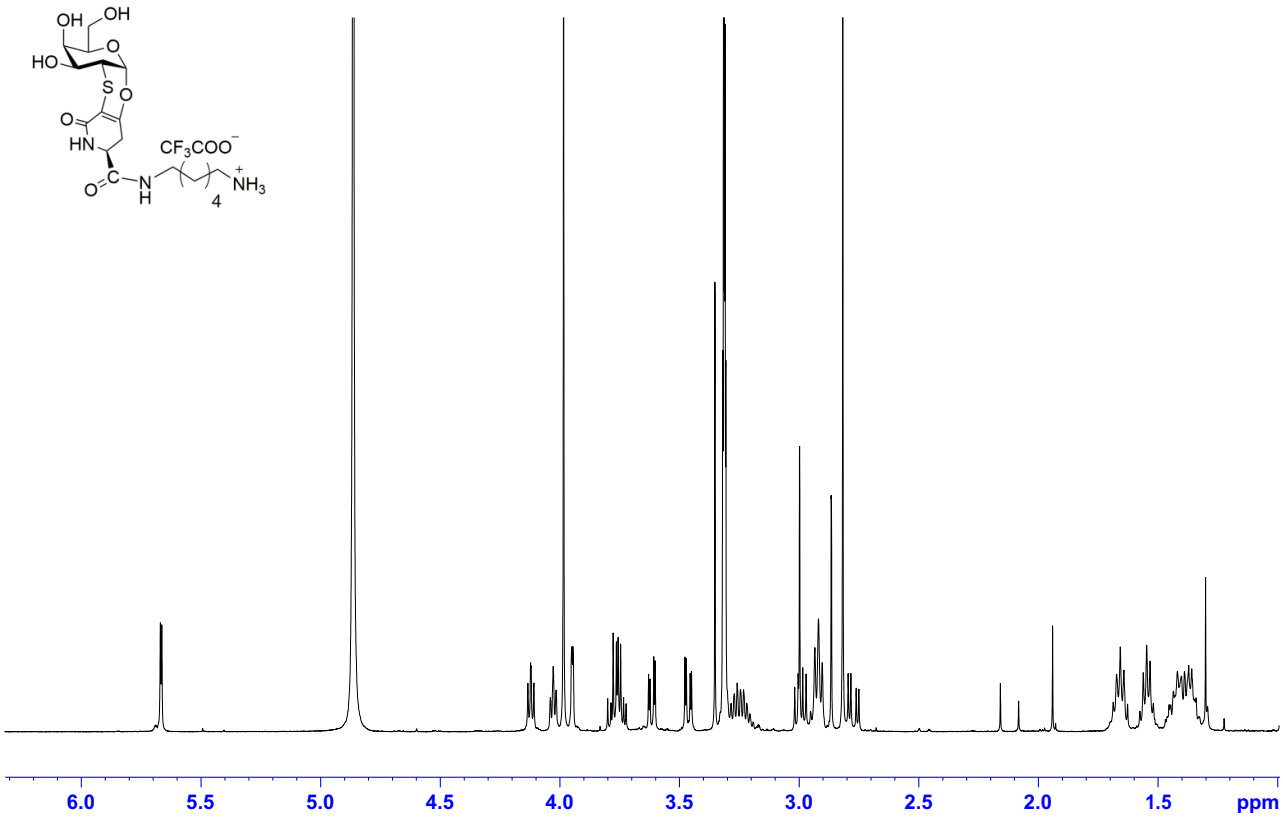

Data S6. Related to Scheme 1. ^{1}H, ^{13}C, 2D NMR and HRMS spectra of compound **8**.

^{1}H at 500 MHz in D_2O - 25 deg

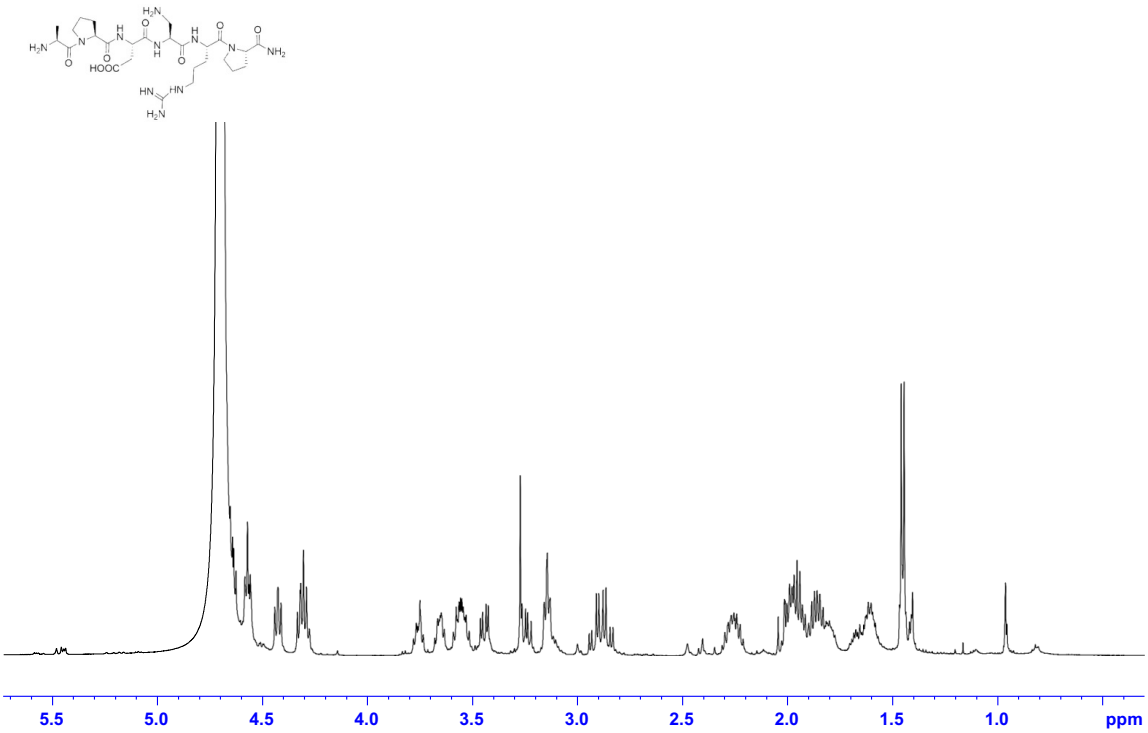

^{13}C at 125 MHz in D_2O - 25 deg

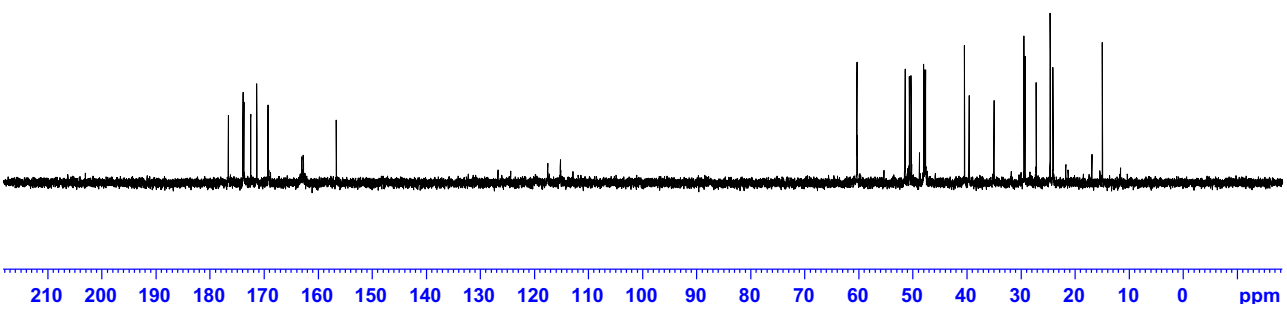

COSY at 500 MHz in D_2O - 25 deg

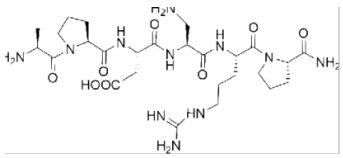

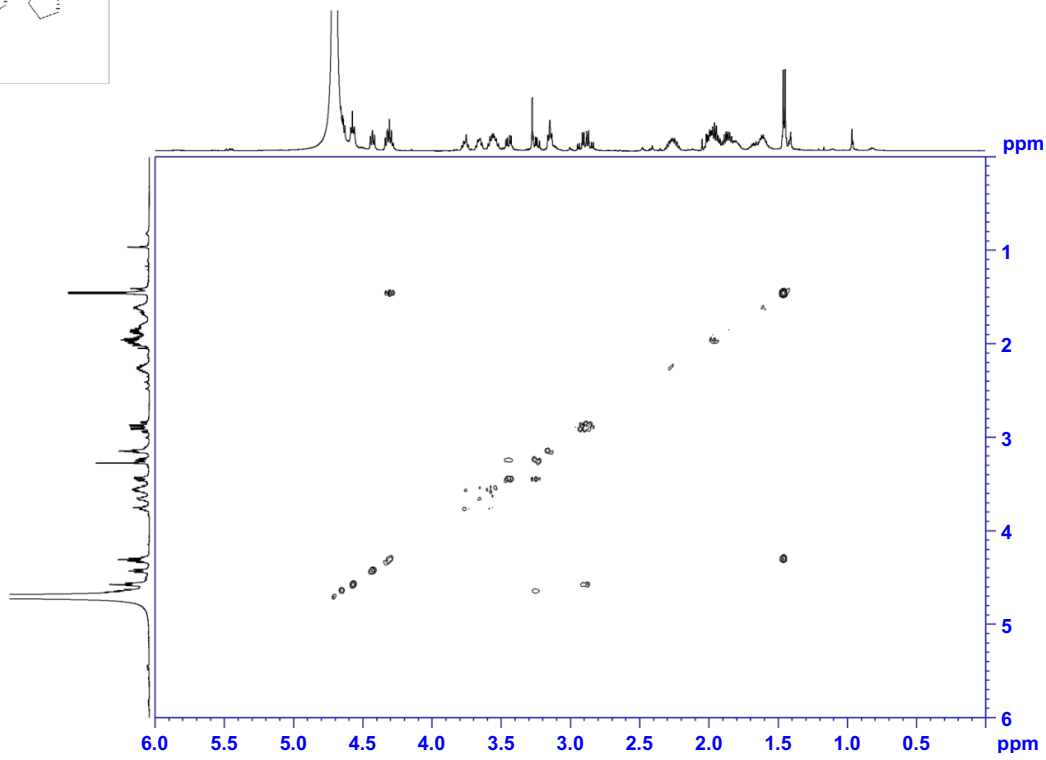

HSQC at 500 MHz in D_2O - 25 deg

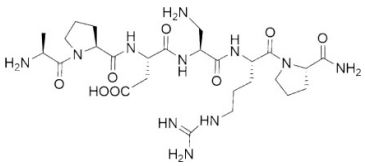

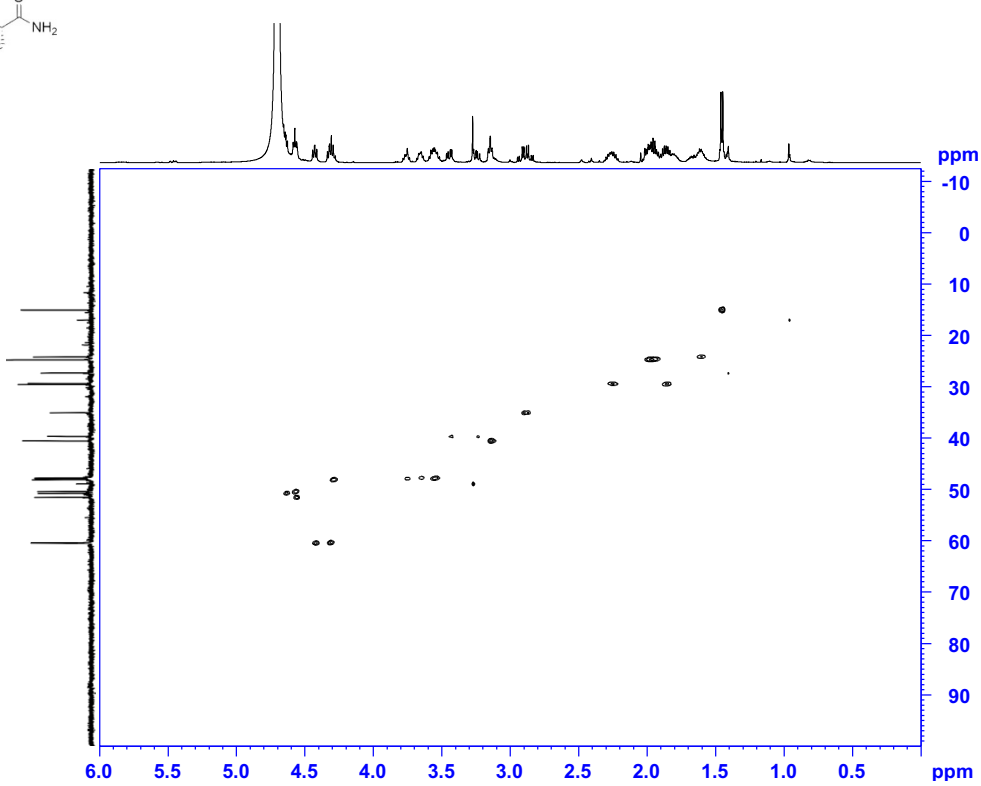

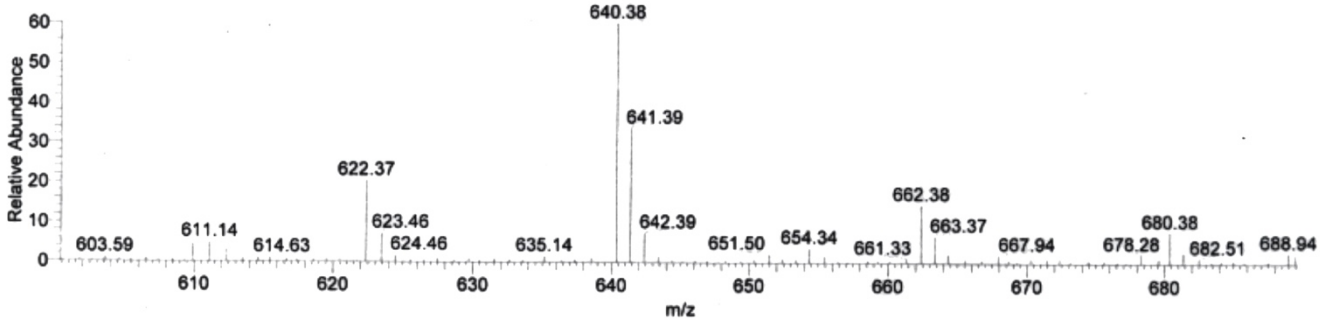
Relative Abundance
m/z
640.38
641.39
622.37
662.38
623.46
642.39
663.37
680.38
611.14
603.59
614.63
624.46
635.14
651.50
654.34
661.33
667.94
678.28
682.51
688.94

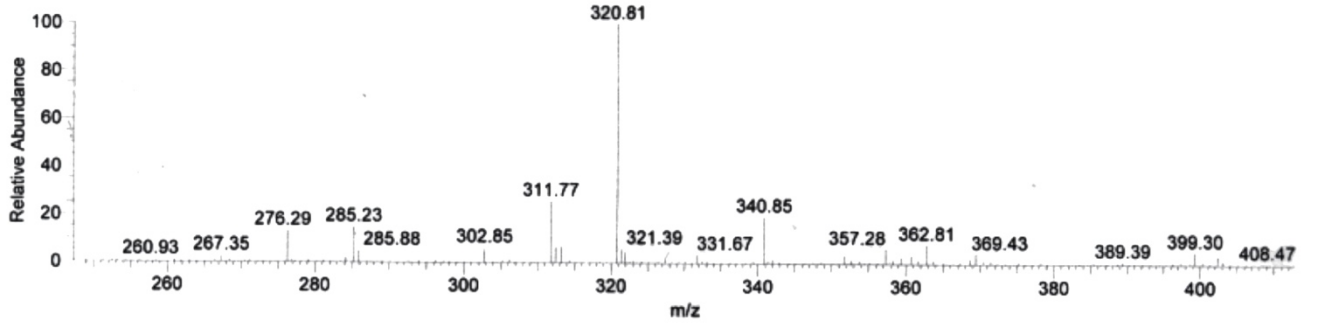
Relative Abundance
m/z
320.81
311.77
340.85
276.29
285.23
260.93
267.35
285.88
302.85
321.39
331.67
357.28
362.81
369.43
389.39
399.30
408.47

Data S7. Related to Scheme 1. ^{1}H, ^{13}C, 2D NMR and HRMS spectra of compound **9**.

^{1}H at 500 MHz in D_2O - 25 deg

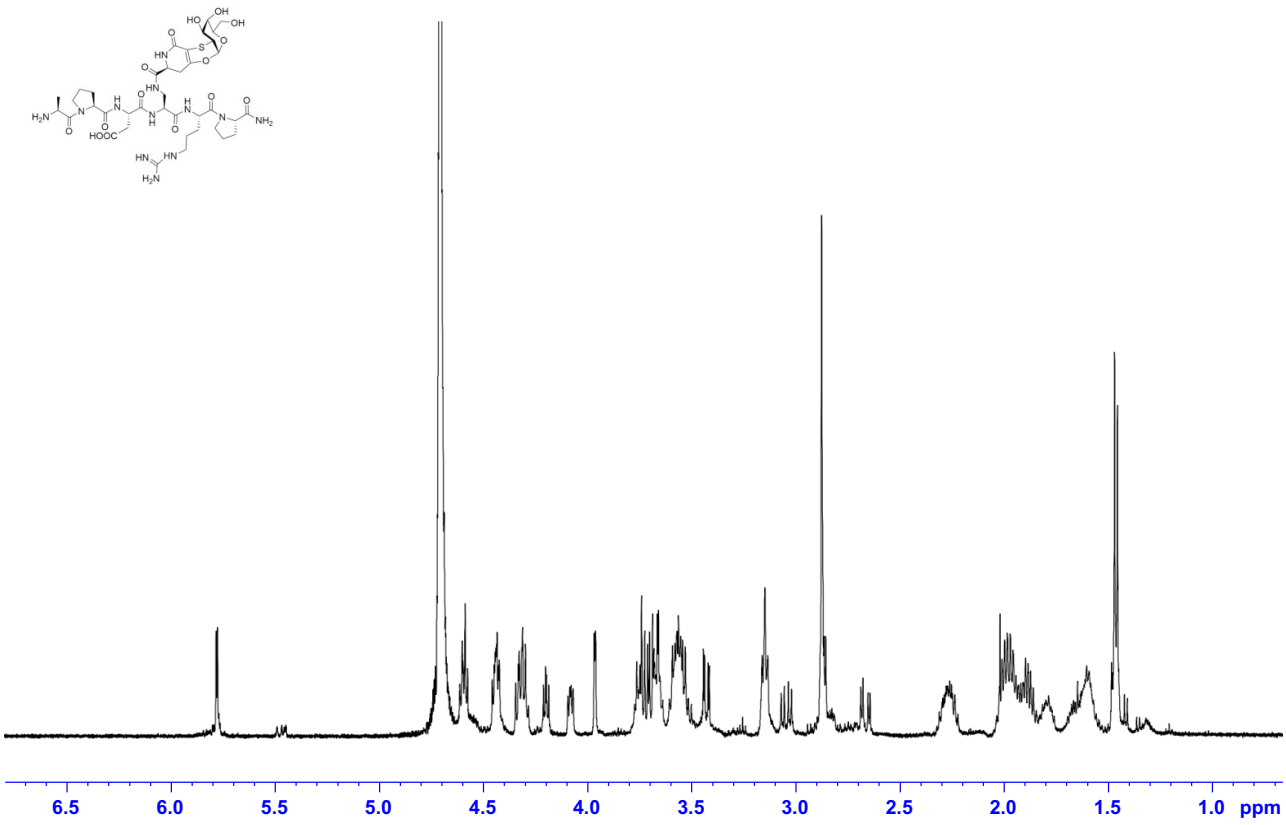

^{13}C at 125 MHz in D_2O - 25 deg

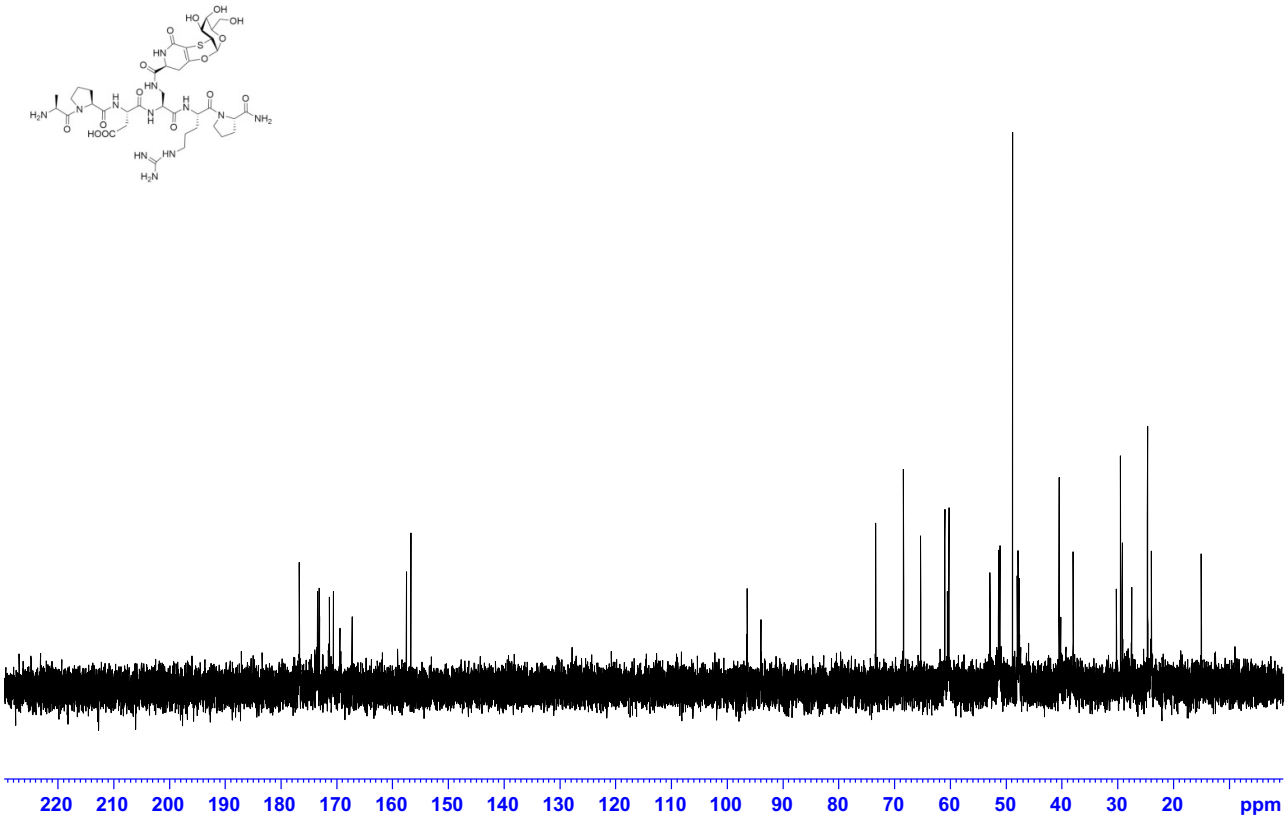

COSY at 500 MHz in D_2O - 25 deg

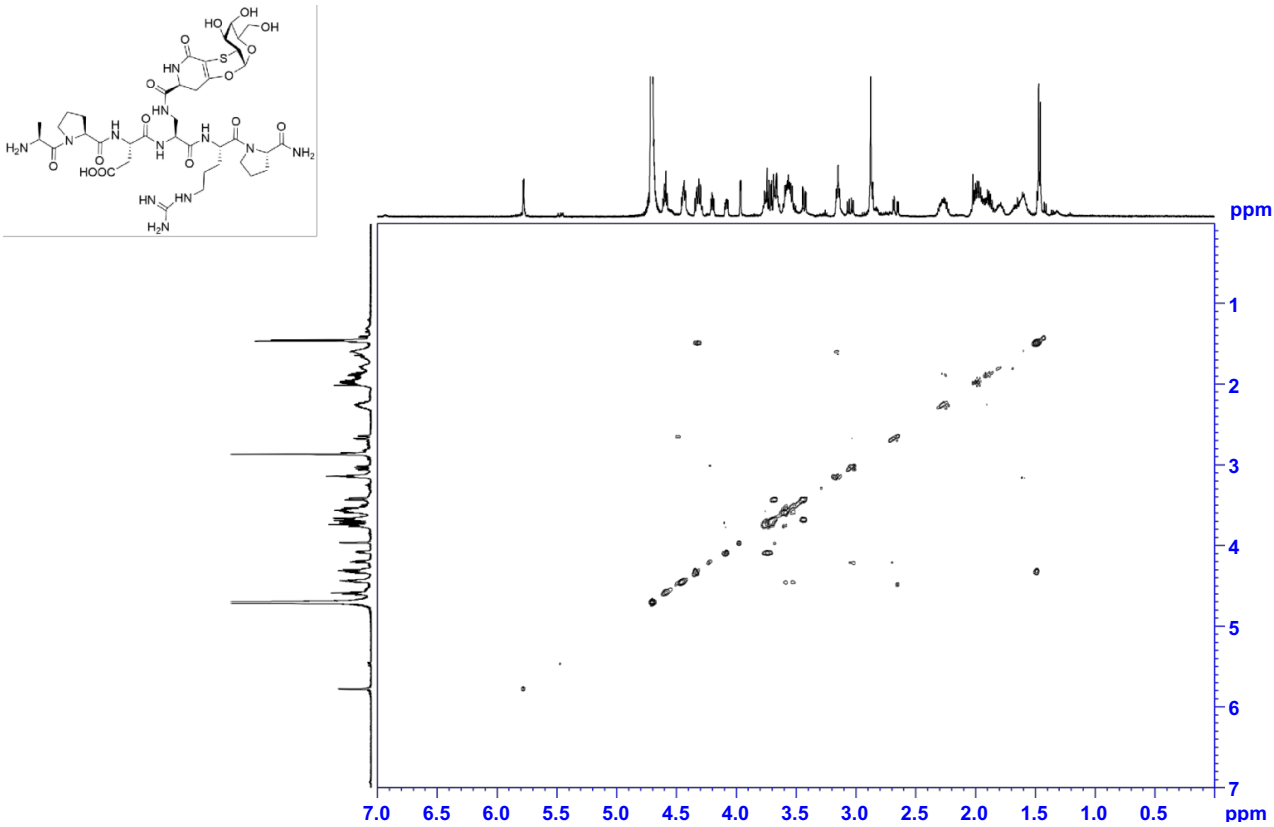

HSQC at 500 MHz in D_2O - 25 deg

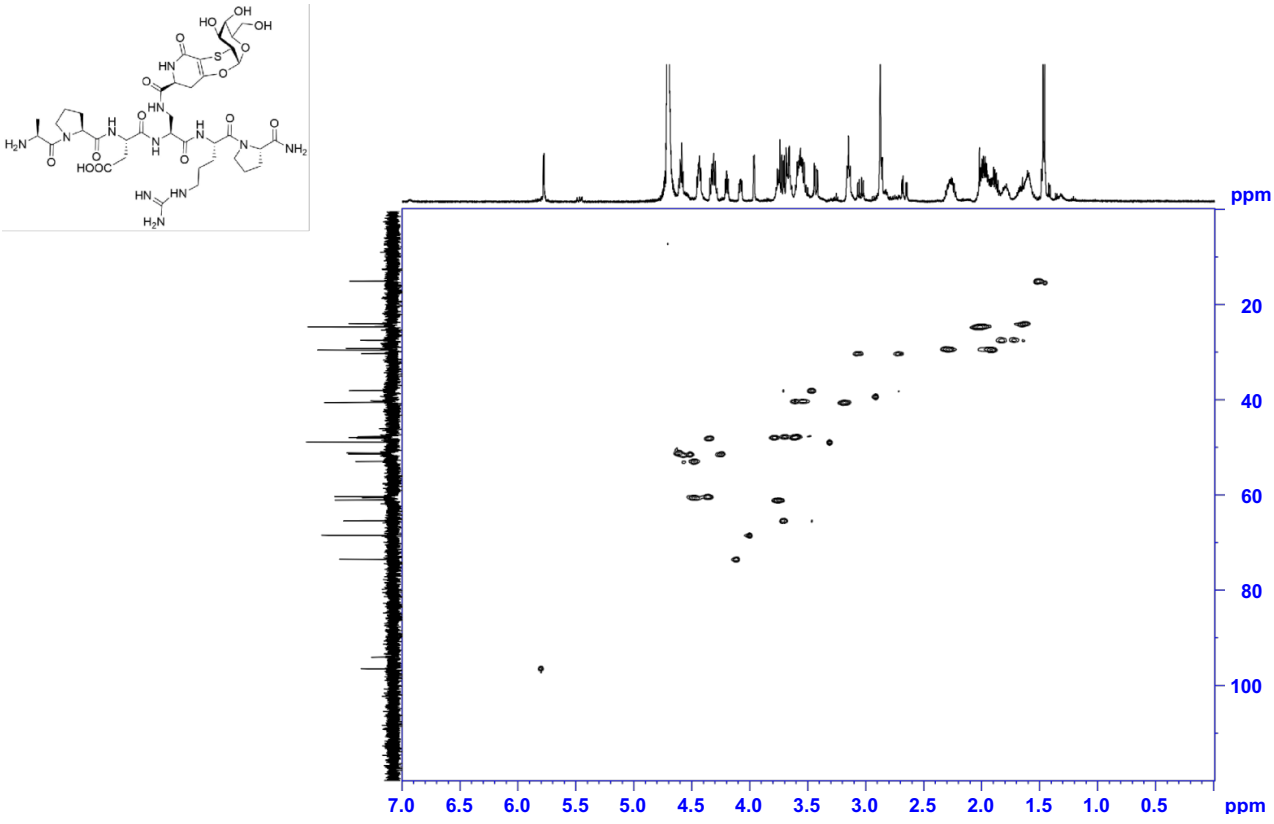

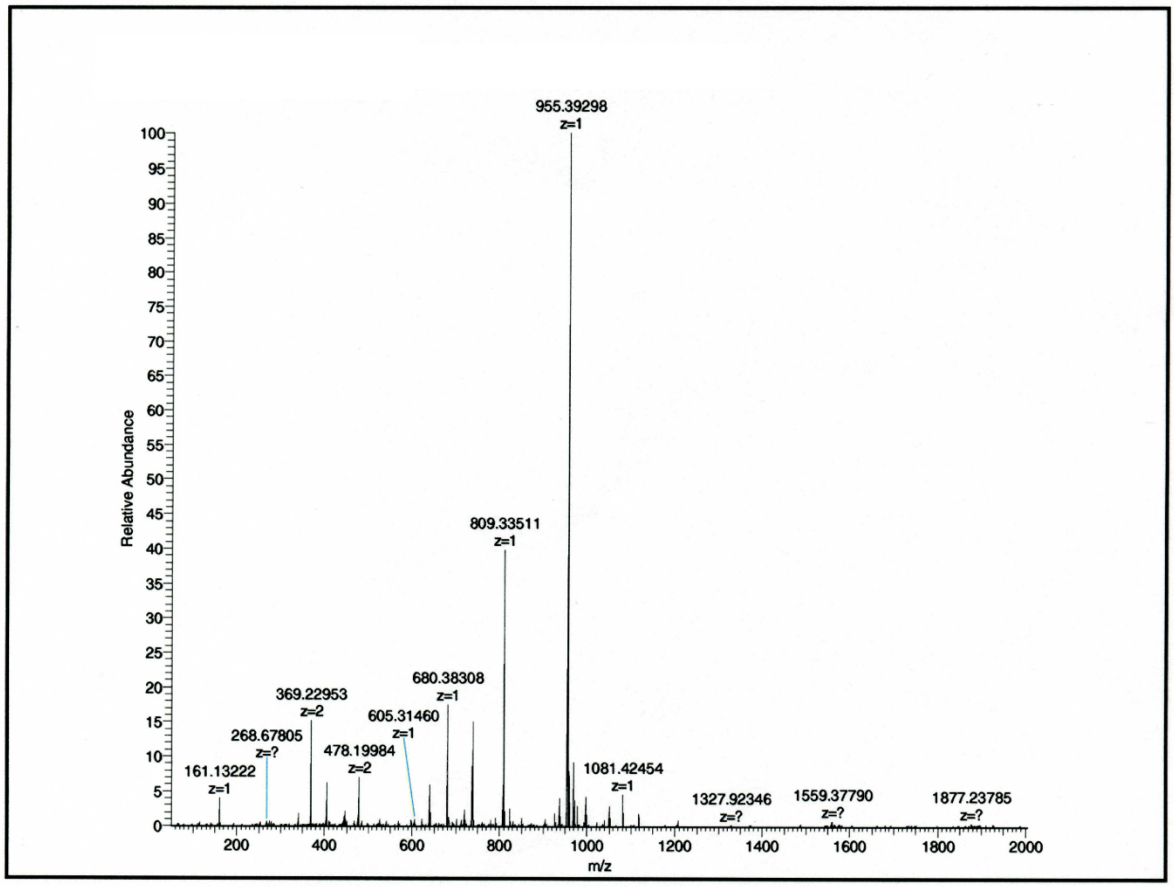

	m/z	Δ (m/z - CRM/ glycoconjugate)	n residues
CRM_{197}	58461.31		
Glc-CRM	67137.50	8676.19	25
mime[4]CRM	60848.95	2387.64	4
mime[19]CRM	68603.24	10141.93	19
mime[34]CRM	76811.90	18350.59	34

Table S3. M/z values for CRM197 and their glycoconjugates (Glc-CRM, **mime[4]CRM**, **mime[19]CRM**, **mime[34]CRM**), found by MALDI-MS analysis and number of saccharide residues (n). Percentage of derivatization with activated antigen was estimated by TNBS assay (Micoli et al., 2012; Palmer and Peters, 1969) and confirmed by MS-MALDI. Related to Figure 2.

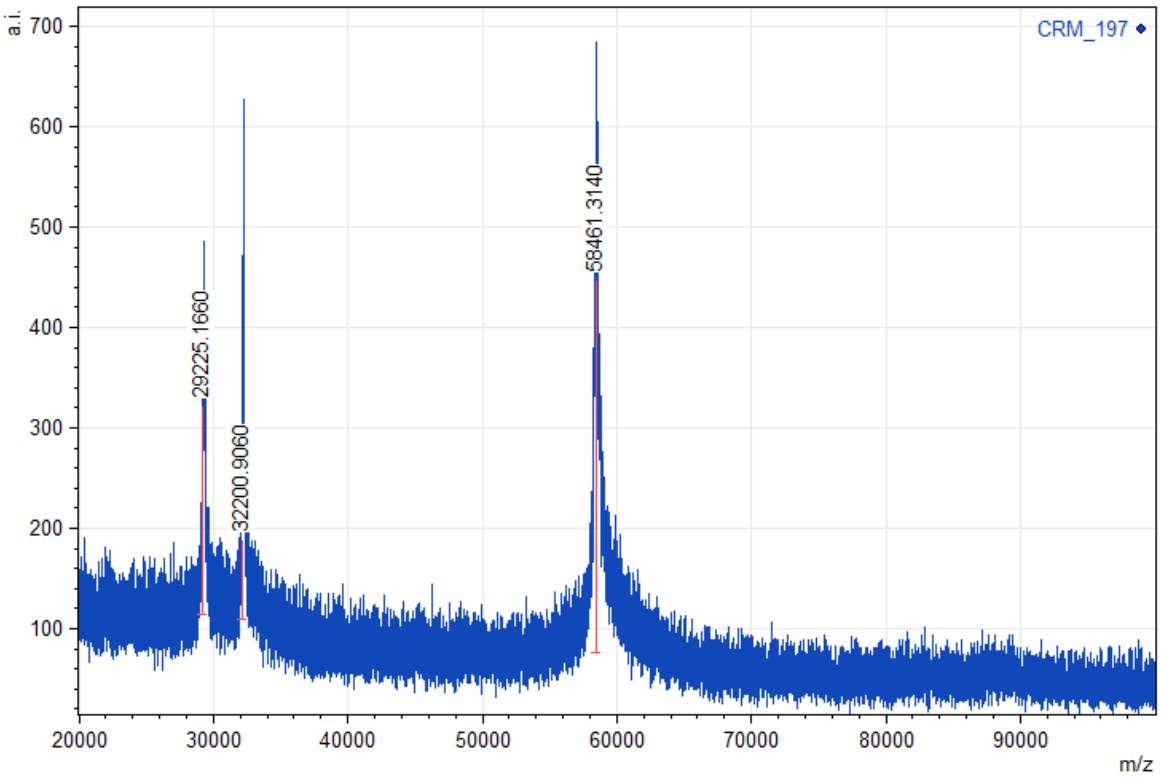

Data S8. Related to Figure 2. MS-MALDI spectrum of non functionalized CRM_{197}.

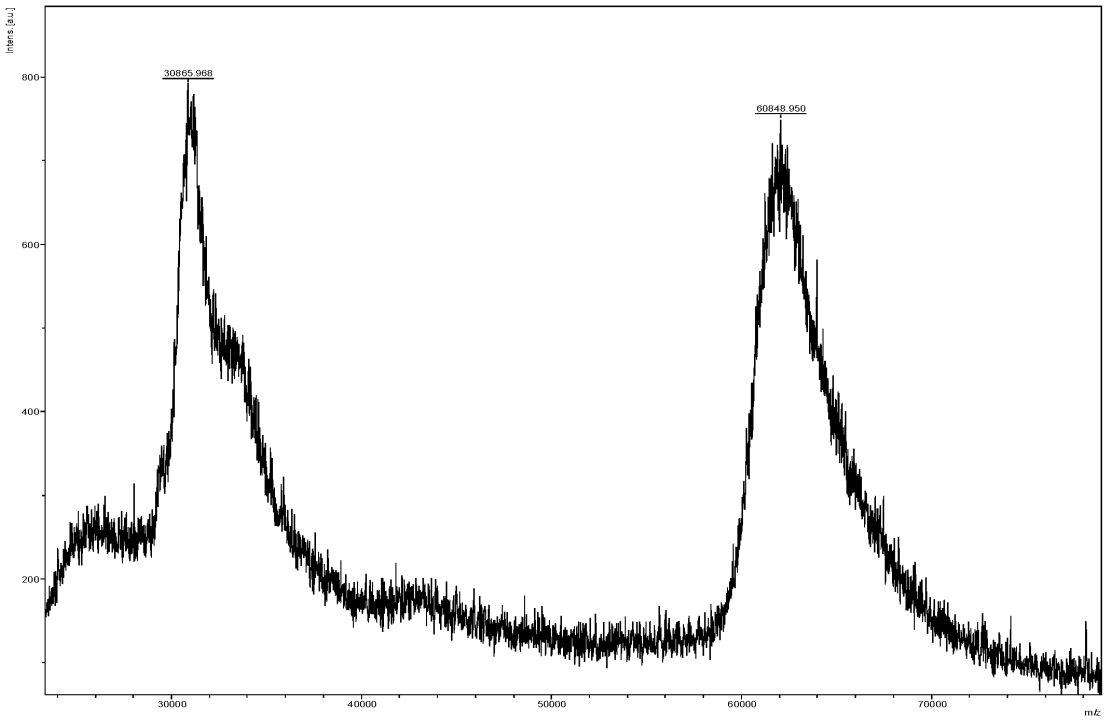

Data S9. Related to Figure 2**.** MS-MALDI spectrum of **mime[4]CRM.**

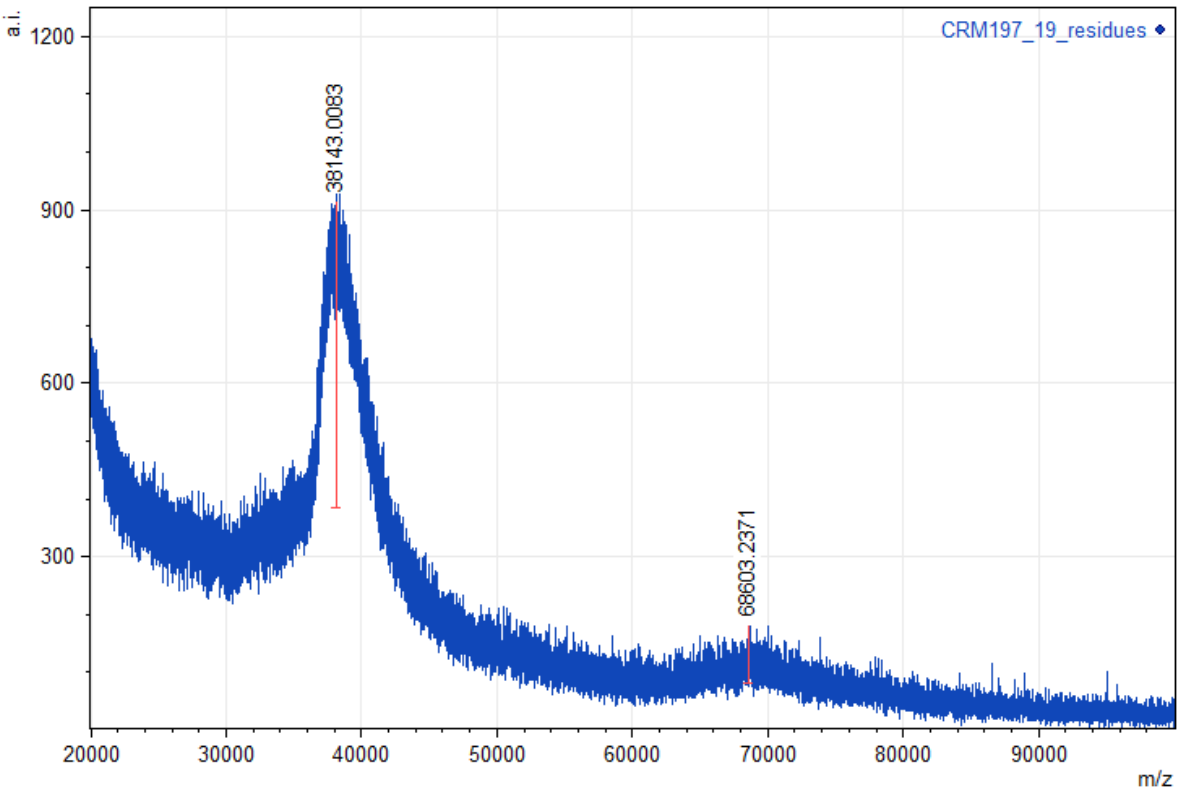

Data S10. Related to Figure2. MS-MALDI spectrum of **mime[19]CRM**.

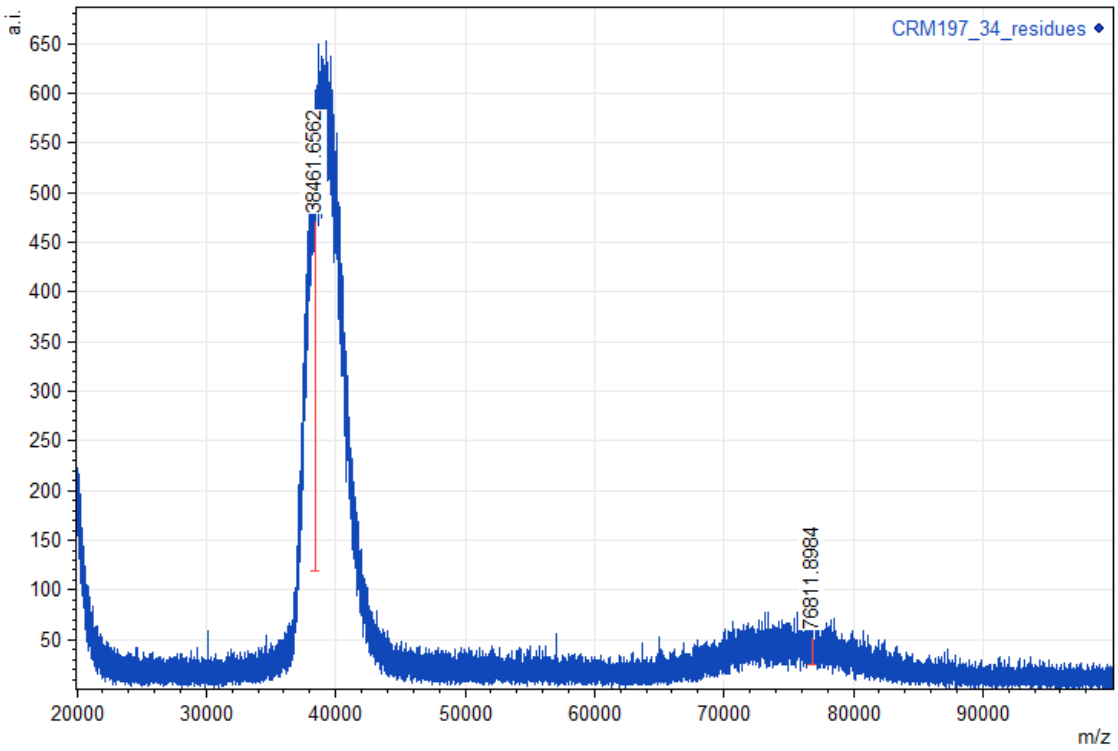

Data S11. Related to Figure 2. MS-MALDI spectrum of **mime[34]CRM**.

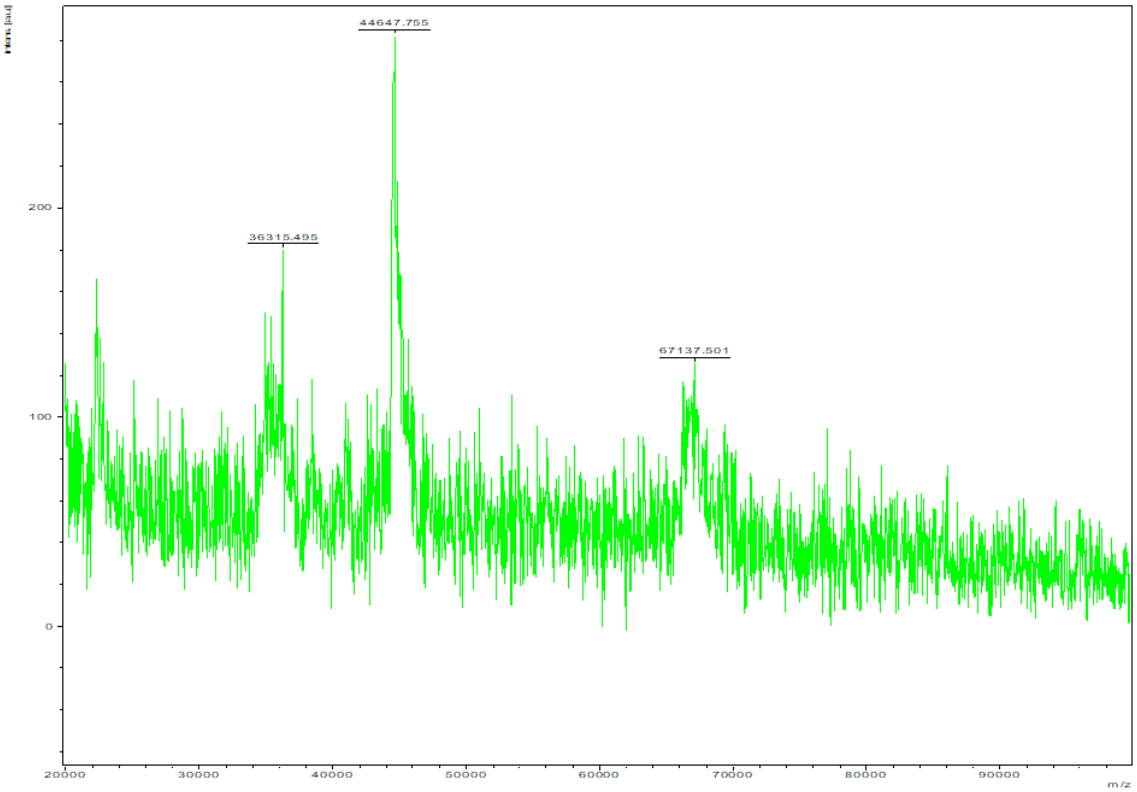

Data S12. Related to Figure 2. MS-MALDI spectrum of **Glc-CRM (**m/z 44647.755, internal standard).

Transparent Methods

Synthesis of compound 2. To a solution of crude derivative **7** (550 mg, 0.76 mmol) and NMM (300 µL, 2.73 mmol) in dry DMF (7.5 mL), a solution of *p*-nitrophenyl adipate (1.2 g, 1.76 mmol) in dry DMF (7.5 mL) was added and the mixture was stirred at room temperature overnight. The solvent was evaporated and the residue purified by flash chromatography (CH_2Cl_2/MeOH 8:1) to give pure **2** (459 mg, 88% over two steps).
$[\alpha]^{D}_{22}$ = + 38.2 (c 0.385, CH_3OH); ^{1}H NMR (500 MHz, CD_3OD) δ: 8.32-8.27 (m, 2H), 7.40-7.36 (m, 2H), 5.67 (d, $J_{1,2}$ = 2.8 Hz, 1H, H-1), 4.14-4.10 (m, 1H, H-5'), 4.04-3.99 (m, 1H, H-5), 3.97-3.94 (m, 1H, H-4), 3.80-3.71 (m, 2H, H-6a, H-6b), 3.62 (dd, $J_{3,2}$ = 10.9 Hz, $J_{3,4}$ = 2.9 Hz, 1H, H-3), 3.46 (dd, $J_{2,1}$ = 2.8 Hz, $J_{2,3}$ = 10.9 Hz, 1H, H-2), 3.27-3.14 (m, 4H, $2CH_2$), 2.98-2.91 (m, 1H, H-4'a), 2.80-2.73 (m, 1H, H-4'b), 2.70-2.64 (m, 2H, CH_2), 2.28-2.23 (m, 2H, CH_2), 1.80-1.69 (m, 4H, $2CH_2$), 1.55-1.46 (m, 4H, $2CH_2$), 1.39-1.26 (m, 4H, 2CH2); ^{13}C NMR (125 MHz, CD_3OD) δ: 175.6 (Cq), 172.7 (Cq), 172.6 (Cq), 167.6 (Cq), 157.8 (Cq), 157.2 (Cq), 146.8 (Cq), 126.1 (Cq), 123.9 (Cq), 98.3 (CH, C-1), 96.8 (Cq), 75.0 (CH, C-5), 70.2 (CH, C-4), 67.2 (CH, C-3), 62.6 (CH_2, C-6), 53.2 (CH, C-5'), 40.4 (CH_2 - CH, C-2), 40.2 (CH_2), 36.7 (CH_2), 34.6 (CH_2), 32.1 (CH_2, H-4'), 30.3 (CH_2), 30.2 (CH_2), 27.5 (CH_2), 27.3 (CH_2), 26.3 (CH_2), 25.3 (CH_2); HR-MS m/z (%): 703.25 (100) $[M+Na]^+$, 719.25 (50) $[M+K]^+$.

Synthesis of compound 3. To a solution of crude **7** (0.18 mmol) and NMM (170 µL, 1.55 mmol) in dry DMF (5 mL), solid bis-succinimide adipate (221 mg, 0.65 mmol) was added. After stirring the mixture overnight at room temperature overnight, the precipitate was eliminated, and the solvent was evaporated. The residue was suspended in EtOAc and the precipitate was purified by flash chromatography (CH_2Cl_2/MeOH 8:1) to give pure **3** (60 mg, 51% over two steps).
^{1}H NMR (500 MHz, CD_3OD) δ: 5.67 (d, $J_{1,2}$ = 2.8 Hz, 1H, H-1), 4.18-4.14 (m, 1H, H-5'), 4.05-4.00 (m, 1H, H-5), 3.98-3.95 (m, 1H, H-4), 3.81-3.71 (m, 2H, H-6a, H-6b), 3.62 (dd, $J_{3,2}$ = 10.9 Hz, $J_{3,4}$ = 2.9 Hz, 1H, H-3), 3.46 (dd, $J_{2,1}$ = 2.8 Hz, $J_{2,3}$ = 10.9 Hz, 1H, H-2), 3.28-3.13 (m, 4H, $2CH_2$), 2.98-2.91 (m, 1H, H-4'a), 2.83 (s, 4H, CH_2), 2.81-2.75 (m, 1H, H-4'b), 2.69-2.63 (m, 2H, CH_2), 2.26-2.20 (m, 2H, CH_2), 1.77-1.68 (m, 4H, $2CH_2$), 1.55-1.45 (m, 4H, $2CH_2$), 1.39-1.30 (m, 4H, $2CH_2$); ^{13}C NMR (125 MHz, CD_3OD) δ: 175.6 (Cq), 172.7 (Cq), 171.9 (Cq), 170.1 (Cq), 167.6 (Cq), 157.8 (Cq), 98.3 (CH, C-1), 96.8 (Cq), 75.0 (CH, C-5), 70.2 (CH, C-4), 67.2 (CH, C-3), 62.6 (CH_2, C-6), 53.2 (CH, C-5'), 40.5 (CH_2), 40.4 (CH, C-2), 40.2 (CH_2), 36.5 (CH_2), 32.2 (CH_2, H-4'), 31.3 (CH_2), 30.3 (CH_2), 30.2 (CH_2), 27.5 (CH_2). 27.3 (CH_2), 26.5 ($2CH_2$), 26.2 (CH_2), 25.2 (CH_2).
HRMS m/z (%): 679.75 (100) $[M+Na]^+$.

Synthesis of compound 5

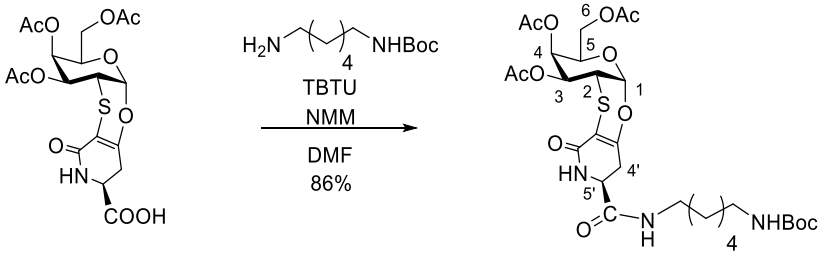

4 **5**

To a solution of **4** (425 mg, 0.93 mmol) in dry DMF (6 mL), a fresh solution of TBTU (597 mg, 1.86 mmol) and NMM (204 µL, 1.86 mmol) in dry DMF (12 mL) was added. Subsequently, N-Boc-1,6-hexanediamine (242 mg, 1.12 mmol) dissolved in dry DMF (2 mL) was added and the solution was stirred at room temperature for 3 h. The solvent was then evaporated and the residue purified by flash chromatography (CH_2Cl_2/MeOH 20:1) to give **5** (526 mg, 86%).
$[\alpha]^D_{22}$ = +77.7 (c 0.6, $CHCl_3$); ^{1}H NMR (500 MHz, $CDCl_3$) δ: 6.96 (bs, 1H, NH), 6.84 (bs, 1H, NH), 5.70 (d, $J_{1,2}$ = 2.7 Hz, 1H, H-1), 5.43-5.41 (dd, $J_{4,3}$ = 3.1 Hz, $J_{4,5}$ = 1.1 Hz, 1H, H-4), 5.02 (dd, $J_{3,2}$ = 11.7 Hz, $J_{3,4}$ = 3.1 Hz, 1H, H-3), 4.63 (bs, 1H, NH), 4.45-4.44 (m, 1H, H-5), 4.18-4.12 (m, 3H, H-5', H-6a, H-6b), 3.63 (dd, $J_{2,1}$ = 2.7 Hz, $J_{2,3}$ = 11.7 Hz, 1H, H-2), 3.30-3.20 (m, 2H, CH_2), 3.14-3.03 (m, 2H, CH_2), 3.02-2.84 (m, H-4'a, H-4'b), 2.15 (s, 3H, $COCH_3$), 2.05 (s, 3H, $COCH_3$), 2.01 (s, 3H, $COCH_3$),1.53-1.41 (m, 13H, $2CH_2$, tBu), 1.36-1.30 (m, 4H, $2CH_2$); ^{13}C NMR (125 MHz, $CDCl_3$) δ: 170.5 (Cq) 170.1 (Cq), 170.0 (Cq), 169.5 (Cq), 165.2 (Cq), 156.3 (Cq), 155.6 (Cq), 96.8 (Cq), 95.9 (CH, C-1), 79.2 (Cq, tBu), 69.0 (CH, C-5), 67.2 (CH, C-4), 65.9 (CH, C-3), 61.6 (CH_2, C-6), 52.3 (CH, C-5'), 40.1 (CH_2), 39.5 (CH_2), 36.3 (CH, C-2), 30.8 (CH_2, C-4'), 29.9 (CH_2), 29.1 (CH_2), 28.5 ($3CH_3$, tBu), 26.0 (CH_2), 25.8 (CH_2) 20.8 ($3CH_3$, Ac); ESI-MS m/z (%): 680.17 (100) [M+Na]+, 696.17 (45) [M+K]+.

Synthesis of compound 6

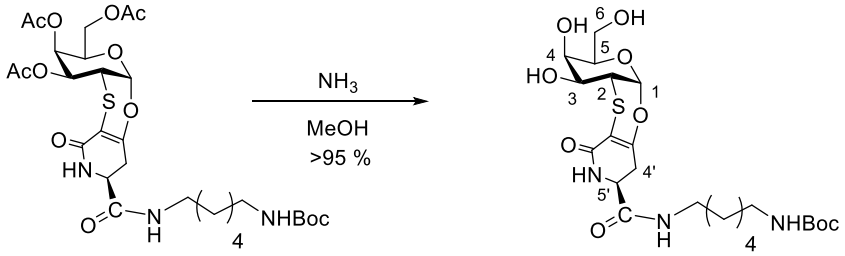

5 **6**

Compound **5** (470 mg, 0.76 mmol) was dissolved in MeOH (8 mL), and NH_3 in MeOH 2M (4.5 mL) was added. After stirring for 2 h, the reaction mixture was concentrated under vacuum to give derivative **6** (410 mg, >95 %), which was used in the next step without further purification.
$[\alpha]^D_{22}$ = + 31.2 (c 0.345, CH3OH); 1H NMR (500 MHz, CD3OD) δ: 5.67 (d, $J_{1,2}$ = 2.8 Hz, 1H, H-1), 4.14-4.10 (m, 1H, H-5'), 4.03-3.99 (m, 1H, H-5), 3.96-3.94 (m, 1H, H-4), 3.80-3.70 (m, 2H, H-6a, H-6b), 3.61 (dd, $J_{3,2}$ = 11.0 Hz, $J_{3,4}$ = 2.9 Hz, 1H, H-3), 3.46 (dd, $J_{2,1}$ = 2.8 Hz, $J_{3,2}$ = 11.0 Hz, 1H, H-2), 3.28-3.16 (m, 2H, CH_2), 3.04 (m, 2H, CH_2), 2.93 (dd, $J_{4'a,4'b}$ = 16.7 Hz, $J_{4\,a',5'}$ = 6.8 Hz, 1H, H-4'a), 2.78 (dd, $J_{4'b\,,4'a}$ 16.7 Hz, $J_{4b',5'}$ = 6.5 Hz, 1H, H-4'b), 1.43 (s, ^{13}H, $2CH_2$, tBu), 1.36-1.30 (m, 4H, $2CH_2$); ^{13}C NMR (125 MHz, CD_3OD) δ: 172.7 (Cq), 167.6 (Cq), 158.6 (Cq), 157.8 (Cq), 98.3 (CH, C-1), 96.8 (Cq), 79.8 (Cq), 75.0 (CH, C-5), 70.2 (CH, C-4), 67.2 (CH, C-3), 62.6 (CH_2, C-6), 53.2 (CH, C-5'), 41.2 (CH_2), 40.5 (CH_2), 40.4 (CH, C-2), 32.1 (CH_2, H-4'), 30.9 (CH_2), 30.2 (CH_2), 28.8 ($3CH_3$, tBu), 27.4 ($2CH_2$); ESI-MS m/z (%): 554.42 (70) $[M+Na]^+$, 570.42 (100) $[M+K]^+$.

Synthesis of compound 7

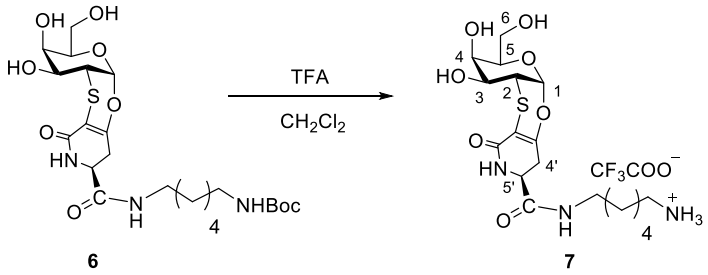

6 **7**

To a suspension of **6** (410 mg, 0.77 mmol) in dry CH_2Cl_2 (13 mL), TFA (2 mL, 26.12 mmol) was added. After 2 h, the reaction mixture was concentrated under vacuum to give crude **7** (550 mg) which was used without further purification. ^{1}H NMR (500 MHz, CD_3OD) δ: 5.66 (d, $J_{1,2}$ = 2.8 Hz, 1H, H-1), 4.14-4.09 (m, 1H, H-5'), 4.04-3.99 (m, 1H, H-5), 3.95-3.93 (m, 1H, H-4), 3.80-3.71 (m, 2H, H-6a, H-6b), 3.61 (dd, $J_{3,2}$ = 10.9 Hz, $J_{3,4}$ = 2.9 Hz, 1H, H-3), 3.46 (dd, $J_{2,1}$ = 2.8 Hz, $J_{2,3}$ = 10.9 Hz, 1H, H-2), 3.29-3.17 (m, 2H, CH_2), 3.02-2.96 (m, 1H, H-4'a), 2.94-2.89 (m, 2H, CH_2), 2.80-2.74 (m, 1H, H-4'b), 1.70-1.62 (m, 2H, CH_2), 1.58-1.50 (m, 2H, CH_2) 1.47-1.32 (m, 4H, $2CH_2$).

Synthesis of hexapeptide 8

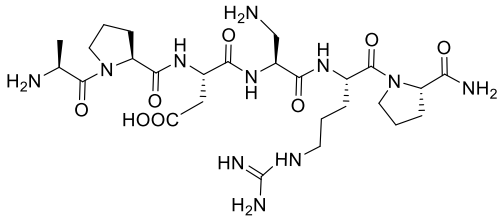

8

Non-glycosylated peptide was synthesized by standard Fmoc solid-phase methodologies starting from Fmoc-Pro-Rink-Amide MBHA resin. Sidechain deprotection and cleavage from the resin were achieved in a standard single-step acidolysis reaction. Hexapeptide **8** was characterized by NMR and MS (see pages S30-S32).
$[\alpha]^D_{22}$ = -71.4 (c 0.22, H_2O); ESI-MS m/z (%): 320.81 (100) $[M+2H]^{2+}$, 640.38 (70) $[M+H]^+$, 662.38 (20) $[M+Na]^+$.

Synthesis of glycosyl hexapeptide 9

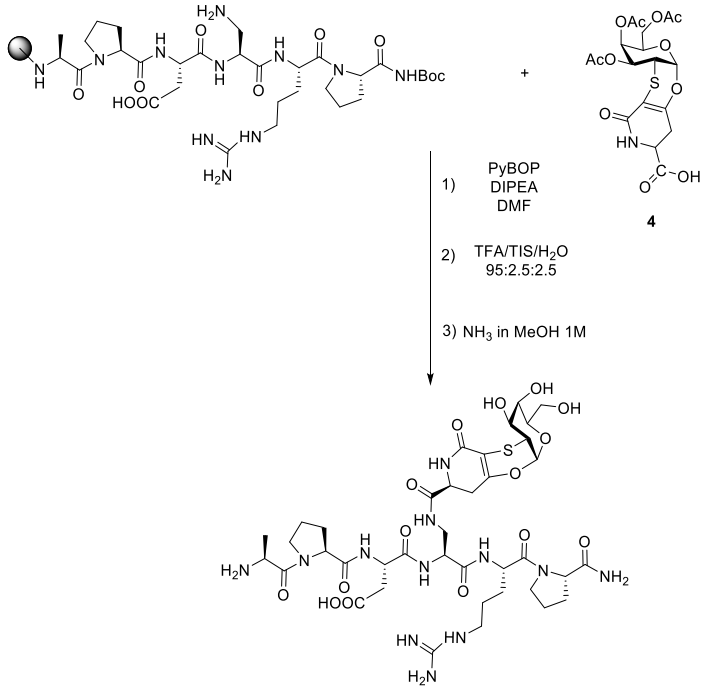

4 **9**

Glycopeptide **9** was synthesized by coupling of derivative **4** to the peptide protected and linked to the resin, with PyBOP and DIPEA in DMF. After 2 h, the resin was washed with DMF and the acetylated glycopeptide was detached and deprotected by acidolysis reaction (TFA/TIS/H_2O 95:2.5:2.5) followed by treatment with NH_3 in MeOH 1 M.

Glycopeptide **9** was purified by C18 reversed-phase chromatography (H_2O/CH_3CN 80:20) and characterized by NMR and HRMS (see pages S33-S35).
ESI-HRMS m/z (%): calculated, $[M+H]^+$ = 955,3938; found, 955.39298 (100) $[M+H]^+$.

General procedure for CRM197 glycoconjugates synthesis

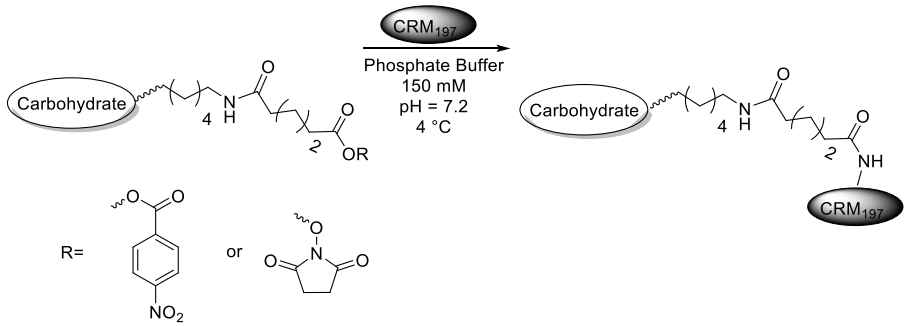

A 0.8 mM solution of CRM197 in NaPi, buffer (150 mM, pH 7.2 buffer) was treated with a 100-200 equiv. of activated carbohydrate, previously dissolved in a minimal amount of the NaPi buffer. The reaction mixture was incubated at 4 °C for 24 h under shaking. The success of the reaction was proved by an SDS-PAGE. The conjugate was then purified from unreacted sugar by multistep washings with water using a 10 kDa MWCO membrane centrifugal device (Millipore). The number of attached moieties was estimated by UltraFlex III MALDI-TOF/TOF instrument (Bruker Daltonics) in linear mode and with positive ion detection (see page S36-37).

SAXS Recording Method and Results.SAXS data were recorded on the BioSAXS beamline BM29 at the European Synchrotron Radiation Facility (ESRF) Grenoble, France, using a 2D Pilatus detector at an X-ray wavelength of 1.008 Å. Data processing and reduction were performed using an automated standard ESRF beamline software (BSxCuBE) (Pernot et al., 2013) and PRIMUS (Konarev et al., 2003). Concentration series (0.5, 1.0, 2.0, 5.0 mg/mL) were recorded for both samples and individual samples and buffers were exposed for 10 times 1s frames and grouped to improve statistics. For CRM197 the radius of gyration RG was extracted by the Guinier approximation (Guinier, 1939) using PRIMUS. In Figure S2 we report the SAXS spectra of CRM197 and **mime[19]CRM** sample measured at 37 °C. The SAXS data showed clear aggregation in the case of **mime[19]CRM** but globular and compact particles in the case of CRM197. The same trend was observed in spectra acquired at 25 °C. A radius of gyration (RG) of 25.8 Å (at T=37 °C) is estimated for the CRM197 from the Guinier fit (inset figure) of the q2 dependence of the scattering intensity in the small angles.

Molecular dynamics (MD) simulations.
The simulations were carried out with AMBER 18 package (Case et al., 2018) implemented with ff14SB (Maier et al., 2015) and GAFF (Wang et al., 2004) force fields. The structure of CRM197 was obtained from the protein data bank web site (PDB id: 4AE0).The parameters and charges for the unnatural Tn and the corresponding linker were generated with the antechamber module of AMBER, using GAFF force field and AM1-BCC method for charges (Jakalian et al., 2002).The conjugated (or compound **1**) was immersed in a water box with a 10 Å buffer of TIP3P water molecules (Kiyohara et al., 1998). If required, the system was neutralized by adding explicit counter ions (Na^+). A two-stage geometry optimization approach was performed. The first stage minimizes only the positions of solvent molecules and the second stage is an unrestrained minimization of all the atoms. The system was then gently heated by incrementing the temperature from 0 to 300 K under a constant pressure of 1 atm and periodic boundary conditions. Harmonic restraints of 30 $kcal \cdot mol^{-1}$ were applied to the solute, and the Andersen temperature-coupling scheme was used to control and equalize the temperature. The time step was kept at 1 fs during the heating stages, allowing potential inhomogeneities to self-adjust. Long-range electrostatic effects were modelled using the particle-mesh-Ewald method (Darden et al., 1993). An 8 Å cut-off was applied to Lennard-Jones interactions. Each system was equilibrated for 2 ns with a 2-fs time step at a constant volume and temperature of 300 K. Production trajectories were then run for additional 0.5 μs under the same simulation conditions.

Binding studies by Surface Plasmon Resonance (SPR).
SPR experiments were performed with a Biacore X-100 apparatus (Biacore, GE) in HBS-EP buffer at pH 7.5 (Hepes 10 mM, NaCl 150 mM, EDTA 3 mM, with 2% DMSO and 0.005% Tween X100 as the running buffer at 25 ºC. Tn218 antibody was immobilized on a CM5 sensor chip (Biacore, GE) following standard amine coupling method. Briefly, the carboxymethyl dextran surface of the flow cell 2 was activated with a 7-min injection of a 1:1 ratio of aqueous 0.4 M 1-ethyl-3-(3-dimethylaminopropyl)carbodiimide (EDC) and 0.1 M sulfo-N-hydroxysuccinimide. Then, the antibody was coupled to the surface during a 7-min injection using several dilutions in 10 mM sodium acetate, pH 4.0. The unreacted active esters on the surface were quenched by a 7-min injection of aqueous 0.1 M ethanolamine-HCl (pH 8.0). The levels

of immobilization were in the range of 3000-5000 resonance units (RU). Flow cell 1 treated as a flow cell 2 (amine coupling procedure) without protein was used as a reference. Prior to use, 50 mM stock solutions of **mime[4]CRM** were diluted to the final concentration in the running buffer. Typically, a series of different compounds was injected onto the sensor chip a flow rate of 30 µl/min for a period of 1min followed by a dissociation period of 1 min. No regeneration was needed. The concentrations used for affinity measurements were in the range of 0.05-1.5 mM. Sensogram data were double-referenced using the Biaevaluation X-100 software (Biacore, GE). The experimental data of affinity measurements were fitted to a one site-specific model binding using Prism software (see also Fig. S3).

DCs markers' expression.
DCs were differentiated from peripheral blood adherent mononuclear cells (PBMC) of healthy donors. PBMC were obtained by cell separation kit Magnetic Cell Separation (MACS - Miltenyi Biotec, Bergisch Gladbach - Germany). The cells were suspended and cultured in 6-well culture plates (2x106/mL) in RPMI-1640 complete medium (Sigma-Aldrich, Milan, Italy) added with GMC-SF (100ng/mL) and IL-4 (200ng/mL) (PeproTech, Rocky Hill, NJ, USA) for 5 days. On the 6th day, we have added the antigens (0.22 mg/mL), and the cells were cultured for 48 h. As positive control to activation, we used the LPS (100ng/mL).

DCs phenotyping.
For the phenotype analysis both active and control DCs were incubated with mAbs for 30 min and washed with PBS containing 0.1% bovine serum albumin (BSA) and 0.1% sodium azide. DCs were labeled with mAbs for CD80 FITC, CD83 PE, CD86 APC (BD Pharmingen, San Jose, CA, USA). Samples were analyzed by FACS Canto II cytometer (Becton-Dickinson, San Jose, CA, USA) using the DIVA software. The error bars are from triplicates of the analysis for one donor (SpSS version 24 sofware).

Cell viability.
Viability of 4T1 cells and PBMC was quantified by PrestoBlue® assay (Thermo Fisher Scientific). Cells were seeded (5,000 cells/well, in triplicate) into 96-well plates. Cells were treated with serial concentrations of **mime[4]CRM**; Glc-CRM or CRM197 and incubated for up 96 h. After, part of the medium was removed, and PrestoBlue® reagent (resazurin-based solution) was added for up to 60 min at 37 °C. During this time, PrestoBlue® reagent is modified by the reducing environment of the viable cell and turns red in color, becoming highly fluorescent. Color change was detected using fluorescence Excitation 535/Emission 615 nm using Microplate Reader InfiniteF200 (Tecan). Experiments were repeated three independent times (Fig. S5).

Cell culture.
4T1-luc, Mouse Mammary Gland Adenocarcinoma Cell Line (stably expressing firefly Luciferase gene) was cultured in RPMI-1640 medium (ECB9006L, Euroclone, Milan, Italy) supplemented with 10% fetal bovine serum (ECS0180D, Euroclone, Milan, Italy), 2 mM L-Glutamine (ECB3000D, Euroclone), and 1% antibiotics (ECB3001D, 10,000 U/mL penicillin, 10 mg/mL streptomycin, Euroclone) at 37 °C in a 5% CO_2 incubator.

Tumor implantation and Bioluminescence imaging (BLI).
4T1-luc (8 x 104 cells in 50 µL PBS) were implanted into the lower right inguinal mammary fat pad (using insulin syringes with 32 G needles) of female (n=19) immunocompetent syngeneic mice model (5 weeks old; strain: BALB/c). Tumor progression of tumor cells were monitored weekly by non-invasive *in vivo* bioluminescence imaging (BLI), using IVIS 3D Illumina Imaging System (Xenogen/Caliper) as previously described (Spano and Zollo, 2012). For *in vivo* BLI acquisitions, mice were anesthetized using 1-3% isofluorane (B104F16C, Piramal/Healthcare) and intraperitoneally injected (100 µL per 10 g body weight) with a 15 mg/mL solution of D-luciferin (122799, Perkin Elmer) in PBS. After 10 min from D-Luciferin injection, BLI acquisitions were performed using the auto-exposure mode. For tumor growth curve, the total flux of photons (photons per sec) within each region of interest (ROI) from bioluminescence image were quantified using the Living Images Software Package 3.2 (Xenogen-Perkin Elmer) (see also Table S1).
Five-week old female BALB/c mice were purchased from Envigo (Italy). Mice were housed in individually ventilated cages in an experimental room. The animals were maintained under standard conditions of light (12 h-light/12 h-dark), temperature (23°-25°C), humidity (50 to 60%) and rodent chow and water ad libitum. Survival analysis was performed using the Kaplan-Meier log-rank survival test with the SPSS16 statistical package.
Ethical approval for mouse use released from Ministero della Sanita` 546/2015 PR to the Director of Studies, Massimo Zollo, 19/6/2015, art. 31 D.lgs. 26/2104.

***In vivo* drug administration.**
For tumor growth evaluation and immune system evaluation, seven days after the implantation of tumor cells, mice (2 groups, n= 9 treated with **mime[4]CRM** and n=10 controls (CRM197), grouped according to their BLI values were administered subcutaneously neck down the back with **mime[4]CRM** at a dose of 17 mg/kg/weekly resuspended in 100 µL PBS or with CRM197 as vehicle for the control group once weekly for 5 weeks. Mice were then sacrificed at days 28,

42 and at the end of the experiment (i.e. on day 54 from the tumor implantation). Serum, primary tumor and different organs were collected for the enzyme-linked immunosorbent assay (ELISA) and immunohistochemistry analyses.

Immunofluorescence staining.
Primary tumors were fixed in 4% paraformaldehyde (PFA) and embedded in paraffin. tissue sections (4-µm-thick) were deparaffinized in Xylene Substitute (A5597; Sigma) 30 min and rehydrated in 100% - 90% -70%- 50% and 30% ethanol and washed with PBS 1X and PBS containing 0.02% TRITON-X 100 (215680010; Acros Organics). For antigen retrieval, the slides incubated in pre-warmed 10 mM sodium citrate buffer (pH 6.0) in microwave for 15 min, The slides were left to cool at room temperature for 30 min. to decrease the non-specific background fluorescence, the sections covered with 0.2 % Trypsin (T2600000; Sigma-Aldrich) and 0.001% $CaCl_2$ and incubated for 10 min at 37 °C in humidified chamber, The tissue sections were washed with phosphate-buffered saline (PBS) and then blocked with a blocking solution containing 6% Bovine serum albumin (A9418; Sigma) and 5% Fetal bovine serum (ECS0180L; EuroClone) 20 mM $MgCl_2$ in PBS containing 0.02% Triton-X 100 for 1 h at room temperature with the following primary antibodies overnight at 4 °C: anti-mouse CD4 FITC-conjugated (22150043, 1:200), FoxP3 (ab47285, 1:500), CD68 (ab53444,1:100), CD163 (sc-33560, 1:100), PD1/CD270 (E-AB-27294, 1:100), F4/80 (sc-52664, 1:100), CD11c/ Integrin alpha-x B-6 (cs-46676, 1:100). Tissue sections were washed in PBS 1X and PBS containing 0.02% TRITON-X 100 and were incubated with secondary antibody, anti-rabbit Alexa Fluor 546 (Thermo Fisher, #A10040, 1:200), anti-mouse Alexa Fluor 594 (ab150116, 1:200). DNA was stained with DAPI (#62254; Thermo Fisher). Confocal microscopy was carried out using a laser scanning confocal microscope (Leica TCS SP5 Confocal Laser Scanning Microscope), with the 63× oil immersion objective.

Statistical analyses for quantitative Immunofluorescences.
Cell counting on immunofluorescence staining was performed using ImageJ software (version 1.52r, 26 October 2019; https://imagej.nih.gov/ij/index.html). More in details, we used the Cell Counter tool (from ImageJ software) to score the number of DAPI positive cells (blue nuclear staining) from three different images per tissue sample previously acquired with Leica TCS SP5 Confocal Laser Scanning Microscope with the 63× oil immersion objective. Then, the same Cell Counter tool was used to score (i) CD4 positive cells (green plasma membrane staining), (ii) FOXP3 positive cells (red nuclear staining), (iii) TCR positive cells (red plasma membrane staining), (iv) CD11c positive cells (red staining plasma membrane staining), (v) PD1 positive cells (red plasma membrane staining), (vi) CD68 positive cells (red plasma membrane staining), (vii) CD163 positive cells (red or green plasma membrane staining), F4/80 positive cells (green plasma membrane staining) per slice (by clicking on the marker feature in the image). The updated number corresponding to each counted marker type was displayed on a table and then export on excel file. Later, the percentage of positive cells were determined as follow: (number of positive cells * 100)/ total number (the total number corresponds to DAPI positive cells (see Table S2). Finally, the Student's t-distribution (i.e., two tailed, type 2 t-test assuming sample equal variance) was applied to determine if the means of the two sets of data (Control: CRM197; or Treated: **mime[4]CRM**) were significantly different from each other. A p-value lower than 0.05 (< 0.05) is assumed statistically significant.

Immunohistochemistry.
The mouse breast cancer and lung specimens, preserved in fixative solution, were taken out from the fixative, washed in 0.1 M phosphate buffered saline (PBS, pH 7.4), dehydrated in a graded ethanol series, cleared in xylene and embedded in paraffin. The sections (5 µm thick) were cut by using a rotary microtome (MR2, Boeckeler Instruments Inc., Tucson, AZ, USA), collected on positively charged slides and processed for either histological or immunohistochemical labeling. The sections were deparaffinized through consecutive passages in xylene and in decreasing ethanol concentration solutions up to the final step in distilled water. To evaluate the tissue organization all the sections were first stained with haematoxylin-eosin (H&E).
The sections underwent to antigen retrieval treatment. Two procedure were used at this aim following antibody data sheets suggestions: 1) boiled 10 min in sodium citrate buffer or 2) treated for 20 min at 90-92 °C in Tris buffer (10 mM) with EDTA (1 mM, pH 9.0), as appropriate, followed by cooling to room temperature (RT). After, the sections were treated with 3% H_2O_2 in PBS for 5 min to block endogenous peroxidase activity. After washing, they were incubated with 1.5% bovine serum albumin (BSA, Sigma-Aldrich, Saint Louis, MI, USA) in PBS for 30 min at RT. The primary antibody, diluted as appropriate in 1.5% BSA in PBS, was applied overnight (ON) at 4°C. The day after, the sections were incubated with the biotinylated secondary antibody in 1.5% BSA in PBS for 2 h, at RT. Then, the sections were washed, treated with ABC Reagent (Vectastain ABC/Elite Kit, Vector Laboratories, Burlingame, CA, USA) for 20 min and developed with 3,3'-diaminobenzidine (DAB, Sigma-Aldrich), as chromogen. After the washing in PBS, the sections were mounted in an aqueous medium (Permafluor, ThermoFiscer Scientific, Rockford, IL, USA) and observed under the Reichert-JungMicrostar IV light microscope. Negative controls were performed omitting the primary antibody to exclude the presence of non-specific staining. As positive control, mouse spleen sections were used.

Primary Ab	Host	IHC	Producer
anti-CD4	Rabbit	1:1000	Cat n. ab183685; Abcam, Cambridge, UK

anti-CD8	Rat	1:100	Cat n. MA1-70041; Thermo Fiscer Scientific, Rockford, IL, USA
anti-CD163	Rabbit	1:500	Cat n. ab182422; Abcam, Cambridge, UK
anti-CD68	Rat	1:100	Cat n. ab53444; Abcam, Cambridge, UK
anti-FOXP3	Rat	1:100	Cat n. 14-5773-82; Invitrogen, Thermo Fiscer Scientific, USA
Secondary Ab	**Host**	**IHC**	**Producer**
anti-Rabbit	Goat	1:300	Cat n. BA1000; Vector laboratories, Burlingame, CA, USA
anti-Rat	Goat	1:300	Cat n. BA-4001; Vector laboratories, Burlingame, CA, USA

Quantitative analysis.
The quantitative analysis of the immunoreactive (IR) structures was done acquiring digitized images of the labeling (2 sections/animal; 2 animals/group) using 10x objectives; attention was made to avoid overlapping between the adjacent portions. The total number of images obtained from the sections of untreated and treated mice was comparable. Each image was analyzed using ImageJ (NIH, Bethesda, ML, USA) to evaluate the intensity of labeling and to quantify the area of the IR structures. The photographs' threshold values were set in the sections of untreated mice in order to analyze the structures of interest exclusively and it was maintained in the treated ones. The optical density of each image was quantified, and the results were expressed as mean±SEM. The significance was evaluated using Graph Pad Prism 3.0 (GraphPad Software Inc., San Diego, CA, USA) applying Student t-test. Differences were considered significant when $P \leq 0.05$.

ELISA Tests.
96-well ELISA plates were coated with 0.5 μg/well of the hexapeptide Ala-Pro-Asp-H2NSer-Arg-Pro (as negative control) or with the glycosylated, Ala-Pro-Asp-HNSer(mimetic **1**)-Arg-Pro hexapeptide overnight at 4 °C. After washing with PBS containing 0,05% Tween 20 (PBST), wells were blocked with 200 μL/well of 5% bovine serum albumin (BSA) in PBS and incubated for 2 h at room temperature. Sera from immunized mice were added to wells as two-fold steps serial dilutions with PBST, compared to wells without sera. After washing with PBST, plates were incubated with HRP conjugated anti-mouse IgG and IgM (GE-Healthcare) at appropriated dilution for 2 h at room temperature. For detection, plates were washed and added with 100 μL/well of 3,3',5,5'-tetramethylbenzidine (TMB - Sigma-Aldrich) substrate solution, and further incubated at room temperature for 10 – 30 min in the dark. Reactions were quenched by adding 100 μl/well of 2 M H_2SO_4 and immediately read at 450 nm using an Infinite F200 microplate reader (Tecan).

Flow Cytometry Analysis.
4T1 cells were grown to sub-confluency, detached from wells by enzyme-free Cell Dissociation Buffer (Gibco) and collected, then resuspended in PBST containing 5% BSA. Sera from immunized mice (1:100 dilution) were added to cells and incubated on ice for 30 min. After washing with PBST-BSA, cells were incubated with APC conjugated donkey anti-mouse IgG (Thermo Fisher Scientific) and incubated on ice for 30 min. After washing, stained cells were measured using BD FACSCanto II, and data analysis was performed using the FLOWJO sofware.

Th1/Th2/Th17 cytokine profile assessment.
Serum samples from mice treated with **mime[4]CRM** or from control mice were analyzed for the presence of Th1, Th2, and Th17 cytokines by using RayBio Quantibody Mouse TH17 Array 1 (RayBio, Norcross, GA), according to the manufacturer's instructions. Eighteen different cytokines were evaluated: interleukin 1 beta (IL-1β), IL-2, IL-4, IL-5, IL-6, IL-10, IL-12p70, IL-13, IL-17, IL-17F, IL-21, IL-22, IL-23, IL-28, interferon gamma (IFN-γ), macrophage inflammatory protein 3 alpha (MIP-3α), transforming growth factor beta 1 (TGFβ1), and tumor necrosis factor alpha (TNF-α). In brief, slides were incubated with blocking solution (RayBio) at room temperature for 30 min. Afterwards, standard cytokines and diluted sera (1:2) were incubated at room temperature for 2 h. Slides were washed 5 times and probed for 1 h at rt with Biotinylated Antibody Cocktail. After washing steps at RT, the slides were incubated 1 h at rt with Cy3 Equivalent Dye-Streptavidin, washed and finally dried by a compressed nitrogen. Signals were scanned on a ScanArray Plus scanner, using ImaGene 8.0 software. Results were analyzed by Prism Graph Pad software. The statistical significance of the differences between groups was determined with Student's two-tailed t-test, while intra-group analysis was determined with two-way ANOVA test. $P < 0.05$ was considered to be statistically significant. The concentration of each cytokine was determined versus standard curves of each cytokine.

Human *ex vivo* tests.
Patients. Twelve patients with breast cancer (BC) were enrolled for the study. All patients, that not received chemotherapy, underwent blood sampling and surgical resection of the primary lesion; patients with evidence of serious illness, immunodeficit, or autoimmune or infectious diseases were excluded.
Patients were enrolled after obtaining informed consent and approval of the local ethical committee.

Detection of mime[4]CRM-specific T cells in the peripheral blood of patients with BC. To assess the presence of **mime[4]CRM**-specific T cells in the peripheral blood of BC patients, PBMCs were re-suspended in medium supplemented with 3% human serum. PBMCs ($3x10^5$) were cultured for 96 h in the presence of medium alone, **mime[4]CRM** (10 μg/mL), or Glc-CRM (as control, 10 μg/mL). At 16 h before harvesting, 0.5 μCi/well [3H]-thymidine (Amersham Pharmacia Biotech, Sweden) was added, and the radionuclide uptake was measured by a β-counter. The mitogenic index (MI) was calculated as the ratio between mean values of cpm (counts for min) obtained in **mime[4]CRM** or Glc-CRM stimulated cultures and those obtained in the presence of medium alone. A MI ≥3 was considered as a positive result.

Generation of T cell clones (Tcc) from TILs of the neoplastic tissue. Surgical specimens of BC tissue were dissociated in order to isolate tumor-infiltrating lymphocytes (TILs). First, tissue pieces were dissociated with the Tumor Dissociation Kit, human (Miltenyi Biotech, UK) in combination with the gentleMACS™ Octo Dissociator (Miltenyi Biotech, Germany), to obtain a gentle and rapid generation of single-cell suspensions. Then, TILs were magnetically isolated with anti-human CD3 microbeads (Miltenyi Biotech, UK) and cloned under limiting dilution. Briefly, single T-cell blasts were seeded in microwells (0.3 cells/well) in RPMI 1640 culture medium (SERO-Med GmbH, Wien) supplemented with 10% FCS HyClone (Gibco Laboratories, Grand Island, NY), in the presence of 2 x 10^5 irradiated (9000 rad) PBMC, phytohemagglutinin (PHA) (0.5% vol/vol), and recombinant human interleukin-2 (IL-2) (50 U/mL) (PeproTech, USA). At weekly intervals, 2 x 10^5 irradiated PBMC and IL-2 were added to each micro-culture to maintain the expansion of growing T cell clones (Tcc).

Phenotypic characterization of isolated Tcc. We analysed the Tcc' surface markers (CD3, CD4, CD8) expression by flow cytometry using FACS Canto II cytometer (Becton-Dickinson, San Jose, CA, USA) and the DIVA software. A total of 10^4 events for each sample was acquired.

Evaluation of mime[4]CRM-specific T cells in the neoplastic tissue of BC. To assess the presence of **mime[4]CRM**-specific T cells in the neoplastic tissue of BC, Tcc were re-suspended in medium supplemented with 3% human serum. Tcc were cultured for 48 h with irradiated autologous mononuclear cells in the presence of medium alone, **mime[4]CRM** (10 μg/mL or Glc-CRM (as control, 10 μg/mL). At 16 h before harvesting, 0.5 μCi/well [3H]-thymidine (Amersham Pharmacia Biotech, Sweden) was added, and the radionuclide uptake was measured by a β-counter. The mitogenic index (MI) was calculated as the ratio between mean values of cpm (counts for min) obtained in **mime[4]CRM** or Glc-CRM stimulated cultures and those obtained in the presence of medium alone. A MI ≥3 was considered as a positive result.

NMR spectra recording

The 1D ^{1}H NMR spectra of free CRM197 and of its glycoconjugates **mime[4]CRM** and **mime[19]CRM** were acquired at 298 K on a Bruker AVANCEIII-HD NMR spectrometer operating at 900 MHz, ^{1}H Larmor frequency, equipped with a cryogenically cooled probe. Free CRM197 in NaPi (10 mM) + sucrose (10% w/v) at pH 7.2 with 10% D_2O, while the glycoconjugates **mime[4]CRM** and **mime[19]CRM** were dissolved in NaPi (150 mM) at pH 7.5 with 10% D_2O.

Supplemental References

Case, D.A., Ben-Shalom, I.Y., Brozell, S.R., Cerutti, D.S., Cheatham, T.E., III, Cruzeiro, V.W.D., Darden, T.A., Duke, R.E., Ghoreishi, D., Giambasu, G., Giese, T., Gilson, M.K., Gohlke, H., Goetz, A.W., Greene, D., Harris, R., Homeyer, N., Huang, Y., Izadi, S., Kovalenko, A., Krasny, R., Kurtzman, T., Lee, T.S., LeGrand, S., Li, P., Lin, C., Liu, J., Luchko, T., Luo, R., Man, V., Mermelstein, D.J., Merz, K.M., Miao, Y., Monard, G., Nguyen, C., Nguyen, H., Onufriev, A., Pan, F., Qi, R., Roe, D.R., Roitberg, A., Sagui, C., Schott-Verdugo, S., Shen, J., Simmerling, C.L., Smith, J., Swails, J., Walker, R.C., Wang, J., Wei, H., Wilson, L., Wolf, R.M., Wu, X., Xiao, L., Xiong, Y., York, D.M., Kollman, P.A., 2018. AMBER 2018. University of California, San Francisco.

Darden, T., York, D., Pedersen, L., 1993. Particle mesh Ewald: An N·log(N) method for Ewald sums in large systems. J. Chem. Phys. 98, 10089–10092. https://doi.org/10.1063/1.464397

Guinier, A., 1939. La diffraction des rayons X aux très petits angles: application à l'étude de phénomènes ultramicroscopiques. Ann. Phys. 11, 161–237. https://doi.org/10.1051/anphys/193911120161

Jakalian, A., Jack, D.B., Bayly, C.I., 2002. Fast, efficient generation of high-quality atomic charges. AM1-BCC model: II. Parameterization and validation. J Comput Chem 23, 1623–1641. https://doi.org/10.1002/jcc.10128

Kiyohara, K., Gubbins, K.E., Panagiotopoulos, Athanassios Z., 1998. Phase coexistence properties of polarizable water models. Molecular Physics 94, 803–808. https://doi.org/10.1080/002689798167638

Konarev, P.V., Volkov, V.V., Sokolova, A.V., Koch, M.H.J., Svergun, D.I., 2003. PRIMUS: a Windows PC-based system for small-angle scattering data analysis. J Appl Cryst 36, 1277–1282. https://doi.org/10.1107/S0021889803012779

Maier, J.A., Martinez, C., Kasavajhala, K., Wickstrom, L., Hauser, K.E., Simmerling, C., 2015. ff14SB: Improving the Accuracy of Protein Side Chain and Backbone Parameters from ff99SB. J. Chem. Theory Comput. 11, 3696–3713. https://doi.org/10.1021/acs.jctc.5b00255

Micoli, F., Rondini, S., Gavini, M., Lanzilao, L., Medaglini, D., Saul, A., Martin, L.B., 2012. O:2-CRM(197) conjugates against Salmonella Paratyphi A. PLoS ONE 7, e47039. https://doi.org/10.1371/journal.pone.0047039

Palmer, D.W., Peters, T., 1969. Automated Determination of Free Amino Groups in Serum and Plasma Using 2,4,6-Trinitrobenzene Sulfonate. Clin Chem 15, 891–901. https://doi.org/10.1093/clinchem/15.9.891

Pernot, P., Round, A., Barrett, R., De Maria Antolinos, A., Gobbo, A., Gordon, E., Huet, J., Kieffer, J., Lentini, M., Mattenet, M., Morawe, C., Mueller-Dieckmann, C., Ohlsson, S., Schmid, W., Surr, J., Theveneau, P., Zerrad, L., McSweeney, S., 2013. Upgraded ESRF BM29 beamline for SAXS on macromolecules in solution. J Synchrotron Rad 20, 660–664. https://doi.org/10.1107/S0909049513010431

Spano, D., Zollo, M., 2012. Tumor microenvironment: a main actor in the metastasis process. Clin Exp Metastasis 29, 381–395. https://doi.org/10.1007/s10585-012-9457-5

Wang, J., Wolf, R.M., Caldwell, J.W., Kollman, P.A., Case, D.A., 2004. Development and testing of a general amber force field. J Comput Chem 25, 1157–1174. https://doi.org/10.1002/jcc.20035